SARAH KWAO

SYNTHESIS, CHARACTERIZATION AND BIOLOGICAL EVALUATION OF NEW ZINC(II)-8-HYDROXYQUINOLINE DERIVED COMPLEXES

2022

SARAH KWAO

SYNTHESIS, CHARACTERIZATION AND BIOLOGICAL EVALUATION OF NEW ZINC(II)-8-HYDROXYQUINOLINE DERIVED COMPLEXES

Mestrado em Qualidade em Análises

Master in Quality in Analytical Laboratories (EMQAL)

UNIVERSIDADE DO ALGARVE

Faculdade de Ciências e Tecnologia

2022

SYNTHESIS, CHARACTERIZATION AND BIOLOGICAL EVALUATION OF NEW ZINC(II)-8-HYDROXYQUINOLINE DERIVED COMPLEXES

Mestrado em Qualidade em Análises

Master in Quality in Analytical Laboratories (EMQAL)

Trabalho efetuado sob a orientação de:

Work performed under the supervision of:

Profª Doutora Maria Isabel Rodrigues Correia

Profª Doutora Isabel Maria Palma Antunes Cavaco

UNIVERSIDADE DO ALGARVE

Faculdade de Ciências e Tecnologia

2022

Synthesis, characterization and biological evaluation of new zinc(II)-8-hydroxyquinoline derived complexes

Declaration of Authorship

I declare that I am the author of this work, which is original. The work cites other authors and works, which are adequately referred in the text and are listed in the bibliography.

Sarah Kwao

Dedication

To my parents;

Margaret Dede Kwao

and

Nene Aflo Akakposu (III), Lawrence Kwao (Late)

Your love and support have made me who I am today.

Acknowledgements

To God be the glory!

He has successfully overseen the opening, progress and ending of another chapter in my life. It's worth trusting You.

My special appreciation and deepest sense of gratitude goes to the Supervisor of this thesis, Professor Maria Isabel Rodrigues Correia at Instituto Superior Técnico (IST), Centro de Química Estrutural (CQE) – University of Lisbon, Portugal. I'm thankful for her leadership, thoughtfulness, critical comments, prompt feedback and inputs, warmth and constant encouragements, patience in reading and correcting this thesis manuscript.

I am deeply grateful to Nádia Raquel Pólvora Ribeiro for her guidance and love in holding my hands and directing me step-by-step along the way in all my laboratory work. Your words of encouragements, prompt feedback, careful inputs, advice and calm disposition helped a lot.
I am also thankful to Dr. Leonor Côrte-Real for her patience and timely assistance anytime in need.

I am profoundly grateful to Professor João Costa Pessoa for allowing me to do this work in his laboratory. I would also like to thank Dr. Pedro Franco Pinheiro for all the biological studies.

A special acknowledgement and appreciation to Professor Isabel Maria Palma Antunes Cavaco, University of Algarve for accepting and introducing me to the research. I would also like to acknowledge Professor Maria Clara Semedo Da Silva Costa for her follow-ups throughout this research work.

My sincere gratitude also goes to the European commission for the financial support from start to finish of this programme. My heartfelt appreciation goes to Professor Bjørn Grung, University of Bergen (UIB) -Norway and Erasmus Mundus Master in Quality in Analytical Laboratory (EMQAL) programme director for his love, care and support throughout the entire programme.
I would like to acknowledge University of Bergen, University of Algarve, University of Lisbon, Instituto Superior Técnico, Centro de Quimica Estrutural and Laboratório de Análises do IST (LAIST) for their immense support in making this programme a reality.

Finally, but not the least, I would like to dedicate this work to my mum, Mrs. Margaret Dede Kwao, for her love and for continuously being an inspiration. To Lt. Cdr. Richard Gerald Nii Lante Lamptey, simply thank you. I am also profoundly grateful to my family, for their immense love and support, making me know distance cannot be a barrier.

Abstract

Metallodrugs like cisplatin and related platinum compounds, widely used for the treatment of cancer patients, have severe side effects and acquired resistance, which are limiting their use. In addition, several cancer conditions are not responsive to available treatments and thus, viable clinical solutions are still lacking.

Metal-based drugs have received a great deal of attention in recent years owing to their properties and benefits in biomedical, therapeutic and diagnostic systems. A wider understanding of the anticancer properties of transition metal complexes like Ru, V, Cu, and Zn and their interactions in biological media is very necessary to ensure their effectiveness and safety.

In the current work, four Schiff base ligands derived from the condensation of 8-hydroxy-2-quinolinecarbaldehyde and benzohydrazides (H_2L^1-H_2L^4), and their corresponding zinc complexes, ZnL^1, ZnL^2, ZnL^3, and ZnL^4 were synthesized. All compounds were characterized by elemental analyses, FTIR, UV–Vis and NMR spectroscopies as well as ESI-MS spectrometry. The stability of the complexes was evaluated in DMSO and under physiological conditions (HEPES buffer (10 mM, pH 7.4) containing DMSO). The interaction between Schiff bases and their corresponding Zn(II) complexes with biological molecules, namely bovine serum albumin (BSA) was investigated using UV-Vis and fluorescence spectroscopies at 298 K. Fluorescence quenching of BSA upon interaction with the complexes was also analyzed at 298, 301, 305 and 310 K. Using the Stern-Volmer formalism, the binding constants indicated moderate to strong binding to albumin with values ranging from K_b = 0.63 to 7.81×10^4 M^{-1} for the first three complexes. These results reveal good binding propensity with the protein. Additionally, evaluation of thermodynamic parameters revealed that hydrophobic interactions are the main interactive forces involved in the zinc complexes binding to BSA.

In vitro cytotoxic activity of the ligands and their complexes was evaluated on prostate carcinoma (LNCaP FGC), acute T-cell leukaemia (Jurkat E6-1), myeloma (MM.1S), and non-cancerous immortalized human HEK-293 cell lines. Strong cytotoxic activities of both ligands and complexes were observed against all three cancer cell lines. In the non-cancer cell line, the ligands exhibited lower IC_{50} values than their counterpart complexes. However, the metal complexes have solubility issues, making it difficult for their evaluation.

Overall, the current ligand system shows high potential for cancer treatment due to the high selectivity towards the studied cancer cells.

***Keywords**: Schiff bases, 8-hydroxyquinoline, Zn(II) complexes, cytotoxicity, albumin binding*

Resumo

Os complexos de metais como a cisplatina e compostos de platina relacionados, amplamente utilizados para o tratamento de doentes com cancro, têm efeitos secundários graves e problemas de resistência adquirida, que limitam a sua utilização. Além disso, várias tipos de cancro não respondem aos tratamentos disponíveis e, por conseguinte, são necessárias soluções clínicas alternativas.

Os fármacos à base de metais têm recebido muita atenção nos últimos anos devido às suas propriedades e benefícios em sistemas biomédicos, quer terapêuticos, quer ~~e~~ de diagnóstico. Uma compreensão mais ampla das propriedades anticancerígenas de complexos metálicos de transição como Ru, V, Cu, e Zn e as suas interacções nos meios biológicos é muito importante para garantir a sua eficácia e segurança.

No trabalho actual, foram sintetizados quatro ligandos base de Schiff derivados da condensação de 8-hidroxi-2-quinolinocarbaldeído e benzohidrazidas (H_2L^1-H_2L^4), e os seus correspondentes complexos de zinco, ZnL^1, ZnL^2, ZnL^3, e ZnL^4. Todos os compostos foram caracterizados por análise elementar, espectroscopias de absorção no IV, UV-Vis e RMN, bem como espectrometria de massa (ESI-MS). A estabilidade dos complexos em solução foi avaliada em dimetilsulfóxido (DMSO) e sob condições fisiológicas (tampão HEPES (10 mM, pH 7,4) contendo DMSO). A interacção entre as bases de Schiff e os seus correspondentes complexos de Zn(II) com macromoléculas biológicas, nomeadamente albumina de soro bovino (BSA) foi investigada utilizando espectroscopias de UV-Vis e fluorescência a 298 K. A extinção da fluorescência da BSA após interacção com os complexos foi também analisada a 298, 301, 305 e 310 K. Usando o formalismo de Stern-Volmer, as constantes de ligação indicaram ligação moderada a forte à albumina com valores que variaram entre K_b = 0,63 a $7{,}81\times10^4$ M^{-1} para os três primeiros complexos. Estes resultados revelam uma boa propensão de ligação para com a proteína. Além disso, a avaliação dos parâmetros termodinâmicos revelou que as interacções hidrofóbicas são as principais forças de interacção entre os complexos de zinco e a BSA.

A actividade citotóxica *in vitro* dos ligandos e seus complexos foi avaliada em células de carcinoma da próstata (LNCaP FGC), leucemia aguda das células T (Jurkat E6-1), mieloma (MM.1S), e uma linha~~s~~ de células humanas não-cancerosas imortalizadas, HEK-293. Foram observadas elevadas ~~fortes~~ actividades citotóxicas de ambos os ligandos e complexos contra as

três linhas de células cancerígenas. Na linha celular não-cancerígena, os ligandos apresentaram valores de IC_{50} inferiores aos dos seus complexos homólogos. No entanto, os complexos metálicos têm problemas de solubilidade, o que dificultou a sua avaliação.
Em geral, o actual sistema de ligandos mostra um elevado potencial para o tratamento do cancro devido à elevada selectividade em relação às células cancerígenas estudadas.

***Palavras-chave**: bases de Schiff, 8-hidroxiquinolina, complexos de Zn(II), citotoxicidade, ligação à albumina.*

Table of Contents

Acknowledgements iii

Abstract v

Resumo vii

Index of Figures xi

Index of Tables xiii

Index of Schemes xiii

Symbols and Abbreviations xiv

1. Introduction 1

1.1 Cancer **1**

1.2 8-Hydroxyquinoline, a privileged drug precursor **1**

1.3 Anticancer metallodrugs based on endogenous metal ions **4**

1.4 Ligand design **6**

1.5 Binding to proteins **8**

1.6 Complex- BSA interaction **8**

2. Experimental 12

2.1 Materials and reagents **12**

2.2 Instrumentation **12**

2.3 Preparation of solutions for biological assays **12**

2.4 Synthesis of the ligands: 8-hydroxyquinoline hydrazones (H_2L^1 – H_2L^4) **13**

H_2L^1 13

H_2L^2 14

H_2L^3 14

H_2L^4 14

2.5 Synthesis of the zinc(II) complexes (ZnL^1 - ZnL^4) **15**

ZnL^1 15

ZnL^2 15

ZnL^3 16

ZnL^4 16

2.7 Stability studies in aqueous medium and in the presence of albumin (BSA) .. 17

2.8 Fluorescence spectroscopy studies 17

2.8.1 Fluorescence in DMSO and in aqueous medium 18

2.8.2 BSA binding studies (fluorescence quenching titration assays) 18

2.8.3 Temperature studies 18

2.9 Biological activity studies 19

2.9.1 Cytotoxic activity 19

2.9.2 Antimicrobial activity 20

3. Result and discussion..... 21

3.1. Synthesis of the compounds 21

3.2 Characterization of the Zn(II) complexes 21

3.3 Characterization by UV-Vis spectroscopy and stability studies 25

3.3.1 DMSO and aqueous medium..... 25

3.3.2 Stability in the presence of albumin 29

3.4 Fluorescence spectroscopy studies in DMSO and aqueous medium..... 30

3.4.1 BSA binding studies (fluorescence quenching titration assay)..... 31

3.5 Quality control (QC)..... 33

3.6 Thermodynamic studies for the zinc(II) complex-BSA interaction 34

3.7 Biological activity study..... 37

3.7.1 Cytotoxic activity 37

3.7.2 Antimicrobial activity 42

4. Conclusions..... 42

References..... 44

Annexes..... 53

Index of Figures

Figure 1: Molecular structure and atom numbering of 8-hydroxyquinoline 1

Figure 2: Overview of the broad-range pharmacological applications of 8HQ derivatives (adapted from Song et al [11]) 2

Figure 3: A few 8-hydroxyquinoline derivatives being explored for drug development 3

Figure 4: Three-dimensional structures of HSA and BSA with tryptophan residues in green (adapted from Belatik et al [51]) 9

Figure 5: FTIR spectra for ZnL^1 and H_2L^1 recorded as KBr pellets. 23

Figure 6: ^{1}H-NMR spectra taken in DMSO_d_6 at 50 ºC of ZnL^2. Arrows show group peaks24

Figure 7: (A) ^{1}H-NMR spectra of ZnL^3 in DMSO_d_6 at 50 ºC. (B and C) HSQC spectra of ZnL^3 in DMSO_d_6 at 50 ºC. 25

Figure 8: Molar absorption coefficient spectra of ZnL^2 and ZnL^3 in DMSO at *ca.* 20.1 – 76.0 µM and *ca.* 3.67-72.44 µM respectively. Measured at initial and final concentrations evidencing the isosbestic points. Arrows indicate changes of higher energy bands (<375 nm) with increasing concentration. 26

Figure 9: A and B shows UV-Vis absorption spectra for ZnL^2 and ZnL^3 respectively, in DMSO. C and D are the molar absorption coefficient spectra. Arrows indicate changes of higher energy bands (<375 nm) with increasing concentration. 27

Figure 10: Graph showing the ratio of absorbance values at λ_{max} (300, 320 and 425 nm) and different concentrations in DMSO for ZnL^1 (A) and ZnL^2 (B) respectively. 27

Figure 11: A) UV-Vis absorption spectra measured for ZnL^2 in HEPES buffer (4.2-38.7 µM); inner chart: time dependence at 38.7 µM. (B) UV-Vis absorption spectra measured for ZnL^3 in HEPES (2.4 - 44.8 µM); inner chart: time dependence at 44.8 µM. (C and D) Molar absorptivity spectra with increasing concentrations for ZnL^1 and ZnL^4 in HEPES aqueous buffer (10 mM, pH 7.4), respectively. 28

Figure 12: (A) UV-visible spectra for ZnL^4 in the presence of albumin (BSA), concentration ration is 1:1~ 2.90×10^{-5} M. (B) UV-visible spectra for ZnL^4 showing changes with time at 1.74×10^{-5} M in HEPES buffer (10 mM, pH=7.4). 30

Figure 13: (A) Fluorescence spectra (λ_{ex} = 350 nm) of the complexes in DMSO at the same concentration (~6.0×10^{-6} M). (B) Linearity of fluorescence intensity of the complexes at maximum wavelength (490 nm) as concentration increases. 31

Figure 14: Fluorescence emission spectra of the titration of BSA (1.5 µM) with ZnL^3 (A) Fluorescence emission spectra and the arrow showing increasing complex concentration from 0 to 2.1 µM. (B) Stern-Volmer plot at 340 nm. 32
Figure 15: (A) Stern-Volmer plots for ZnL^3 – BSA interaction at the minimum and maximum temperatures..... 35
Figure 16: (A) Stern-Volmer constant of ZnL^3 at different temperatures. (B) Stern-Volmer plots of ZnL^3-BSA complex at different temperatures. (C) Fluorescence intensity of ZnL^3-BSA complex as temperature increases..... 37
Figure 17: Dose-response curves of (A and C) ligands (B and D) Zinc(II) complexes and $ZnCl_2$. LNCaP and HEK cells were exposed to different concentrations of each test compound for 48 hours. Cell viability was determined using the resazurin reduction assay. Results were normalized to vehicle control and are presented as the mean ± SD of two independent assays. 40

Index of Tables

Table 1: Assignment of ESI-MS ion peaks for Schiff base ligands and their corresponding zinc(II) complexes. 22

Table 2: Values of K_{sv}, K_q, the binding constant K_b and regression coefficients R^2, for the complexes. 33

Table 3: Quenching constants K_{sv} and regression coefficients R^2 for fresh and aged stock solutions of the zinc complexes. 34

Table 4: The binding constants; K_b and the thermodynamic parameters for the interaction between ZnL^3 and BSA at 298, 301, 305 and 310 K. 36

Table 5: Cell viability recorded at maximum tested concentrations (LNCaP = 25 µM, HEK, Jurkat and MM .1S = 50 µM). 38

Table 6: IC_{50} values of the ligands and corresponding zinc(II) complexes 39

Index of Schemes

Scheme 1: Synthesis of 8-hydroxyquinoline hydrazones. 13

Scheme 2: Synthesis of the zinc(II) complexes 15

Scheme 3: Synthesis of ZnL^3 16

Scheme 4: Synthesis of ZnL^4 16

Symbols and Abbreviations

8HQ	8-Hydroxyquinoline
DNA	Deoxyribonucleic Acid
^{1}H NMR	Proton Nuclear Magnetic Resonance
DMSO	Dimethyl sulfoxide
ESI-MS	Electrospray Ionization Mass Spectrometry
FTIR	Fourier Transform Infra-Red Spectroscopy
NMR	Nuclear Magnetic Resonance
UV-Vis	Ultra-violet-Visible
OD	Optical Density
MS	Mass Spectrometry
HSA	Human Serum Albumin
BSA	Bovine Serum Albumin
DMEM	Dulbecco′s Modified Eagle′s Medium
RPMI-1640	Roswell Park Memoria Institute 1640 medium
µM	Micromolar
I	Fluorescence emission intensity
IC_{50}	Half-inhibitory concentration
MIC	Minimal Inhibitory Concentration
m/z	mass/charge
LNCaP FGC	Prostate carcinoma cell line
Jurkat E6-1	T-cell leukaemia cell line
MM.1S	Myeloma cell line
HEK-293	Non-cancerous human embryonic kidney cell line
MeOH	Methanol
MTT	3-(4,5-Dimethylthiazol-2-yl)-2,5-diphenyltetrazolium bromide
HEPES	(4-(2-hydroxyethyl)-1-piperazineethanesulfonic acid)
FBS	Foetal Bovine Serum
PBS	Phosphate-Buffered Saline
Trp	Tryptophan residue
δ	Chemical shift
ε	Molar extinction coefficient
λ_{em}	Fluorescence emission wavelength

λ_{ex}	Fluorescence excitation wavelength
λ_{max}	Maximum wavelength
$\pi \rightarrow \pi^*$	Electronic transition from the π orbital to the π* orbital
$n \rightarrow \pi^*$	Electronic transition from the n orbital to the π* orbital
τ	Fluorescence lifetime

1. Introduction

1.1 Cancer

Cancer prevalence is rising in economically developing nations, where reportedly it is the second biggest cause of death and the first in developed nations.[1] Prostate cancer alone accounts for about 62 % of tumours worldwide, being the most prevalent form of cancer in males. Other gender unrelated cancers such as leukaemia and multiple myeloma follows with 9.1 % and 3.3 % respectively.[1,2]

According to Khalil *et al* all forms of cancers are mostly characterized by high levels of genetic instability, leading to continuous DNA damage and mutations. Accumulation of these mutations enables the cancer cells to adapt and resist interventions thereby becoming more aggressive.[3,4]

During the process of invasion, cancerous cells undergo several physiological processes and any failure to complete even a single step of the process would lead to the arrest of the entire process.[3] Therefore, designing drugs that can target specific sites of the cancer cells, stop the division and cause cancer cells' death without the adverse side effects associated with the traditional platinum anticancer drug cisplatin, is the preoccupation of medicinal scientists and chemists. [3,4].

1.2 8-Hydroxyquinoline, a privileged drug precursor

8-Hydroxyquinolines (8HQs) are metal ion chelators that have been used in a range of analytical and pharmaceutical applications over the last 100 years, attracting considerable interest regarding other therapeutic applications.[5–7] Their mode of bioactivity is related to the chelating capacity of the nitrogen of the quinoline ring and the 8-hydroxyl, which bind to divalent ions [8,9] (**Fig. 1**).

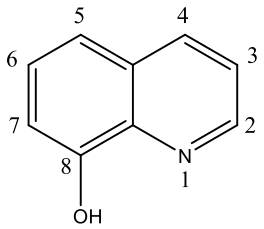

Figure 1: Molecular structure and atom numbering of 8-hydroxyquinoline

Among the quinoline core compounds, 8HQ is the most frequently encountered in medicinal chemistry, making it an excellent scaffold exploited for a wide spectrum of pharmacological applications such as iron-chelators for neuroprotection, anticancer agents, chelators of metalloproteins, anti-HIV agents,[10] antifungal agents, antileishmanial agents, antischistosomal agents, Mycobacterium tuberculosis inhibitors, botulinum neurotoxin inhibitors etc[11] (**Fig. 2**).

Figure 2: Overview of the broad-range pharmacological applications of 8HQ derivatives (adapted from Song *et al* [11])

A number of 8HQ derivatives, notably clioquinol (5-chloro-7-iodo-8-hydroxyquinoline) and 5-((4-(prop2-ynyl)piperazin-1-yl)methyl)quinolin-8-ol (HLA-20) (**Fig. 3**) utilized in the clinic, have been shown to exert strong anti-neurodegenerative and anticancer activity. [11–14] In addition, clioquinol has been reported to act as antifungal and antimicrobial agent by destroying the fungal/protozoa cell wall and altering the metal homeostasis.[7] 5-Nitro-8-hydroxyquinoline, or nitroxoline (NX), was also reported to be active against Gram-positive and Gram-negative bacteria and has therefore been used in the therapy of urinary infections. It is also being studied for its anti-HIV, and *Mycobacterium tuberculosis* inhibition properties and has been found that

it can be used as antimicrobial adjuvant to revert microbial resistance.[8,15,16] Moreover, 8HQ has also been reported as a diabetogenic agent owing to its ability to destroy β-cells.[17] Acting as Zn ionophore, 8HQ carries Zn into cells in the form of lipophilic, uncharged complexes and releases Zn inside the cells to promote Zn-dependent phosphorylation, thereby leading to oxidative damage and apoptosis of β-cells. In addition, proton released from the –OH group of 8HQ causes damage to β-cells.[9,17]

Derivatives of 8-hydroxyquinoline are known to form stable complexes with various metal ions that also have interesting pharmacological characteristics.[5] Recent studies have reported 8HQ metal complexes as potent antioxidants, enhancing superoxide dismutase (SOD) activity. Among these, 5-iodouracil-Mn-8HQ complex was shown to exert the highest activity, with an IC_{50} *ca.* three fold lower than that of the free ligand 8HQ.[9,18] The therapeutic importance of 8HQ coordinated with metals in the treatment and management of neurodegenerative diseases and cancers cannot be overemphasized. However, most of these metal complexes have several limitations and may impose severe side effects.

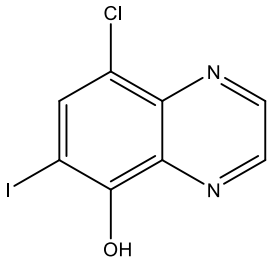

(A) Clioquinol

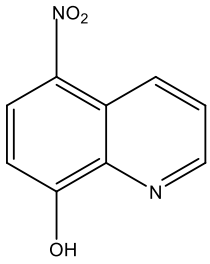

(B) Nitroxoline

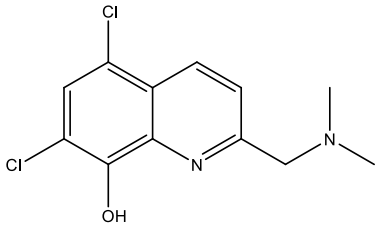

(C) PBT2

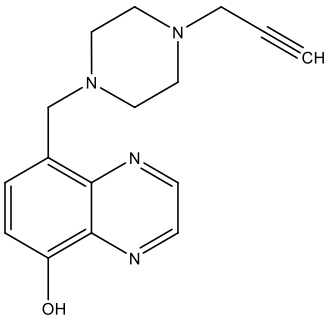

(D) HLA-20

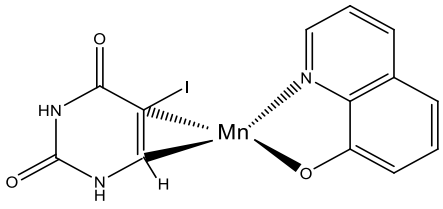

(E) 5-iodouracil-Mn-8HQ

Figure 3: A few 8-hydroxyquinoline derivatives being explored for drug development

At present, drugs used for Parkinsons' Disease (PD) therapy can only improve clinical symptoms (symptomatic) but cannot mitigate progression of the disease process underlying PD. The only therapeutically active drugs are cholinesterase inhibitors and glutamate antagonists, which have severe side effects in the long-term treatment. Therefore, other approaches are critically needed for these progressive neurodegenerative diseases. In order to overcome these disadvantages, and impose neurotoxic effect, the 8HQ scaffold is being studied by conjugation through a number of ways to neuropeptides.[19,20]

Clioquinol and nitroxoline for instance, have been associated with neurotoxic effects resulting in withdrawal from the market. Currently both compounds are under drug repurposing due to their wide therapeutic importance.[5,6]

A new class of therapeutic agents for the treatment of amyloidogenic diseases is the metal-protein attenuating compounds (MPACs). They prevent oligomerization, restore metal homeostasis, and reduce oxidative stress by competing with the aggregating protein for zinc and redox-active metal ions.[21] A second-generation 8-hydroxyquinoline derivative, 5,7-dichloro-2-[(dimethylamino) methyl]-8-hydroxyquinoline (PBT2), for instance was proposed to show greater blood-brain barrier (BBB) penetration than clioquinol.[22]

All the relevant biological properties reported for 8HQ derivatives, and its metal complexes highlight their importance in drug development for Medicinal Chemistry.

1.3 Anticancer metallodrugs based on endogenous metal ions

The dose-limiting side-effects often associated with the well-known platinum-based anticancer cisplatin, such as neuro-, hepato- and nephrotoxicity, including acquired or inherent resistance, has prompted organic and medicinal chemists to develop alternative strategies based on less toxic endogenous metals such as Cu and Zn, aimed at different targets. [23] The major trend recently is using metal ions as scaffolds rather than reactive centres and the departure from the cisplatin paradigm of activity towards a more targeted, cancer cell-specific approach. [23]
Less expensive transition metals including Co(II), Cu(II), Ni(II), V(IV/V), and Zn(II), are in frontline demonstrating superior pharmacological profiles, and are among rational therapeutic ways to generate novel metal-based biologically active molecules.[24]

To reduce the toxicity and to broaden the spectrum of activity, many research groups have focused their attention on endogenous metals, particularly copper and zinc, to develop metal based anticancer agents[25,26] mainly because both these metals are bio-essential elements and their complexes are capable of binding to DNA and proteins.[27] Copper and vanadium complexes, for example, showed a significantly higher activity against cisplatin resistant human ovarian adenocarcinoma and a much lower resistant factor than cisplatin (0.52 *vs.* 3.36).[28]

Metal complexes of 8HQ-hydrazone derivatives have proven to have various degrees of antiproliferative cytotoxicity against human cancer cell lines, and even *in vitro* anti-HIV activity. 3,4,5-Phenyl, methyl and fluoro substituted-8-HQs were cytotoxic against HeLa (cervix cancer cells), MCF-7 (breast cancer cells), A-549 (lung cancer cells) and MDA-MB-231 (triple negative breast cancer cells) with IC_{50} values ranging from 26.30 to 58.69 μM, with maximum selectivity of 2.4 over normal cells. [10] Copper(II) and zinc(II) Schiff base complexes were all found to have high antiproliferative cytotoxic activities against HeLa, A-549 and HCT-116 (human colon cancer) with promising IC_{50} values.[29,30]

Zn(II) possesses unique properties. In addition to generating nucleophiles and undergoing Lewis activation, it also controls apoptosis. Several biological processes, including DNA synthesis, gene expression, enzyme synthesis, and catalytic activities, are regulated by zinc. In addition, Zn(II) complexes demonstrate reduced *in vivo* cytotoxicity to normal cells, unique multi-modes of action, and cellular targets.[31]

When compared to Cu(II), fewer Zn(II) complexes have been studied for therapeutic applications. Nonetheless, the Zn complexes studied have demonstrated remarkable bioactivities.[32,33] Given that the coordination sphere can be altered *in vivo*, Zn(II) complexes may be unique as powerful anticancer treatments because of their structural stability.[31]

The promising results obtained with similar zinc complexes of 8HQ derivatives,[32,34,35] coupled with our group's recent success in developing new 8HQ hydrazone metallodrugs based on oxidovanadium(IV) that showed low IC_{50} values against both melanoma (A-375) and A-549 cell lines, prompted us to prepare new 8HQ Schiff base zinc complexes with potential biological activity.[5]

1.4 Ligand design

To optimize its biological properties and increase the stability and activity, the 8HQ scaffold can easily be functionalized or modified at various positions by the assembly with different bioactive organic moieties. The hydroxyl group of 8HQ is a strong activating ortho-/para-directing substituent, and therefore the 5- and 7-positions (**see Fig. 1**) can easily be functionalized by electrophilic aromatic substitutions (i.e. sulfonation, nitration, nitrosation).[36] Furthermore, poly-substitution can readily take place at the 2- or 4-positions.[37] Functionalization has improved selective permeability, increased toxicity, and increased lipophilicity of the 8HQ molecule, which have all been discovered to ease transport of the molecule to the cell membrane and absorption to the target location.[6,38–40] As stated earlier, to impose neurotoxic effect, the 8HQ scaffold has also been conjugated through a number of ways to neuropeptides.[19,20] This allows the mitigation of some of the main drawbacks of 8HQs as drugs, related to absorption, distribution, metabolism, excretion, and toxicity. For instance, clioquinol was associated with neurotoxic effects and was withdrawn from the market.[6]

The hydrazide-hydrazone derivatives (compounds with a -CO-NHN=CH- group) are a significant family of substances that have attracted growing interest for therapeutic development. They are Schiff bases with a broad range of bioactivity, such as antibacterial, antitubercular, antifungal, anticancer, and anti-inflammatory properties.[5,41] Moreover, in addition to their anticancer activities, hydrazine derivatives of quinolines are currently being explored for other anti-infective potentials. *e.g.* anti-HIV-1.[10]

Benzothiazole is another emerging privileged structure in anticancer research[34] and zinc benzothiazole Schiff bases are presenting very promising results,[31] exhibiting high therapeutic potential on colon cancer, the third in incidence and second in cancer-related mortality.[42]
In our research group a new Schiff base incorporating two bioactive moieties, 8-hydroxyquinoline and benzothiazole, and two Zn(II) complexes (M:L=1: and 1:2) were successfully developed and characterized. Both zinc complexes displayed promising IC_{50} values against human and murine colon cancer lines. The zinc benzothiazolyl-ligand acetate complex, [ZnL(AcO)] displayed a higher antiproliferative capacity than [ZnL_2] and was incorporated in long-blood-circulating and pH-sensitive liposomes.[34] The *in vivo* study demonstrated that the optimized [ZnL(AcO)] complex after liposomal incorporation

maintained its high antiproliferative properties while using 3-fold lower dosages relative to positive control to reduce tumour volume of murine colon cancer in mouse. [34]

Schiff bases are privileged ligand scaffolds exhibiting a wide range of applications in the field of medicinal inorganic chemistry.[41,43] They have been categorized as versatile ligand moieties due to their structural stability, synthetic flexibility, and excellent chelating ability with metal ions.[44] They are endowed with potential biological and pharmacological activities, such as antimicrobial activity, anti-oxidant, and anticancer.[45,46]

We recently reported a series of new benzohydrazones (Ln, n = 1-6) synthesized from 2-carbaldehyde-8-hydroxyquinoline and benzylhydrazides with various substituents in the para position. The synthesized Schiff base ligands were characterized and used in the synthesis of oxidovanadium(IV) complexes.[5] All complexes show antiproliferative activity when evaluated against malignant melanoma (A-375) and lung (A-549) cancer cells. Much lower, IC_{50} < 6.3 µM values were obtained on A-375 cells compared with cisplatin, with the Fluoro-substitute being the most active against both cell lines.[5]

The anti-neurodegenerative and anticancer effects of 8HQ derivatives are found to be related to their ability to behave as ionophores and to coordinate Cu(II) and Zn(II). As metal ionophore, the 8HQ moiety has low to moderate metal affinity allowing it to bind the metal ion in higher concentration areas and release them at lower concentrations areas. They are also easy to protonate because they have suitable acid dissociation constant values (pKa) inducing the release of the metal ions from the complex at the suitable site at lower pH.[9,47]

Continuing our recent pursuit for the design of smart metal−based drug entities, we have prepared a series of Zn(II) complexes with substituted benzohydrazide Schiff bases. Substituents of different nature, such as fluoro, hydroxyl, methyl along with unsubstituted one were used to study their effect on anticancer and antimicrobial activity.[5,34,35] These studies clearly demonstrate the interest and relevance of zinc complexes with 8HQ-derived ligands in the development of new anticancer drugs.

1.5 Binding to proteins

There is ample evidence in literature supporting serum proteins as drug transporters for anticancer agents.[48] Their ability to bind various substances in a reversible manner, is one of the most important characteristics.[49] One of the proteins that binds and transports endogenous and exogenous molecules, human serum albumin (HSA), is the most prevalent circulating protein in human blood plasma.[48] Once in the bloodstream, these endogenous and exogenous substances are transported and eliminated as a result of forming a complex with serum albumins. Additionally, members of this class of proteins help maintain blood pH and colloid blood osmotic pressure. The protein frequently improves the perceived solubility of hydrophobic medicines in plasma and impacts drug circulation, metabolism, and efficacy.[49] Consequently, many researchers have chosen to explore drug-protein interactions using HSA for effective and efficient anticancer agent development.

1.6 Complex- BSA interaction

Numerous mononuclear and polynuclear metals, Cu^{2+}, Ni^{2+}, Zn^{2+}, Co^{2+}, and Pt^{2+} complexes with aromatic ligands, with known pharmacologically active moieties, have been studied for their BSA interaction and binding properties.[49]

Majority of these metal complexes being synthesized are only soluble in organic solvents but not in water or aqueous medium. As such their concentrations in biological media are minute and therefore the required therapeutic amounts may not be present in the extracellular fluid as required. Moreover, if the complex is being transported by albumin to the target site, structural changes may occur leading to changes in the compound's activity, which could affect efficacy. It is therefore necessary to evaluate the structural stability of the complex *in vitro* using spectroscopic techniques to ascertain changes. This is done with the synthesized complex using conditions similar or close to the biological medium (HEPES buffers).

BSA, (**Fig. 4**) is not only similar in composition and structure (~ 76% sequence homology), but also comparable in physicochemical properties with HSA. It is also cheaper than HSA, hence mostly preferred by scientists for experimental studies and often used instead to study the binding interaction of serum albumin with drugs.[50] It shares structural similarities with HSA, and has been the most extensively researched of this category of proteins. It is a heart-shaped protein of 583 amino acid residues. Three homologous domains (I, II, and III) constitute

the BSA biomolecule, which is further subdivided into nine loops (L1–L9) by 17 disulphide bonds. The loops in each domain are composed of a triplet of large-small-large loops with each domain resulting into two subdomains (IA, IB, etc.). Unlike HSA, BSA has two tryptophan residues as fluorophores responsible for the majority of the intrinsic fluorescence of the protein.[51] In the first domain, Trp-134, found on the molecule's surface and in the second, Trp-212 located in the protein's hydrophobic binding pocket. Trp-134 is easily quenched by solvent molecules, while Trp-212 is the one responsible for the fluorescence quenching upon drug binding

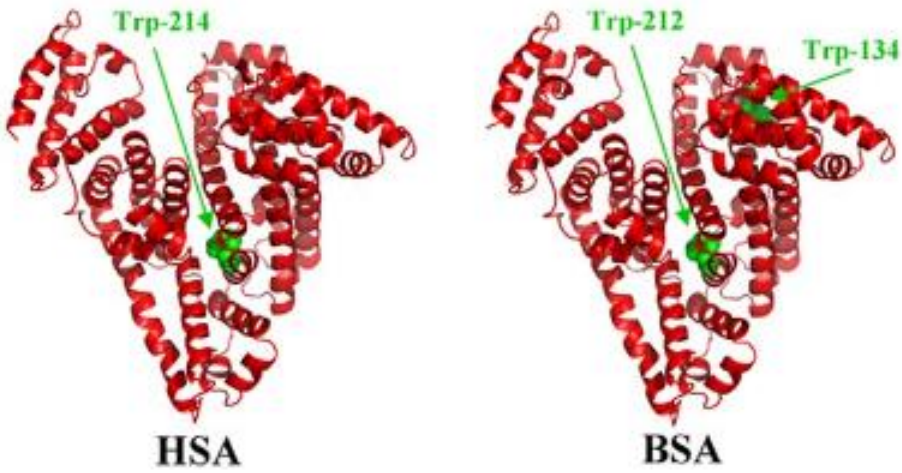

Figure 4: Three-dimensional structures of HSA and BSA with tryptophan residues in green (adapted from Belatik *et al* [51])

One effective technique considered useful for determining binding affinities is fluorescence quenching. It utilizes the intrinsic fluorescence of the protein whose emission can be quenched by a small molecule binding at or near the Trp residue which is highly susceptible to environmental changes. Fluorescence quenching can therefore be used to directly study the binding at the main binding site.[52]

Due to the presence of Trp-212, BSA exhibits a characteristic fluorescence emission band at about 340 nm after being excited at 295 nm. This fluorescence can be quenched upon binding of small molecules near the Trp residue.[52,53]

The quenching constant of the interaction can be determined using the Stern-Volmer equation (**Eq. 1**), used to analyze the quenching of fluorescence in order to assess the binding strength of the compound. The quenching rate constant value 2×10^{10} M^{-1} s^{-1} is typically used as a maximum limit for diffusion collision quenching of various quenchers.[53]

$$\frac{Io}{I} = 1+K_{sv}[Q] = 1+K_q\tau^0[Q] \qquad \textbf{(1)}$$

where I_0 and I are BSA fluorescence intensities in the absence and presence of a quencher, respectively. K_q, K_{sv}, τ^0 and [Q] are the quenching rate constant, the Stern-Volmer quenching constant, the average biomolecule lifetime in the absence of quencher and the quencher concentration, respectively.[54,55]

If this process involves the formation of a complex between BSA and the species being studied, static quenching will be observed, and the Scatchard equation (**Eq. 2**) can be used to determine the binding constant and the number of binding sites;[50]

$$\log\left(\frac{Io-I}{I}\right) = \log K_b + n \log [Q] \qquad \textbf{(2)}$$

where Io, I and [Q] have their meanings defined above, and K_b and n are the binding constant and the number of binding sites, respectively.[50] Thus, a plot of log [(Io-I)/I] versus log[Q] can be used to determine K_b from the intercept on y-axis and *n* from the slope.

As stated earlier, drug binding to serum albumin is often a reversible process, allowing the drug to be released and rebound with serum albumin at an equilibrium, dictated by their respective binding or dissociation constants. High binding constant values suggest a drug has a great affinity for serum albumin, and high dosages of the drug are typically needed to maintain the free fraction and achieve the therapeutic level for successful course of treatment. A low binding constant, on the other hand, results in weak binding to serum albumin. This means that most of the compound will be in its unbound state, where it can exert its activity, but it may well show low solubility and/or be removed. Therefore, it is critical to comprehend how a potential drug interacts with serum albumin and how well it binds to it in order to identify the pharmacokinetics and pharmacodynamics that have a big impact on a drug's effectiveness. [53]

Thermodynamic parameters can also be used to explain the types of forces that promote drug interactions with proteins, most notably hydrogen bonds, van der Waals forces, electrostatic forces, and hydrophobic interactions.[53] By studying the binding process at different temperatures and fitting the Van't Hoff equation (**Eq. 3**), the enthalpy (ΔH) and entropy (ΔS) of the BSA-complex interaction can be computed.[50]

$$\ln K_b = \frac{-\Delta H}{RT} + \frac{\Delta S}{R} \qquad \textbf{(3)}$$

where K_b is the binding constant at the corresponding temperature of T (in K) and R is the gas constant (8.314 J mol^{-1} K^{-1}).[56]

The Gibb's free energy (ΔG) can then be determined to evaluate the spontaneity of the interaction between the compounds and BSA.[50,53]

$$\Delta G = \Delta H - T\Delta S \qquad \textbf{(4)}$$

2. Experimental

2.1 Materials and reagents

4-Flourobenzoic hydrazide, 4-hydroxybenzoic hydrazide, 4-methoxybenzoic hydrazide, benzoic hydrazide and 8-hydroxy-2-quinoline carbaldehyde (all from Sigma) were used as received. The metal salt, zinc acetate-2-hydrate (Panreac) was used as supplied. Methanol (MeOH, Aldrich) and dimethyl sulfoxide (DMSO, Carlo Erba) were p.a. grade and used without further purification. Millipore® water used throughout all the experiments with biological macromolecules was double deionized. HEPES (4-(2-hydroxy ethyl)-1-piperazine ethane sulfonic acid) was purchased from Sigma-Aldrich as a salt readily soluble in water (deionized water) and the buffer was prepared with 0.01M and containing potassium chloride (KCl 0.10 M), pH 7.4 at 25º C. Fatty acid free Bovine Serum Albumin (BSA) was purchased from Sigma-Aldrich. All other materials not mentioned here were either p.a. or reagent grade.

2.2 Instrumentation

Elemental analysis for C, H and N were carried on a FISONS EA 1108 CHNS-O apparatus at *Laboratório de Análises of Instituto Superior Técnico*. A Bruker Avance II + 400 (UltraShieldTM Magnet) spectrometer operating at 400.13 MHz for proton and at 81 MHz for carbon was used to obtain the ^{1}H, ^{13}C and correlation NMR spectra. The chemical shifts are reported in ppm using tetramethylsilane as internal reference. The Infra-Red spectra were recorded on a JASCO FT/IR 4100 spectrophotometer as KBr pellets, while the UV-Visible absorption spectra were recorded on a Perkin Elmer Lambda 35 UV-Vis spectrophotometer with 10.0 mm cuvettes. A 500-MS Varian Ion Trap Mass Spectrometer was used to measure ESI-MS spectra of methanolic solutions of the compounds in both positive and negative ion modes. Fluorescence measurements were carried out on a SPEX® Fluorolog spectrofluorimeter (Horiba Jobin Yvon) in a FL3-11 configuration, equipped with a Xenon lamp and in a 10.0 × 10.0 mm quartz cuvette. The instrumental response was corrected by means of a correction function provided by the manufacturer. The experiments were all carried out at room temperature and are all steady-state measurements.

2.3 Preparation of solutions for biological assays

Fatty acid free BSA stock solutions were prepared and used within a week by dissolving the protein in HEPES buffer (10 mM, pH 7.4, KCl 0.10 M), swirled gently and kept at 4°C overnight for complete homogeneity. The BSA concentrations were spectrophotometrically

determined using the molar extinction coefficient, ε_{280} = 43890 M^{-1} cm^{-1} at 280 nm.[57,58] Initial concentrations of *ca.* 500 µM of the zinc complexes were prepared by dissolving ~1.0 mg in 5 mL of DMSO and used within the same day.

2.4 Synthesis of the ligands: 8-hydroxyquinoline hydrazones (H_2L^1 – H_2L^4)

H_2L^1 was synthesized by dissolving 8-hydroxy-2-quinolinecarbaldehyde (122 mg, 0.705 mmol) in *ca*. 10 mL of methanol and stirred with a few drops of glacial acetic acid. Solid benzoic hydrazide (123 mg, 0.90 mmol) was added and the mixture, left to reflux for 5 h with continuous stirring during which a light-yellow solid separated out. The mixture was allowed to cool to room temperature and then 10 min in the freezer for further precipitation. The final solid was collected by filtration, washed with ice-cold MeOH and dried under vacuum overnight. Yield: 148.8 mg, 72.6%. Elem. analysis for $C_{17}H_{13}N_3O_2 \cdot 0.1H_2O$ [found (calcd)]: C, 69.7% (70.09%); H, 4.5% (4.50%); N, 14.2% (14.42%). ESI-MS *m/z* (+): 292.2 (calcd for $[C_{17}H_{13}N_3O_2+H]^+$ 292.12). FTIR (KBr pellet, cm^{-1}): 3359, 3319, 3051, 1687 (carbonyl), 1678 (quinol. C=N), 1547 (imine), 1266 (δ, CO phenol). UV-Vis [DMSO, λ, nm (ε, $M^{-1}cm^{-1}$)]: 264 (2.09×10^4), 293 (shoulder, 4.86×10^4), 303 (5.10×10^4), 328 (3.10×10^4), 337 (2.90×10^4), 377 (shoulder, 5.30×10^3). ^{1}H NMR [300 MHz, DMSO_d_6, δ (ppm)]: 12.22 (1H, s, NH), 9.83 (1H, s, OH), 8.66 (1H, imine), 8.39 – 7.13 (10H, aromatic). ^{13}C NMR [75.4 MHz, DMSO_d_6, δ (ppm)]: 163.5 (carbonyl), 147.7 (imine), 152.9 – 111.9 (aromatic).

H_2L^2, H_2L^3 and H_2L^4 were all previously prepared, using the same procedure (see **Scheme 1**), by Nádia Ribeiro and only their characterization will be presented.

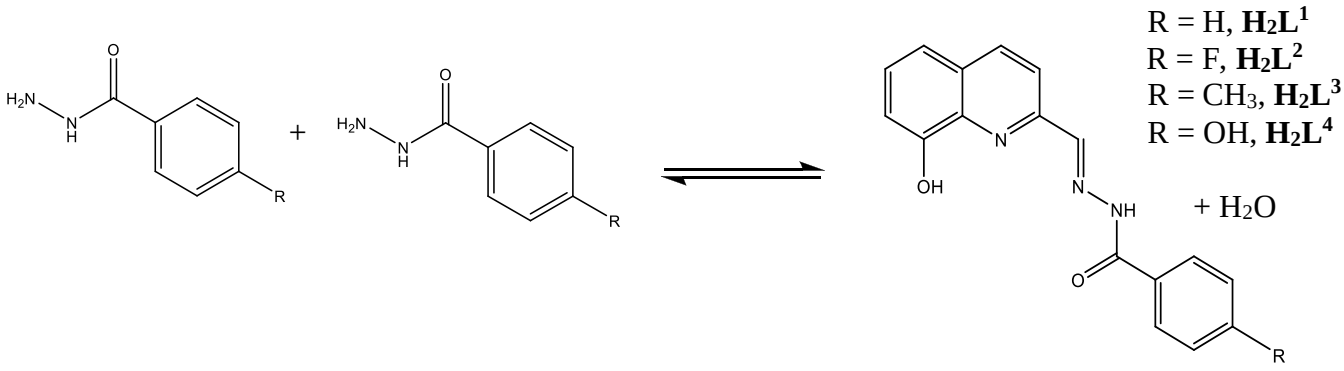

Scheme 1: Synthesis of 8-hydroxyquinoline hydrazones.

H_2L^2: Pale yellow solid. Yield: 87.0%. Elem. analysis for $C_{17}H_{12}FN_3O_2$ [found (calcd)]: C, 65.9% (66.02%); H, 3.8% (3.91%); N, 13.8% (13.59%). ESI-MS *m/z* (−) 308.3 (calcd for $[C_{17}H_{12}FN_3O_2-H]^-$ 308.28); (+) 310.2 (calcd for $[C_{17}H_{12}FN_3O_2+H]^+$ 310.30). FTIR (KBr pellet, cm^{-1}): 3401 (sharp, OH), 3212, 3041, 1653 (carbonyl), 1645 (quinol. C=N), 1559 (imine), 1506, 1465, 1286 (δ, CO phenol), 1234, 1154, 1099, 836, 762, 662 (aromatic F), 603. UV-Vis [DMSO, λ, nm (ε, $M^{-1}cm^{-1}$)]: 267 (1.50×10^4), 297 (3.70×10^4), 301 (3.80×10^4), 330 (2.20×10^4), 375 (4.00×10^3). ^{1}H NMR [300 MHz, DMSO_d_6, δ (ppm)]: 12.25 (1H, s, NH), 9.85 (1H, s, OH), 8.64 (1H, imine), 8.36 – 7.13 (9H, aromatic). ^{13}C NMR [75.4 MHz, DMSO_d_6, δ (ppm)]: 162.5 (carbonyl), 148.0 (imine), 153.5 – 112.2 (aromatic).

H_2L^3: Light yellow solid. Yield: 69.7%. Elem. analysis for $C_{18}H_{15}N_3O_2$ [found (calcd)]: C, 70.6% (70.81%); H, 4.8% (4.95%); N, 13.6% (13.76%). ESI-MS *m/z* (+): 306.1 (calcd for $[C_{18}H_{15}N_3O_2+H]^+$ 306.13). FTIR (KBr pellet, cm^{-1}): 3386, 3284, 3050 (aromatic CH), 2919 (aliphatic CH), 1668 (carbonyl), 1634 (quinol. C=N), 1553 (imine). UV-Vis [DMSO, λ, nm (ε, $M^{-1}cm^{-1}$)]: 260 (2.00×10^4), 300 (4.70×10^4), 310 (5.00×10^4), 350 (3.00×10^4), 375 (5.00×10^3). ^{1}H NMR [300 MHz, DMSO_d_6, δ (ppm)]: 12.17 (1H, s, NH), 9.85 (1H, s, OH), 8.65 (1H, imine), 8.34 – 7.14 (9H, aromatic), 2.40 (3H, CH_3). ^{13}C NMR [75.4 MHz, DMSO_d_6, δ (ppm)]: 163.1 (carbonyl), 147.6 (imine), 152.5 – 112.1 (aromatic), 20.9 (methyl).

H_2L^4: Light yellow solid. Yield: 75.4%. Elem. analysis for $C_{17}H_{13}N_3O_3$ [found (calcd)]: C, 66.0% (66.44%); H, 4.2% (4.26%); N, 13.5% (13.67%). ESI-MS *m/z* (−): 306.33 (calcd for $[C_{17}H_{13}N_3O_3-H]^-$ 306.29); (+) 308.08 (calcd for $[C_{17}H_{13}N_3O_3+H]^+$ 308.31). FTIR (KBr pellet, cm^{-1}): 3359, 3303, 3205, 1668 (carbonyl), 1657 (quinol. C=N), 1541 (imine), 1275-1224 (δ, CO phenol). UV-Vis [DMSO, λ, nm (ε, $M^{-1}cm^{-1}$)]: 263 (1.70×10^5), 296 (shoulder, 2.75×10^4), 306 (3.00×10^4), 340 (1.85×10^4), 364 (shoulder, 9.50×10^3). ^{1}H NMR [300 MHz, DMSO_d_6, δ (ppm)]: 15.67 (1H, s, NH), 10.85 (1H, s, OH, hydroxyquinoline), 10.26 (1H, s, OH, phenol), 7.83 (1H, imine), 8.54 – 6.96 (9H, aromatic). ^{13}C NMR [75.4 MHz, DMSO_d_6, δ (ppm)]: 164.0 (carbonyl), 137.2 (imine), 161.2 – 112.8 (aromatic).

2.5 Synthesis of the zinc(II) complexes (ZnL^1 - ZnL^4)

To an amount (0.5 mmol) of the ligand precursor, an equimolar amount of the zinc-metal salt, $Zn(CH_3COO)_2•2H_2O$, was added after dissolution in ca. 10 mL of MeOH. The mixture was left to reflux for 5 h with continuous stirring until a coloured solid separated out from the reaction mixture. The mixture was allowed to cool to room temperature and then subsequently 10 min in the freezer for further precipitation. The final solid was collected by filtration, washed with ice-cold MeOH and dried under vacuum overnight.

ZnL^1: Yellowish-red solid. Yield: 79.2 mg, 45.6%. Elemental analysis for $C_{17}H_{11}N_3O_2Zn•3.5\ H_2O$ [found (calcd)]: C, 48.9% (48.88%); H, 3.1%; (4.34%); N, 9.8% (10.06%). ESI-MS *m/z* (+): 386.1 (calcd for $[C_{17}H_{11}N_3O_2Zn+CH_3OH+H]^+$ 385.50). FTIR (KBr pellet, cm^{-1}): 3432 strong and broad (O-H), 1672 strong and sharp imine (C=N), 1538 strong and sharp imine (C=N). UV-Vis [DMSO, λ, nm (ε, $M^{-1}cm^{-1}$)]: 300 (2.79×10^4), 318 (2.55×10^4), 445 (3.08×10^3).

ZnL^2: Yellowish-red solid. Yield: 218.8 mg, 82.98%. Elemental analysis for $C_{17}H_{12}FN_3O_2Zn•0.75H_2O$ [found (calcd)]: C, 52,7% (52.87%); H, 3.0% (3.00%); N, 10.6% (10.88%). ESI-MS (DMSO), *m/z* (+) [Found (Calcd.)]: [372.2 (372.01 for for $[C_{17}H_{12}FN_3O_2Zn+H]^+$)] and [Found (Calcd.)]: 403.4 (404.04 for $[C_{17}H_{12}FN_3O_2Zn+CH_3OH+H]^+$). FTIR (KBr pellet, cm^{-1}): 3381 strong and broad (O-H), 1645, 1599 strong and sharp imine (C=N). UV-Vis [DMSO, λ, nm (ε, $M^{-1}cm^{-1}$)]: 300 (3.00×10^4), 302 (1.42×10^4), 320 (2.30×10^4), 440 (2.58×10^3).

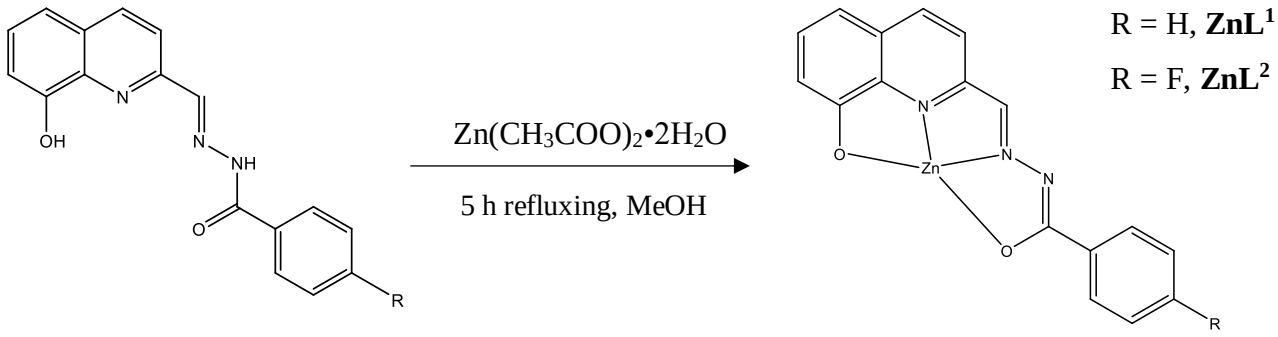

Scheme 2: Synthesis of the zinc(II) complexes

ZnL^3: Brick-red solid. Yield: 142.1 mg, 70.5%. Elemental analysis for $C_{20}H_{17}N_3O_4Zn•H_2O$ [found (calcd)]: C, 54.0% (53.77%); H, 4.0% (4.29%); N, 9.5% (9.41%). ESI-MS *m/z* (-) [Found (Calcd.)]: 458.1 (458.09 for $[C_{20}H_{17}N_3O_4Zn+CH_3OH-H]^-$) and *m/z* (+) [Found (Calcd.)]: 368.1 (369.05 for $[C_{20}H_{17}N_3O_4Zn-AcO]^+$). FTIR (KBr pellet, cm^{-1}): 3490 strong and broad (O-H), 3242 medium and broad amine (N-H), 1682 strong and sharp carboxyl (C=O), 1557 strong and sharp imine (C=N). UV-Vis [DMSO, λ, nm (ε, $M^{-1}cm^{-1}$)]: 303 ($3.36x\times10^4$), 320 ($3.20x10^4$), 420 (5.24×10^3).

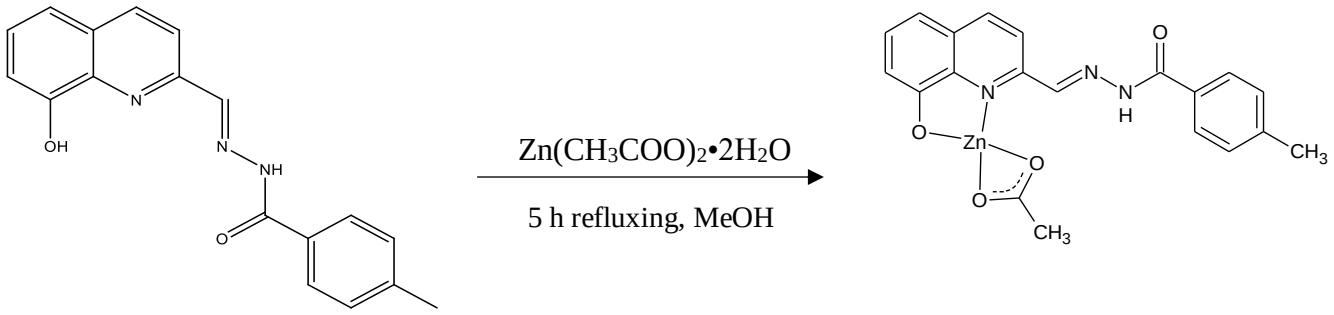

Scheme 3: Synthesis of ZnL^3

ZnL^4: Yellowish-red solid. Yield: 129.1 mg, 38.0 %. Elemental analysis for $C_{34}H_{24}N_6O_6Zn•2H_2O$ [found (calcd)]: C, 57.2% (57.19%); H, 3.3% (3.95%); N, 11.6% (11.77%). ESI-MS *m/z* (+) [Found (Calcd.)]: 676.9 (677.11 for $[C_{34}H_{24}N_6O_6Zn+H]^+$). FTIR (KBr pellet, cm^{-1}): 3403 weak and broad (O-H), 3208 strong and broad hydroxyl (O-H), 1663, 1604 strong and sharp carboxyl (C=O), 1552, 1509 strong and sharp imine (C=N). UV-Vis [DMSO, λ, nm (ε, $M^{-1}cm^{-1}$)]: 307 (6.08×10^4), 325 (5.47×10^4), 440 (6.90×10^3).

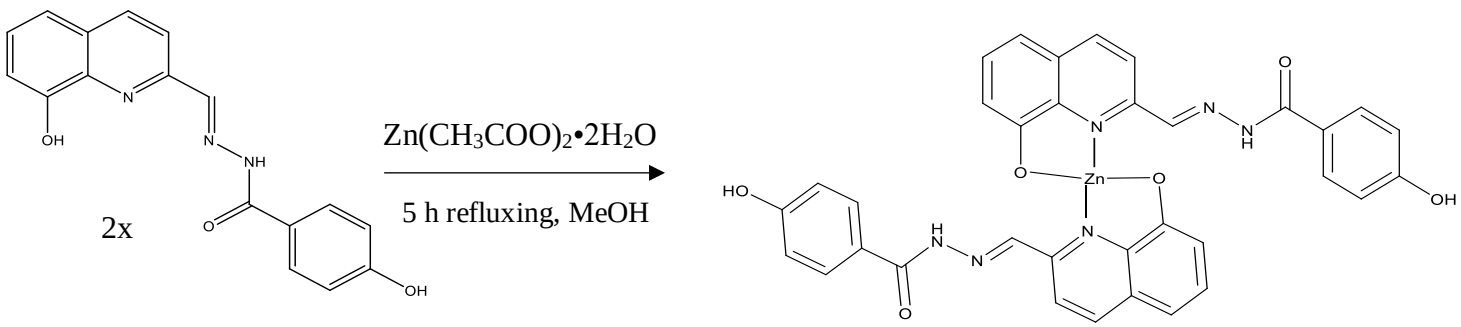

Scheme 4: Synthesis of ZnL^4

2.6 Solubility evaluation

Solubility tests were carried out for all complexes in toluene, acetonitrile, MeOH, $CHCl_3$, CH_2Cl_2 and DMSO. The complexes (~1.0 mg) were tentatively dissolved in 5.0 mL of each solvent. They were found fully soluble only in DMSO. The degree of solubility in DMSO was determined by dissolving the same amount in incremental volumes of 0.001 L of solvent. ZnL^1 and ZnL^4 have solubility of 200 mg/L, solubility of ZnL^2 is 250 mg/L while that of ZnL^3 is 1000 mg/L. The complexes were insoluble in aqueous medium.

2.7 Stability studies in aqueous medium and in the presence of albumin (BSA)

The stability of the Zn(II) complexes was evaluated using UV-Vis spectroscopy. Stock solutions of the complexes were prepared by dissolving approximately 1.0 mg in 5.0 mL DMSO and used immediately. Successive dilutions were prepared from the stock solutions of the complexes in 3000 μL HEPES buffer (10 mM, pH 7.4) using a 1.0 cm cuvette. UV-Vis spectra (260 – 700 nm) of each dilution were recorded until final concentrations (*ca*. 17.4 - 44.8 μM) were obtained. UV-Vis spectra were then recorded at these final concentrations at 60 min intervals for 5 consecutive hours and after 24 h for each complex.

The stability of the complexes in the presence of albumin was studied using solutions of BSA (*ca*. ~ 29 μM) and the complexes (stock solutions *ca*. 290 to 523 μM in DMSO) in HEPES buffer (10 mM, pH 7.4) containing a small amount of DMSO (< 5% v/v). Using a total volume of 3.0 mL in a 1.0 cm cuvette, UV-Vis spectra (260 – 700 nm) were recorded for final concentrations of 29 μM of the complexes for 5 consecutive hours and after 24 h.

2.8 Fluorescence spectroscopy studies

Fluorescence spectroscopy studies were done in DMSO, in aqueous medium (HEPES; 10 mM, pH 7.4) and also in the presence of albumin (quenching titration assay). Fluorescence emission spectra were recorded between 310 and 650 nm with excitation at λ_{ex} = 290 and 350 nm in DMSO and DMSO/HEPES aqueous medium. All spectra were recorded after gently shaking the cuvette containing a total volume of 3000 μL HEPES and BSA mixture about 5-6 times to equilibrate.

2.8.1 Fluorescence in DMSO and in aqueous medium

Stock solutions of the complexes (1.0 mg in 5 mL DMSO) were successively diluted with DMSO or HEPES (10 mM, pH 7.4) in a 1.0 cm cuvette to obtain final concentrations between *ca*. 15 and 50 μM. Fluorescence emission spectra (310-650 nm) were recorded for each successive dilution in DMSO and in the aqueous medium (HEPES; 10 mM, pH 7.4).

2.8.2 BSA binding studies (fluorescence quenching titration assays)

Fluorescence quenching spectroscopy studies were carried out in buffered medium in the presence of *ca*. 1.5 μM BSA (in HEPES; 10 mM, pH 7.4). The fluorescence emission spectra were recorded between 310 and 650 nm with λ_{ex} = 295 nm. This excitation wavelength was selected because proteins have absorption maxima near 280 nm due to the presence of phenylalanine, tyrosine and tryptophan residues. At 295 nm the absorption is due primarily to tryptophan. [59]

The complexes were successively added to a 1.0 × 1.0 cm cuvette containing HEPES buffer and *ca.* 1.5 μM BSA to obtain final complex concentrations of 0 to ~2.0 μM. Fluorescence emission spectra were then recorded after each addition under the same conditions (room temperature).

Fluorescence spectra were also recorded for blank assays for solutions containing the same concentrations of the complexes in HEPES without BSA. UV-Vis spectra were measured for each solution to determine correction factors for the inner filter effect.[54]

The effect of "shell life" in the binding of the zinc(II) complexes to BSA was determined with aged stock samples prepared and stored over a period of two months. Fluorescence quenching titrations were performed using these aged stock solutions under the same conditions as fresh samples prepared and used on the same day.

2.8.3 Temperature studies

The temperature effect on the binding of the complexes to albumin was studied using ZnL^3 as model complex at four different temperatures (25, 28, 32, and 37 ± 1 ºC) in the presence of *ca.* 1.5 μM BSA (in HEPES; 10 mM, pH 7.4). The fluorescence emission spectra of the final mixtures were recorded between 310 and 650 nm with λ_{ex} = 295 nm.

The stock solution of BSA was diluted to *ca.* 1.5 µM final concentration in a 3000 µL HEPES buffer contained in 10.0 x 10.0 mm quartz cuvette. The complex was thereafter successively added to make a final complex concentration between *ca.* 0 and ~2.0 µM and after allowing the mixture to equilibrate to the desired temperature for some few minutes, the fluorescence emission spectrum was recorded for each addition under all the four temperature conditions.

2.9 Biological activity studies

This procedure was performed by Dr. Pedro Pinheiro at Instituto Superior Técnico, Universidade de Lisboa, as described below.

2.9.1 Cytotoxic activity

The *in vitro* cytotoxicity of the zinc complexes and counterpart ligands was evaluated by employing MTT assay [60] on human cancer cell lines from prostate carcinoma (LNCaP FGC, ATCC CRL-1740), acute T-cell leukaemia (Jurkat E6-1, ATCC TIB-152) and multiple myeloma (MM.1S, ATCC CRL-2974), and on non-cancerous immortalized human embryonic kidney cell line HEK-293 (ATCC CRL-1573), using the resazurin reduction assay after a 48 h treatment. Stock solutions of each test compound were prepared in cell culture-grade DMSO (Panreac AppliChem) at a concentration of 5 mM.

Cells were seeded in appropriate culture medium (RPMI-1640 (Sigma-Aldrich) with 10% FBS (Gibco) for LNCap, Jurkat and MM.1S, and DMEM (Sigma-Aldrich) with 10% FBS for HEK-293 cells) in 96-well plates at a density of 50 000 cells/cm^2. After overnight incubation, the compound solutions were added to the final test concentrations and the plates were incubated at 37 ºC in a humidified atmosphere with a 5% CO_2 in air. After 48 h, 20 µL of a 0.15 mg/mL solution of resazurin (Stem Cell Technologies) in PBS were added to each well, and the plates incubated for further 3 hours before absorbance data recording.

Absorbance at 570 and 600 nm were recorded and used to determine cell viability according to **Equations 5** and **6**, respectively.[61]

$$Viability\ per\ well = (Abs_{570\ nm} . \varepsilon_{600\ nm}) - \ (Abs_{600\ nm} . \varepsilon_{570\ nm}) \quad \textbf{(5)}$$

$$\varepsilon_{600\ nm} = 117216\ M^{-1}cm^{-1}$$

$$\varepsilon_{570\ nm} = 80586\ M^{-1}cm^{-1}$$

$$\%Cell\ viability = \frac{Viability_{test\ well} - \overline{Viability_{control-}}}{\overline{Viability_{conrol+}} - \overline{Viability_{control-}}} \quad \textbf{(6)}$$

Negative control (Control -) cells were incubated in medium containing 10% DMSO, while positive controls (Control +) were carried out using culture medium containing 0.5% DMSO (vehicle). Data was processed using the GraphPad Prism 6 software. Results were normalized to the vehicle control and are presented as the mean ± SD of two independent assays.

2.9.2 Antimicrobial activity

Antimicrobial activity was evaluated using minimal inhibitory concentration (MIC) assays with *Escherichia coli* ((Migula) Castellani and Chalmers (ATCC 25922)).

Conical flasks (15 mL) were inoculated with 2 mL of a bacterial suspension at 0.04 OD (600 nm) in Mueller-Hinton culture medium (NZY Tech). To these, 2 mL of culture medium containing different concentrations of each test compound were added. Each condition was prepared in triplicate and the tubes were incubated at 37ºC for 24 h with continuous orbital shaking at 250 rpm. Solvent controls were prepared in the same way.

Following incubation, the OD (600 nm) value of each tube was recorded using a spectrophotometer (Spectrostar Nano, BMG Labtech). OD values for each condition were compared with vehicle controls (0.5% DMSO).

3. Result and discussion

3.1. Synthesis of the compounds

All new zinc complexes in this work were synthesized by reacting zinc(II) with the Schiff base ligand precursors, 8-hydroxyquinoline-2-hydrazones. The Schiff base ligands were synthesized in MeOH by condensation of 8-hydroxy-2-quinolinecarbaldehyde with benzoic hydrazides bearing different substituents. The mixtures were refluxed for 4-5 h with continuous stirring yielding the four ligand precursors; H_2L^1, H_2L^2, H_2L^3 and H_2L^4, bearing no substituent, 4-fluoro, 4-methyl and 4-hydroxy substituents, respectively.

The zinc(II) complexes were synthesized by reacting equimolar amounts of the ligand precursors with $Zn(CH_3COO)_2 \bullet 2H_2O$ in MeOH for 5 h at 50 ºC (see Scheme 2). Upon complexation, stable yellow-reddish zinc(II) complexes separated out from the reaction mixtures which were filtered out, washed and dried under vacuum overnight for further analysis. Percentage yields of the complexes were moderate to excellent, ranging from 38 to 83%, and the complexes' solubility was very poor in water but reasonable in DMSO.

3.2 Characterization of the Zn(II) complexes

Three different complex structures were observed from the complexation reactions despite all being carried out under the same conditions with a 1:1 molar ratio (L:M) of ligand precursor to $Zn(CH_3COO)_2.2H_2O$. The elemental analysis done on the complexes obtained indicated 1:1 ratios for ZnL^1, ZnL^2 and ZnL^3 with ZnL^4 having a 2:1 ratio. Amongst these, the structural features proposed for ZnL^1 and ZnL^2 are similar but different from ZnL^3 and ZnL^4. In the case of H_2L^1 and H_2L^2, the ligands are proposed to suffer enolization and double deprotonation, having a −2 charge necessary to balance the +2 charge of the zinc ion. ZnL^3 is proposed to have one acetate group and one ligand molecule complexing the zinc metal, while ZnL^4 is proposed to have two ligand molecules (see Schemes 2, 3 and 4). In ZnL^3 and ZnL^4 the ligand is proposed to be monodeprotonated. These claims were corroborated by the results obtained from the ESI-MS studies, shown in Table 1 and by the NMR and FTIR spectroscopic characterization. The use of the denominations ZnL^n for all Zn-complexes is just to simplify the text, despite them having different structures/stoichiometries.

Table 1: Assignment of ESI-MS ion peaks for Schiff base ligands and their corresponding zinc(II) complexes.

Compound	*m/z* (%)	
	Calculated	Found
$[H_2L^1 + H]^+$	292.12	292.2
$[H_2L^2 - H]^-$	308.28	308.3
$[H_2L^2 + H]^+$	310.30	310.2
$[H_2L^3 + H]^+$	306.13	306.1
$[H_2L^4 + H]^+$	308.31	308.1
$[ZnL^1 + CH_3OH+H]^+$	385.50	386.1
$[ZnL^2 +H]^+$	372.01	372.2
$[ZnL^2 + CH_3OH+H]^+$	404.04	403.4
$[ZnL^3 - AcO]^+$	369.05	368.1
$[ZnL^3 + CH_3OH-H]^-$	458.09	457.1
$[Zn(L^4)_2 + H]^+$	677.11	676.9

Figure 5 shows the FTIR spectra of H_2L^1 and ZnL^1 as example and Annex A2 contains the spectra for all other compounds. The FTIR spectra of the zinc(II) complexes shows peak changes when compared to that of the corresponding ligands, indicating complex formation. The deprotonation of the phenolic O-H on the ligand precursors, complexation with the zinc metal and the presence of lattice water molecules in the zinc(II) solid complex is evidenced by the disappearance of sharp, strong bands between 3201 and 3400 cm^{-1} on the spectra of the ligands and the appearance of a broad band between 3180 and 3484 cm^{-1} on that of the zinc complexes. The bands corresponding to the carbonyl (C=O) group in ZnL^3 and ZnL^4 are shifted from the ranges between 1644 and 1688 cm^{-1} to 1602 and 1688 cm^{-1}, upon complexation. The imine (C=N) group bands suffered a slight shift downfield from the ranges of 1605 and 1547 cm^{-1} to between 1599 and 1538 cm^{-1} respectively. Moreover, bands appearing in this region are seen for ZnL^1 and ZnL^2 corresponding to the second imine formed in the enolization process of the ligand precursors.

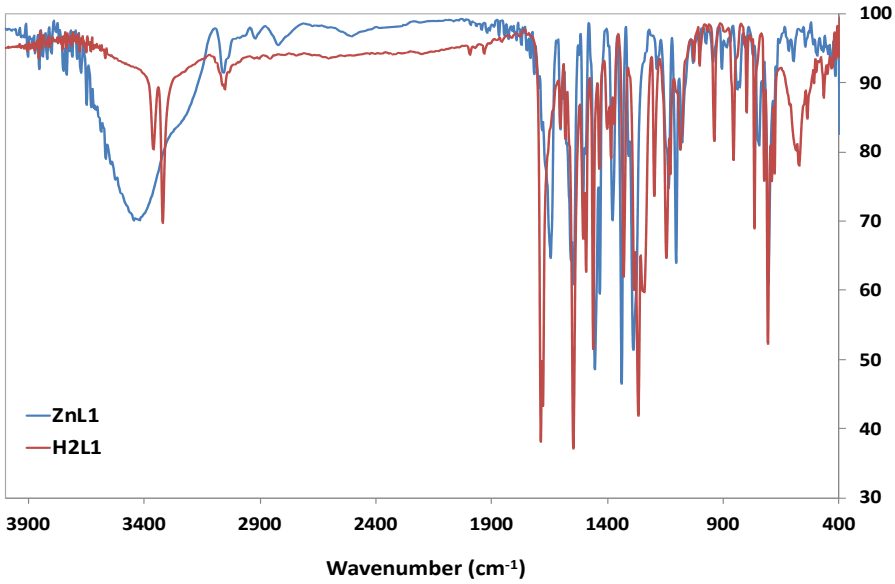

Figure 5: FTIR spectra for ZnL^1 and H_2L^1 recorded as KBr pellets.

Zinc(II) complexes are diamagnetic and therefore, to further confirm the proposed structures, proton (^1H), carbon (^{13}C) and Heteronuclear Single Quantum Coherence (HSQC) nuclear magnetic resonance (NMR) spectroscopies were carried out to characterize the compounds. The NMR measured at room temperature could not produce clear spectra (very weak peaks) and thus, the experiments were carried out overnight at 50 ºC. Under these conditions, the ^{13}C-NMR still did not show clear peaks, as such, only ^1H- NMR and HSQC spectra are presented (**Fig. 6, 7 and Annex A2)**. The ^1H-NMR spectra of ZnL^2 (**Fig. 6**) show amine (N-H) peaks around δH = 12.5 ppm, which is not expected for this complex and ZnL^1. However, it is possible that these complexes lack stability in solution and upon heating to 50 °C there is an un-coordination, maybe only partial, of the ligand and that is why the NH signal is appearing in the complexes' spectra.[62,63]

The uncertainty with the NMR spectroscopy could be attributed to the complexes' inability to completely solubilize in the deuterated solvents. Also, at high temperature conditions, there could be the dissociation of weak bonds causing the nitrogen on the ligands to be protonated, or different binding modes occurring at higher temperatures. [62,63] After complexation, the O-H peak of the 8-hydroxyquinoline moiety of the ligand around δH = 9.0 ppm disappears in the spectra of all Zn complexes. The imine proton (**H**C=N) peak appearing between δH = 8.5 - 9.0 ppm on the ligands' spectra also suffered a downfield shift to above δH = 9.0 ppm. Except for ZnL^1. This claim is corroborated by the HSQC spectra, except for ZnL^1, for which signal is not

observed and this assignment is based on the other complexes' spectra. Aromatic proton peaks of the ligand precursor have all shifted *i.e.* the peaks between δH = 7.0 - 7.5 ppm and those between δH = 8.0 - 8.5 ppm have all experienced some level of shift after complexation. The proposed structures for ZnL^3 and ZnL^4 indicates that while ZnL^3 has an amine proton, complex ZnL^4 has two hydroxyl substituents on the two bound ligands and these peaks are all observable in the NMR spectra.

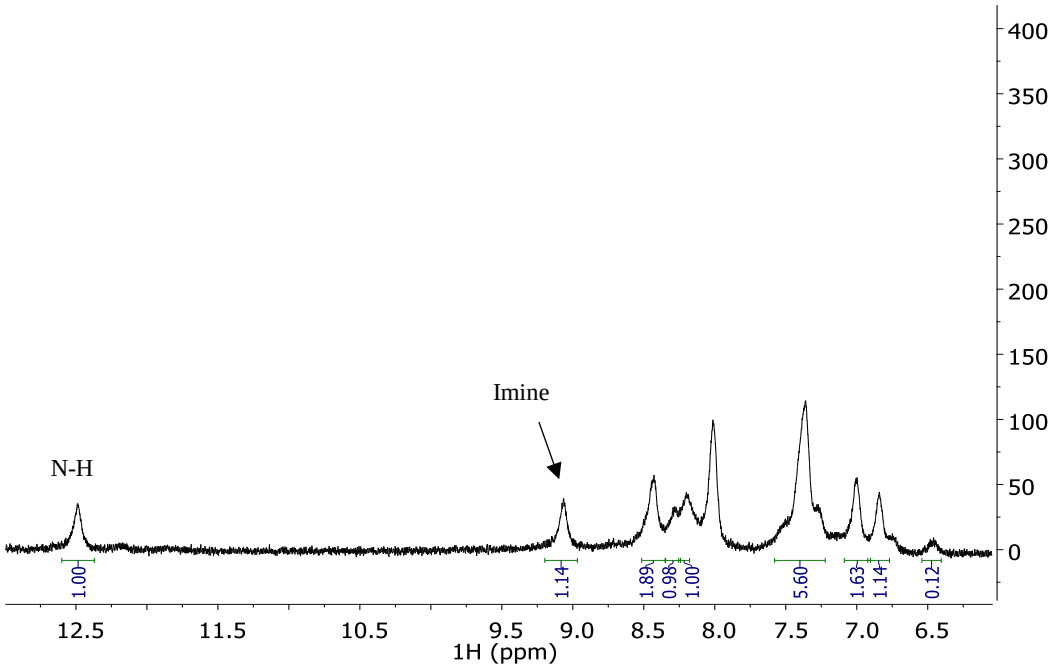

Figure 6: ^{1}H-NMR spectra taken in DMSO_d_6 at 50 ºC of ZnL^2. Arrows show group peaks

In the case of ZnL^3 (**Fig. 7**) there are two different peaks corresponding to two methyl groups in the complex. One is the substituent on the benzohydrazide moiety, appearing at δH = 2.38 ppm and δC = 20.81 ppm. The other corresponds to an acetate group from the original zinc salt that shows peaks at δH = 1.82 ppm and δC = 21.70 ppm, in good agreement with previous work.[34]

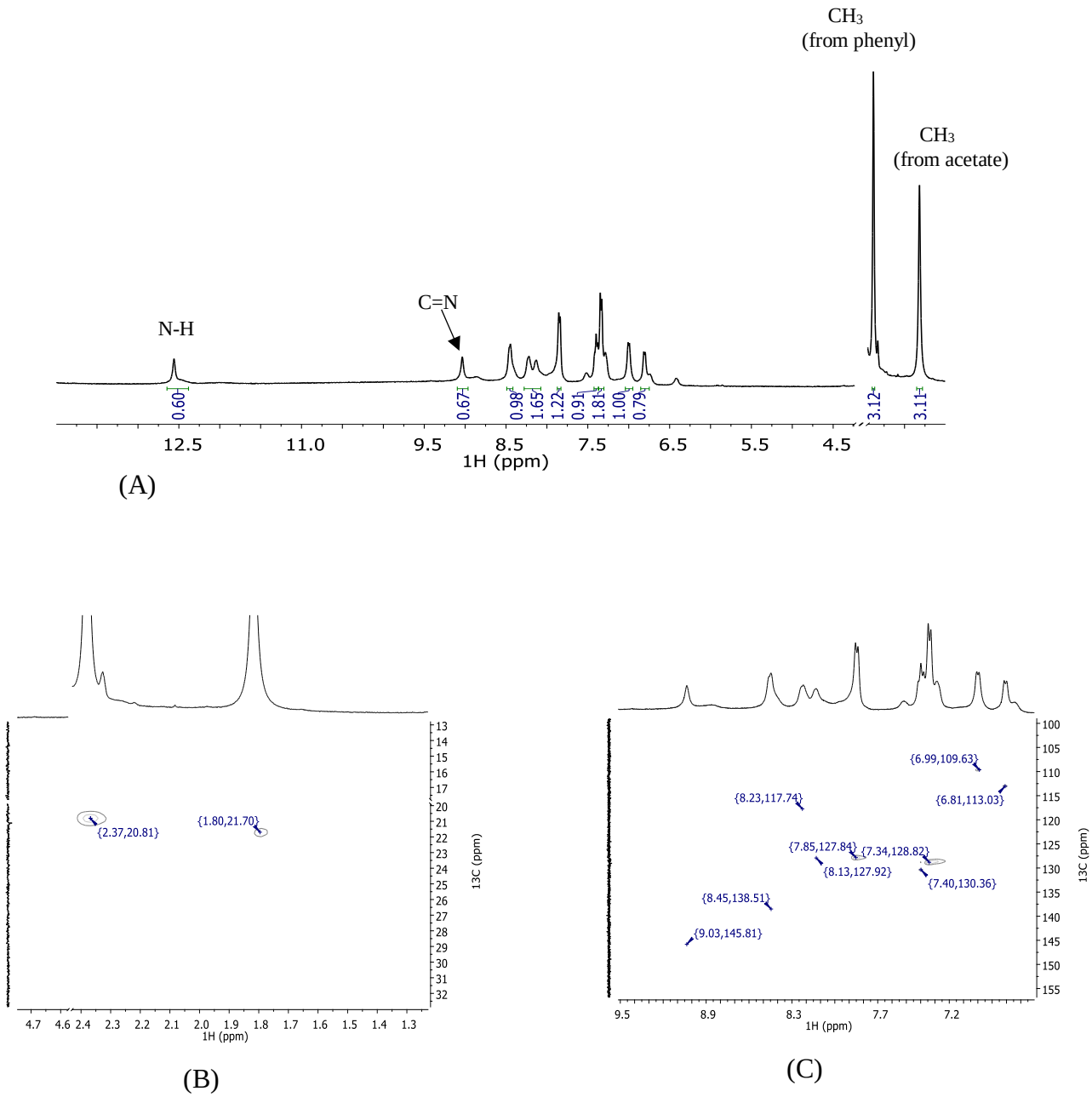

Figure 7: (A) ^{1}H-NMR spectra of ZnL^{3} in DMSO_d_6 at 50 ºC. (B and C) HSQC spectra of ZnL^{3} in DMSO_d_6 at 50 ºC.

3.3 Characterization by UV-Vis spectroscopy and stability studies

3.3.1 DMSO and aqueous medium

By employing UV-Vis spectroscopy the characterization and stability of the zinc(II) complexes was evaluated in both DMSO and in aqueous medium using HEPES buffer (10 mM, pH 7.4). In DMSO, as concentration is increased, it seems that the Beer-Lambert law is being obeyed

at individual wavelengths (300, 320 nm). However, the molar absorptivity spectra changes at λ_{max} with the observance of isosbestic points, **Fig. 8**. This is also clear in **Fig. 10**, where the ratio of the absorbance at two maximum wavelengths, such as A300/A320 is represented. In principle, the ratio should be constant, but in this case, it is not, giving clear indications that probably aggregation occurs as the concentration is increased.

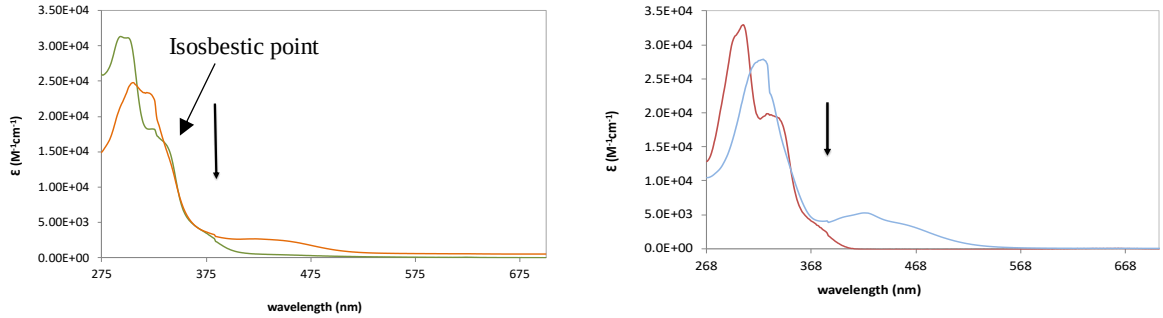

(A) ZnL^2 (B) ZnL^3

Figure 8: Molar absorption coefficient spectra of ZnL^2 and ZnL^3 in DMSO at *ca.* 20.1 – 76.0 µM and *ca.* 3.67-72.44 µM respectively. Measured at initial and final concentrations evidencing the isosbestic points. Arrows indicate changes of higher energy bands (<375 nm) with increasing concentration.

The UV–Vis absorption spectra of DMSO solutions of these compounds present intense bands, with ε values in the order of 10^4 M^{-1} cm^{-1} in the region 260–360 nm, characteristic for the π → π* and n→ π* transitions within the different moieties of the compound which are in good agreement with previously published structures. [5,12,64] At higher wavelengths (λ >400 nm), less intense bands developed coming from the charge transfer between the ligand and the Zn^{2+}. The molar absorption coefficient spectra show that even for the lowest concentrations the Beer-Lambert law isn't followed since the spectra in ε values are not constant (**Fig. 9**). The same is also easily seen in the graphs of ratio of absorbance values at λ_{max} for different concentrations that are not constant (**Fig. 10**). This suggests that the molecules suffer aggregation in solution, probably through π–π stacking of the aromatic rings.

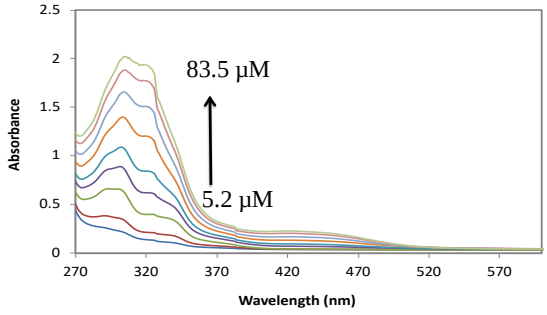

(A) ZnL^2

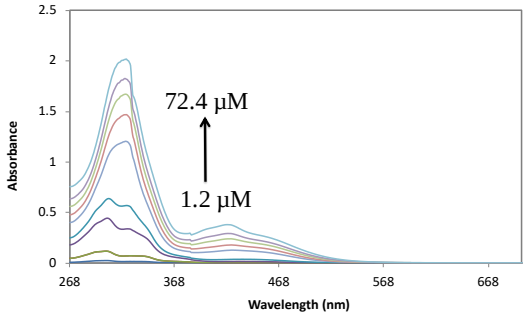

(B) ZnL^3

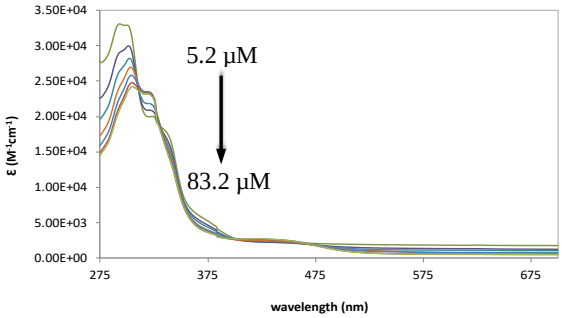

(C) ZnL^2

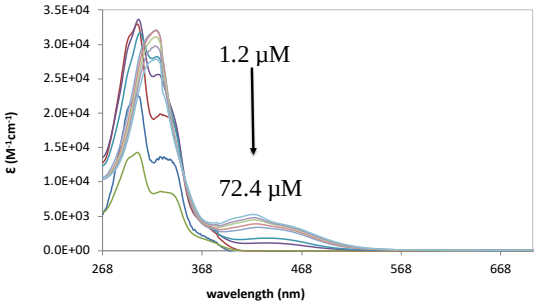

(D) ZnL^3

Figure 9: A and B shows UV-Vis absorption spectra for ZnL^2 and ZnL^3 respectively, in DMSO. C and D are the molar absorption coefficient spectra. Arrows indicate changes of higher energy bands (<375 nm) with increasing concentration.

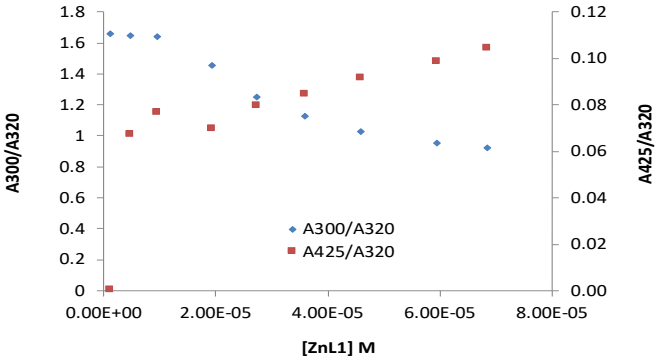

(A)

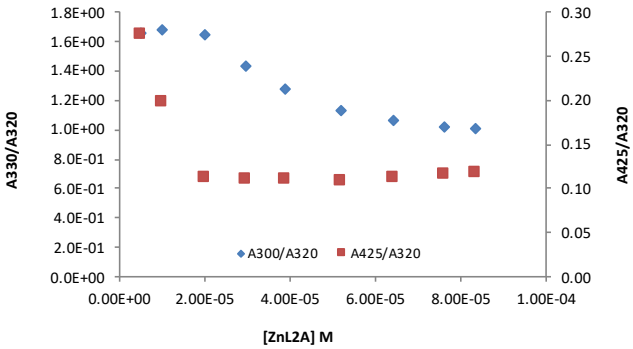

(B)

Figure 10: Graph showing the ratio of absorbance values at λ_{max} (300, 320 and 425 nm) and different concentrations in DMSO for ZnL^1 (A) and ZnL^2 (B) respectively.

The complexes' spectra in HEPES aqueous buffer show increase in absorption bands while concentration increases. This corresponds with observed precipitation until at a specific concentration where absorption bands begin to decrease. At this point, there were no further concentration increases and hourly spectra readings were recorded. As depicted in **Fig. 11** insets, all spectra recorded at 60 min intervals decreased over time. Moreover, **Fig. 10** again shows the molar absorptivity spectra follow the trend observed in DMSO, with decreases in absorbance as concentration increases. In aqueous buffer the behaviour suggests precipitation for ZnL^1-ZnL^3, even in the low µM range concentration, while for ZnL^4 the different behaviour suggests aggregation in solution. Failure to obey the linear dependence of absorbance on concentration, according to the Beer–Lambert Law, may be due to aggregate formation or the presence of other absorbing species.[54]

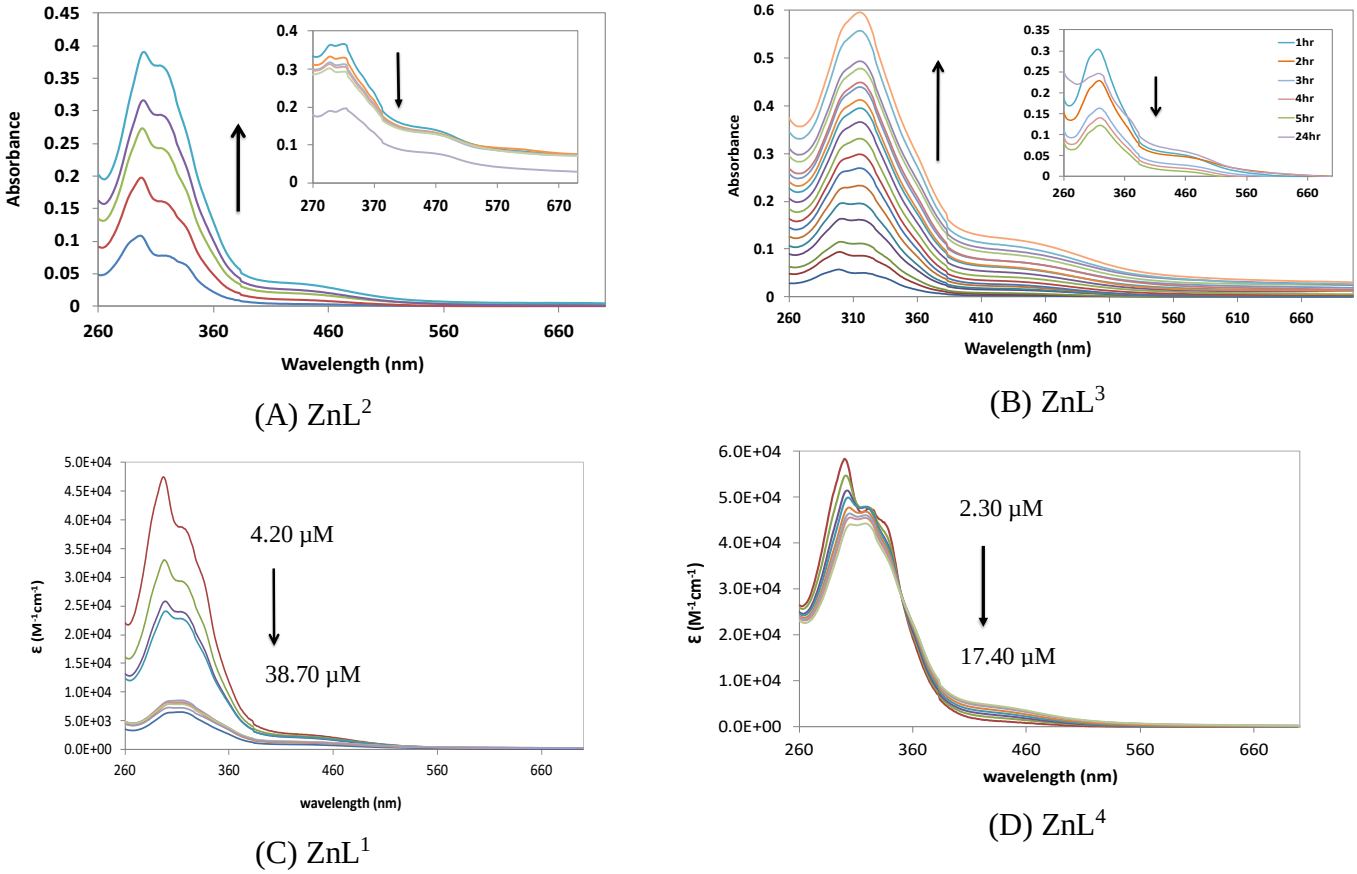

(A) ZnL^2

(B) ZnL^3

(C) ZnL^1

(D) ZnL^4

Figure 11: A) UV-Vis absorption spectra measured for ZnL^2 in HEPES buffer (4.2-38.7 µM); inner chart: time dependence at 38.7 µM. (B) UV-Vis absorption spectra measured for ZnL^3 in HEPES (2.4 - 44.8 µM); inner chart: time dependence at 44.8 µM. (C and D) Molar absorptivity spectra with increasing concentrations for ZnL^1 and ZnL^4 in HEPES aqueous buffer (10 mM, pH 7.4), respectively.

The formation of tiny particles even at lower complex concentrations during spectra recordings can be said to be an evidence of complex aggregation. As such, the zinc complexes ZnL^1-ZnL^3 can be considered insoluble and precipitate in aqueous media.

3.3.2 Stability in the presence of albumin

Knowledge of the extent of zinc(II) complexes binding to albumin is necessary, particularly if the synthesized complexes are to be applied as active antitumour agents. Binding to albumin may perhaps increase the complex solubility in aqueous media. It is also important that they remain effectively stable until released at the target site.[23] For this reason, the stability of the complexes was studied in the presence of BSA by UV-Visible spectroscopy. Eight spectral readings were recorded for each of the complex-BSA systems, *i.e.* time zero, 30 min, 1 to 5 consecutive hourly readings and 24 hours' reading, after addition of the complexes to the protein solution in buffered media (HEPES, 10 mM, pH=7.4) **(Fig. 12)**.

Analysis of the **Fig. 12,** exemplifies how the zinc complexes remained fairly stable with little or no variation in the spectra over time (see data for all complexes in **Annex A4**).

The coordination geometry and ligand donor atom type play key roles in determining the binding extent of the complexes to the protein.[4] The ligands developed in this work have different binding abilities and can easily change their binding mode, from tetra, to tri or bidentate to accommodate covalent binding of the metal ion to protein residues. Or strong hydrophobic interactions can simply be established between the aromatic groups of the ligands and amino acids in hydrophobic pockets. In aqueous medium and in the absence of albumin, the intensity of the spectra was reduced over time, indicating precipitation of the lipophilic complexes. In the presence of albumin however, no precipitation was observed, and the spectra hardly change. This is relevant because BSA is present in the growth media used in *in vitro* anticancer cytotoxicity studies.[65,66] This means that complex precipitation is avoided, and the complexes may be uptaken while bound to the protein by endocytosis and then be released due to the lower tumour intracellular pH.

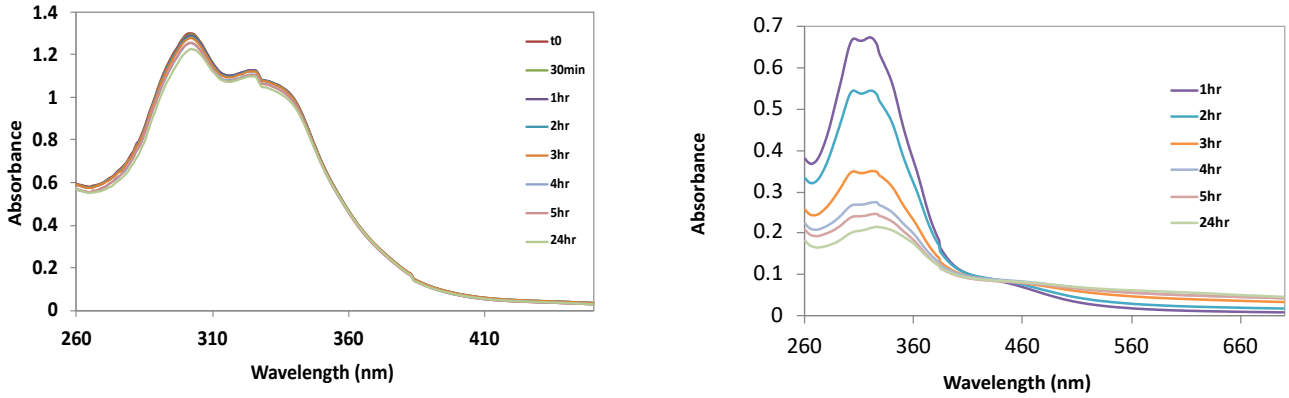

(A) (B)

Figure 12: (A) UV-visible spectra for ZnL^4 in the presence of albumin (BSA), concentration ration is 1:1~ 2.90×10^{-5} M. (B) UV-visible spectra for ZnL^4 showing changes with time at 1.74×10^{-5} M in HEPES buffer (10 mM, pH=7.4).

3.4 Fluorescence spectroscopy studies in DMSO and aqueous medium

All zinc complexes showed fluorescence emission in DMSO as concentrations increased from *ca.* 1.20 to 52.76 µM. However, in HEPES aqueous medium, there was no fluorescence emission in the same concentration range (see **Annex A5** for spectra). This is so because the presence of water quenches all fluorescence activity. The spectra were recorded between 360 and 700 nm with λ_{ex} at 350 nm because this is one of the absorption bands of the complexes. The emission maximum of tryptophan in water occurs near 350 nm and is highly dependent on polarity and/or local environment.[54]

Comparing the spectra of the Zn(II) complexes at approximately the same concentration (~ 6.0×10^{-6} M), the maximum fluorescence intensity is observed at 490 nm (**Fig. 13).** However, at this wavelength, ZnL^2 and ZnL^3 emit with much higher intensity than ZnL^4 followed by ZnL^1 while still showing linearity between the fluorescence intensity and the concentration.

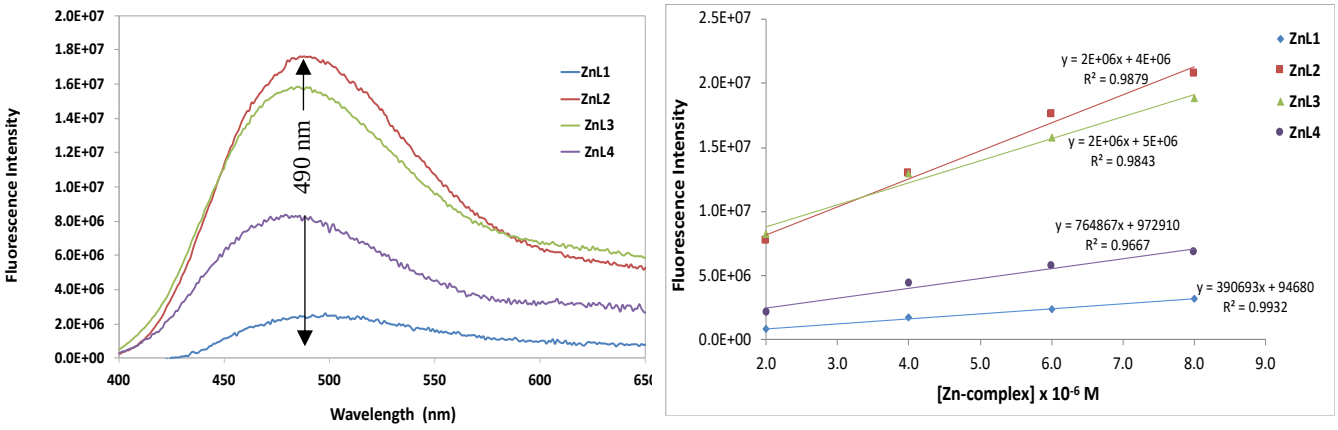

(A) (B)

Figure 13: (A) Fluorescence spectra (λ_{ex} = 350 nm) of the complexes in DMSO at the same concentration (~6.0×10^{-6} M). (B) Linearity of fluorescence intensity of the complexes at maximum wavelength (490 nm) as concentration increases.

3.4.1 BSA binding studies (fluorescence quenching titration assay)

The BSA fluorescence quenching titrations were carried out in buffered HEPES aqueous medium (10 mM, pH 7.4) and *ca*. 1.5 µM BSA. Concentrations of the complexes were increased from 0 to ~ 2.0 µM and the emission spectra were recorded between 310 and 650 nm with λ_{ex} = 295 nm under the same room temperature (25 ± 1 ºC) conditions.

Addition of the metal complexes to the solution of BSA resulted in the quenching of its fluorescence emission suggesting that the complex formed between the metal hydrazones and BSA is responsible for the quenching of BSA while the complex concentration increases [67] (**Fig. 14A**). The fluorescence quenching phenomenon can be analysed by the Stern-Volmer equation (**Eq. 1**) where the fluorescence intensity ratio is proportional to the concentration of the quencher [Q] which in this case is the zinc(II) complex. [55]

The ratio I_0/I is plotted against the quencher concentration (Stern–Volmer plot; (**Fig. 14B**). A linear Stern-Volmer plot is generally indicative of quenching by a single class of fluorophores.[59] The variation in this case was found to be linear for the Zn complexes, and the slopes therefore gave the Stern–Volmer constant, K_{sv} (**Table 2**).[54]

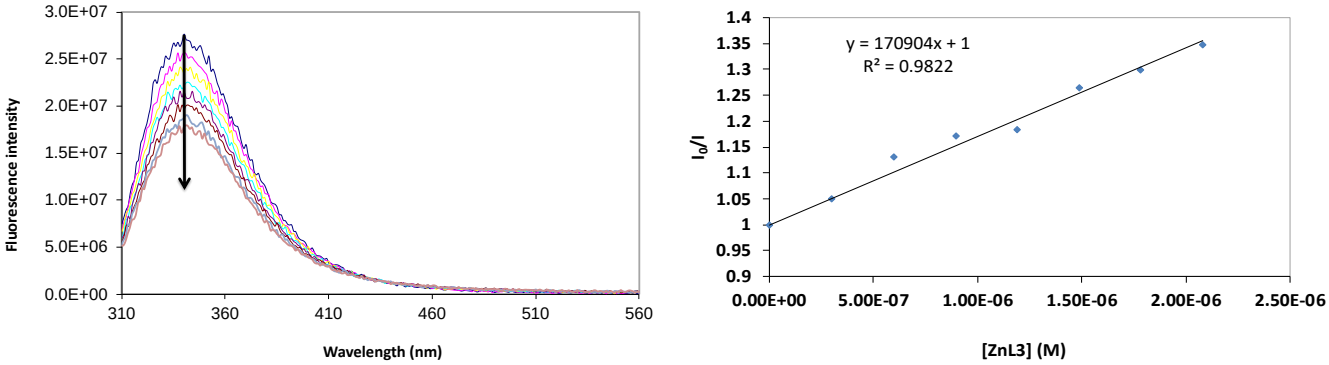

(A) (B)

Figure 14: Fluorescence emission spectra of the titration of BSA (1.5 µM) with ZnL^3 (A) Fluorescence emission spectra and the arrow showing increasing complex concentration from 0 to 2.1 µM. (B) Stern-Volmer plot at 340 nm.

Taking the excited-state lifetime of the protein as 10 ns,[68] the K_q, which reflects the efficiency of quenching was then calculated (**Table 2**). [54,59]

For static quenching a linear relationship from the Stern-Volmer plot should be observed in principle with no change in the excited-state lifetime and indeed it is (**Fig. 14B**). Moreover, since Trp emission in albumins has a lifetime (τ^0) in the nanoseconds range, this means that the calculated K_q values will be above the collisional limit, and therefore, the quenching process will have a static component from the formation of a complex between the Zn complexes and albumin.[34]

The obtained K_{sv} values were used to calculate the quenching rate constants K_q, which are 1000 times higher than the maximum scattering collision quenching rate constant (2.0×10^{10} $M^{-1}s^{-1}$), further stressing the point that the fluorescence quenching mechanism is static.[56,69]

Table 2: Values of K_{sv}, K_q, the binding constant K_b and regression coefficients R^2, for the complexes.

	ZnL^1	ZnL^2	ZnL^3	ZnL^4
K_{sv} ($\times 10^5$ M^{-1})	1.11 ± 0.05	1.20 ± 0.08	1.71 ± 0.08	0.77 ± 0.15
K_q ($\times 10^{13}$ $M^{-1}s^{-1}$)	1.11	1.20	1.71	0.77
K_b ($\times 10^4$ M^{-1})	0.63 ± 0.05	2.36 ± 0.05	7.81± 0.07	NA
R^2	0.968	0.968	0.982	0.818
$R^{2\,b}$	0.966	0.984	0.972	NA

R^2 and $R^{2\,b}$ are for K_{sv} and K_b values respectively.

The Scatchard equation (**Eq. 2**) for static quenching can be employed when the Zn complexes bind independently to a set of equivalent sites (n) on BSA.[69]

Analysis of the results reveal that the binding constant, K_b, increased from ZnL^1 to ZnL^3 following the K_{sv} trend. The increase in binding constants of the complexes can also be attributed to the coordination geometry and ligand donor atom type which play key roles in determining the binding extent of complexes to protein.[4]

The observed K_b values range between 6×10^3 to *ca.* 8×10^4 M^{-1} from ZnL^1 to ZnL^3 and are considered to represent moderate to strong binders, which indicates that the complexes can be transported in the serum by the protein and released at the target site.[34] A linear fit of the data yields n = 0.8, 0.9 and 0.9 for ZnL^1, ZnL^2 and ZnL^3 respectively, suggesting that the Zn complex binds to BSA at about 1:1 stoichiometry.

The K_b value for ZnL^4 is not reported because the calculations yielded a very high value that is not consistent with the rest of the data. Data linearization typically introduces errors. However, in terms of binding strength it is the complex that shows the lowest K_{SV} value, and thus, lower binding to BSA.

3.5 Quality control (QC)

Quality control measures were taken where appropriate. For spectrophotometric measurements such as NMR, because the magnitude of the energy changes involved in the NMR spectroscopy are very small, sensitivity can be a limitation when looking at very low (mM) concentrations. As such, overnight measurements were taken for quality control purposes in order to record many spectra and then add them together to increase sensitivity. As noise is random, it adds as

the square root of the number of spectra recorded. For example, if one hundred spectra of a compound were recorded and summed, then the noise would increase by a factor of ten, but the signal would increase in magnitude by a factor of one hundred – giving a large increase in sensitivity.[70] Moreover, the biological studies experiments were all based on replicates.

For purposes of determining if old stock solutions of the complexes have decomposed in a two months period, and if this has any influence on the binding and quenching (K_{sv}) properties of the complexes to BSA , fluorescence quenching titrations were performed as well on old stock solutions prepared over a period of two months. In general, the values in **Table 3** show that although there are some differences between the K_{sv} values of fresh and aged stock solutions, for ZnL_2, ZnL^3 and ZnL^4 the Stern-Volmer equation could still fit the data and yield K_{sv} values of the same magnitude. However, comparatively the errors associated with the use of aged stocks are much greater. Data obtained for ZnL^1 could not be fitted. Thus, we can conclude that the complex must be completely decomposed.

Table 3: Quenching constants K_{sv} and regression coefficients R^2 for fresh and aged stock solutions of the zinc complexes.

Fresh stock	ZnL^1	ZnL^2	ZnL^3	ZnL^4
K_{sv} ($\times 10^5$ M^{-1})	1.11 ± 0.05	1.20 ± 0.08	1.71 ± 0.08	0.77 ± 0.15
R^2	0.968	0.968	0.982	0.818
Aged stock				
K_{sv} ($\times 10^5$ M^{-1})	0.74 ± 0.34	2.15 ± 0.12	1.35 ± 0.14	1.14 ± 0.14
R^2	0.254	0.977	0.925	0.902

3.6 Thermodynamic studies for the zinc(II) complex-BSA interaction

The binding interaction between small drug molecules and biological macromolecules can be mainly driven by one or more of the four main types of intermolecular forces, namely: hydrogen bonding, hydrophobic interaction, van der Waal's forces and electrostatic interactions.[71] In order to further understand the binding interaction between the Zn(II) complexes and BSA, a temperature study was conducted at 298, 301, 305 and 310 K (± 1)

using ZnL^3. Fluorescence intensities decreased as complex concentration increased and linear Stern–Volmer plots were obtained at all temperatures (**Fig. 15**).

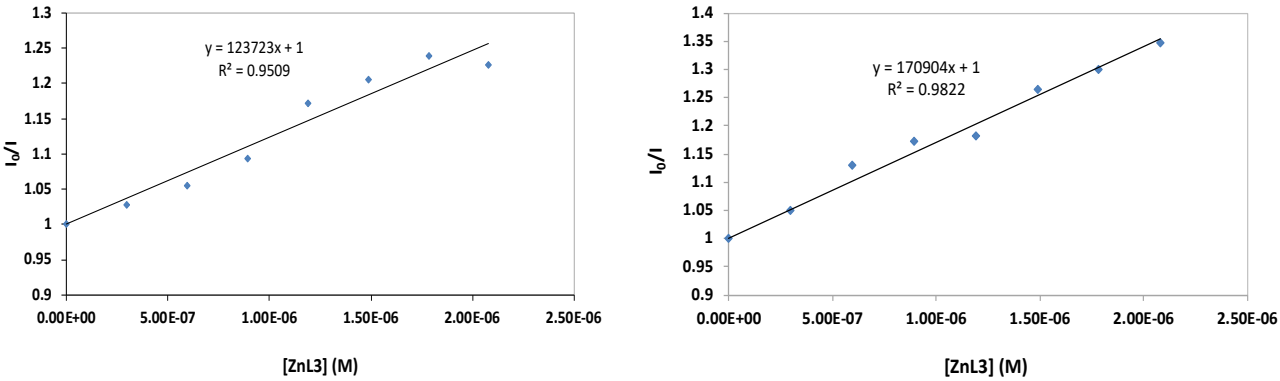

(A) 298K (B) 310K

Figure 15: (A) Stern-Volmer plots for ZnL^3 – BSA interaction at the minimum and maximum temperatures.

A thermodynamic analysis was performed to investigate the interaction using the van't Hoff equation. [56]

The entropy (ΔS) and enthalpy changes (ΔH) were calculated from a plot of R $\ln K_b$ against $\frac{1}{T}$ and then, using the figures, the Gibbs free energy (ΔG) can be calculated with **Eq. 4**.

ΔG determines the spontaneity of the interaction between the compounds and BSA.[56] Negative Gibbs energy changes mean that the reaction is spontaneous while a positive value refers to a non-spontaneous reaction.[69]

The values of ΔH and ΔS can then help to elucidate the major binding force of the protein-complex, which include hydrogen bonds and van der Waals forces ($\Delta H < 0$ and $\Delta S < 0$), electrostatic interactions ($\Delta H < 0$ and $\Delta S > 0$), and hydrophobic interactions ($\Delta H > 0$ and $\Delta S > 0$).[69,72] Herein, the thermodynamic parameters of BSA–Zn(II) complex interaction are included in **Table 4**. The ΔG values were negative at all four different temperatures, giving an indication that the Zn(II) complex spontaneously binds to BSA.

Additionally, hydrophobic forces were found to mainly drive the interaction between the zinc complex and BSA owing to the positive values of both ΔH and ΔS. The positive enthalpy change (ΔH) also indicates an endothermic process. [50,69,73]

To demonstrate the association by hydrophobic interactions in the Zn(II) complex-BSA binding process, when the temperature of the system's interaction is increasing, K_b values are expected to rise. This is because the temperature tends to enhance the strength of hydrophobic interactions in aqueous medium and then enlarge the association constant.[69,74] In this case, values for both K_{sv} and K_b follows the same trend by increasing, but the increases though were inconsistent. The narrow temperature ranges chosen for the study could be attributed to the observed inconsistencies in the increase of the K_b values. This shows no clear tendency regarding the behaviour of the complexes with increasing in temperature. Or it is another indication that several processes are taking place in solution at the same time, including precipitation.

Table 4: The binding constants; K_b and the thermodynamic parameters for the interaction between ZnL^3 and BSA at 298, 301, 305 and 310 K.

T (K)	K_{sv} (M^{-1})	K_b (M^{-1})	n	R^2	ΔG (KJ mol^{-1})	ΔH (KJ mol^{-1})	ΔS (J $mol^{-1}K^{-1}$)
298	$(1.2\pm0.1)\times10^5$	$(1.73\pm 0.09)\times10^6$	1.2	0.974	-35.7		
301	$(1.83\pm0.09)\times10^5$	$(8.17 \pm 0.09)\times10^5$	1.1	0.969	-38.2	216 ± 2	847± 2
305	$(1.5\pm0.1)\times10^5$	$(3.0 \pm 0.1)\times10^8$	1.6	0.969	- 41.6		
310	$(1.6\pm0.2)\times10^5$	$(1.3 \pm 0.2)\times10^7$	1.3	0.935	- 45.8		

R^2 is the correlation coefficient for K_b values.

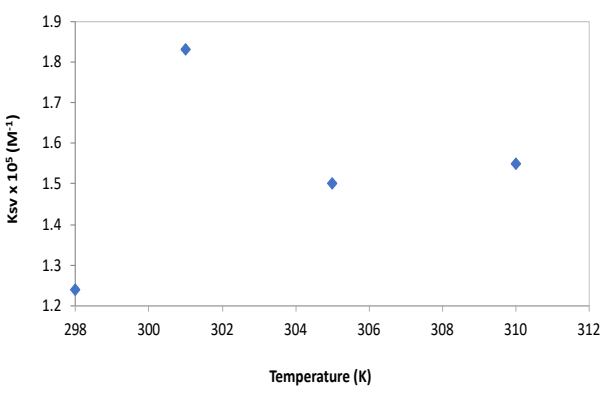

(A)

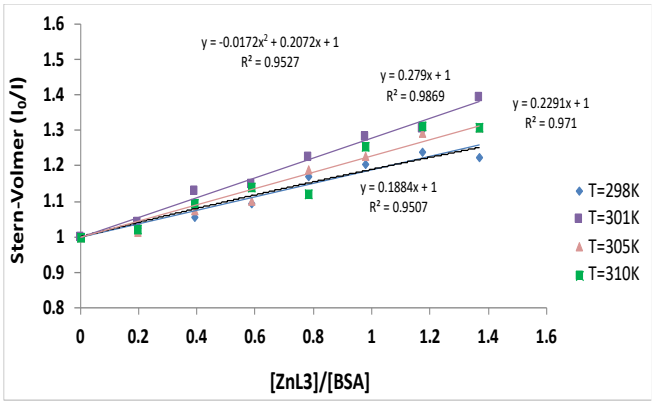

(B)

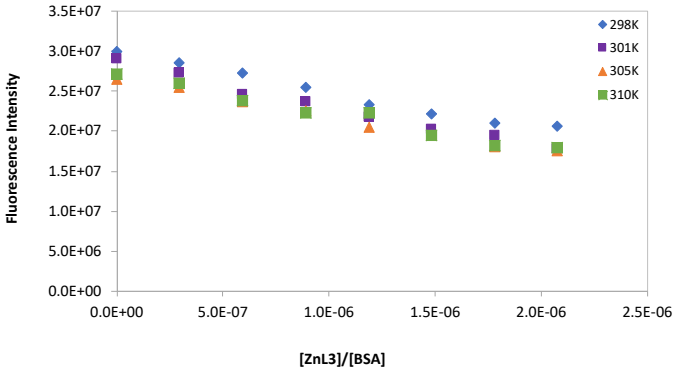

(C)

Figure 16: (A) Stern-Volmer constant of ZnL^3 at different temperatures. (B) Stern-Volmer plots of ZnL^3-BSA complex at different temperatures. (C) Fluorescence intensity of ZnL^3-BSA complex as temperature increases

3.7 Biological activity study

3.7.1 Cytotoxic activity

All cell lines (LNCaP FGC, Jurkat E6-1 and MM.1S) including the non-cancerous human cell line, HEK-293, were exposed for 48 h to concentrations of both ligands and zinc complexes ranging from 0.098 to 25 µM. Due to time constraints, no further concentrations were tested. Additionally, zinc chloride was tested in parallel to rule out effects of free Zn^{2+} ions in cell viability. Cell viability was determined using the resazurin reduction assay.

The ligands were readily soluble in DMSO and, when stock solutions of these compounds were further diluted in culture medium, no precipitates were formed. In the case of the zinc complexes, stock solutions in DMSO were difficult to prepare and dilutions in culture medium

presented some precipitates at higher concentrations. However, this was not observed for ZnL^4, which was easily dissolved in DMSO and did not form any precipitate when further diluted in culture media. Microscopic observation of the wells treated with ZnL^1, ZnL^2 and ZnL^3 showed the presence of deposited clumps of these compounds. Regarding the interference of the test compounds with the cell viability detection reagents, no interference was observed in terms of absorption maxima, media pH alterations or resazurin reduction potential. **Fig. 17** shows some assay data and **Table 5 and 6** cell viability data and IC_{50} values, respectively.

Table 5: Cell viability recorded at maximum tested concentrations (LNCaP = 25 µM, HEK, Jurkat and MM .1S = 50 µM).

LNCaP	**ZnL^1 *vs* HL^1**	**ZnL^2 *vs* HL^2**	**ZnL^3 vs HL^3**	**ZnL^4 vs HL^4**
Complex	91.6 %	64.6 %	7.14 %	11.2 %
Ligand	43.3 %	59.6 %	15.9 %	32.2 %
HEK-293				
Complex	94.4 %	97.6 %	97.6 %	52.1 %
Ligand	74.6 %	91.6 %	102.1 %	68.0 %
Jurkat				
Complex	73.6 %	20.4 %	26.1 %	61.6 %
Ligand	9.94 %	73.8 %	25.8 %	39.0 %
MM .1S				
Complex	11.2 %	43.2 %	67.5 %	48.6 %
Ligand	11.9 %	34.9 %	43.3 %	41.9 %

Table 6: IC_{50} values of the ligands and corresponding zinc(II) complexes

Ligands	**JURKAT**	**MM.1S**	**LNCaP**
	IC_{50} (µM)	IC_{50} (µM)	IC_{50} (µM)
H_2L^1	10 ± 1	7 ± 1	23 ± 1
H_2L^2	67 ± 1	18 ± 1	36 ± 1
H_2L^3	8 ± 1	30 ± 1	12 ± 1
H_2L^4	~ 11.78*	24 ± 1	16 ± 1
Complexes			
ZnL^1	~ 52.06*	~ 43.97*	–
ZnL^2	35 ± 1	18 ± 1	38 ± 1
ZnL^3	~ 11.74*	68 ± 1	12 ± 1
ZnL^4	24 ± 1	20 ± 1	8 ± 1

* SD reading failure, (-) New model required

The data presented demonstrate cytotoxic activities for both ligands and complexes. Cytotoxicity was stronger against cancer cells when compared with the non-cancer cell line HEK-293. The ligands on the other hand, showed higher cytotoxic activity with good IC_{50} values than their corresponding zinc complexes. The effect is predominantly observed in cancer cell lines, whereas in the non-cancer cell line the cytotoxicity of the ligands was not significant. This suggests that the ligands may be interfering with a pathway important in cancer cells, or with a protein that is overexpressed in cancer cells.[3] It is interesting to note that the ligands seem to have higher cytotoxic activities against blood cancer cell lines in suspension cultures (Jurkat E6-1 and MM.1S). The cytotoxic effect was not so strong in adherent cell lines being LNCaP and HEK-293 cells. This could be due to the fact that suspension cultures tend to be more sensitive than adherent cultures, or the fact that the compounds may be interfering with a pathway more relevant in blood cancers. However, these assertions are purely speculative as we only have cytotoxic results and more data will be needed to further support these claims.

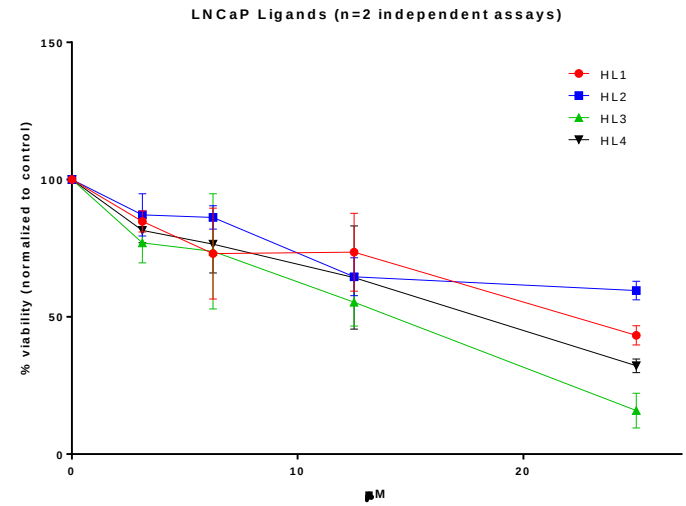

(A)

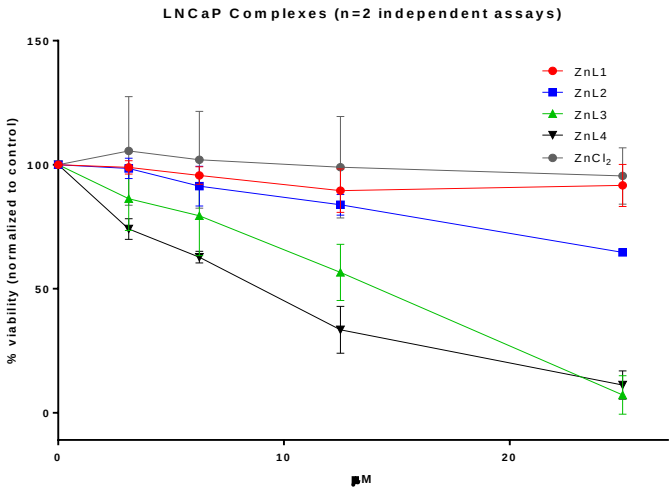

(B)

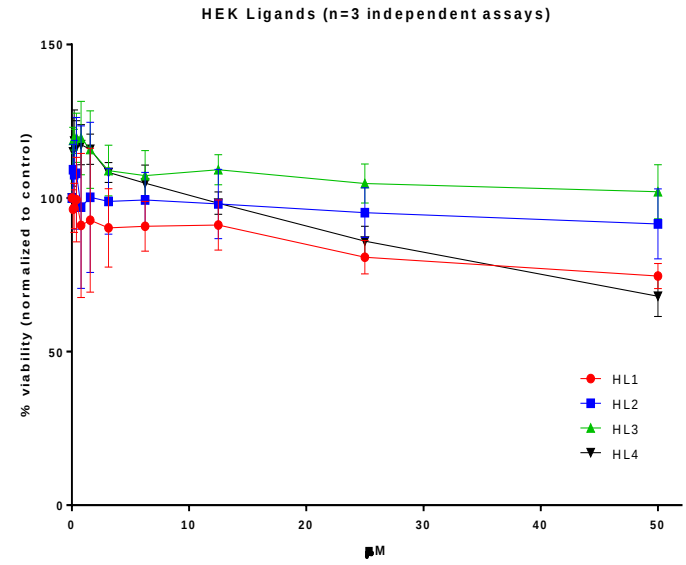

(C)

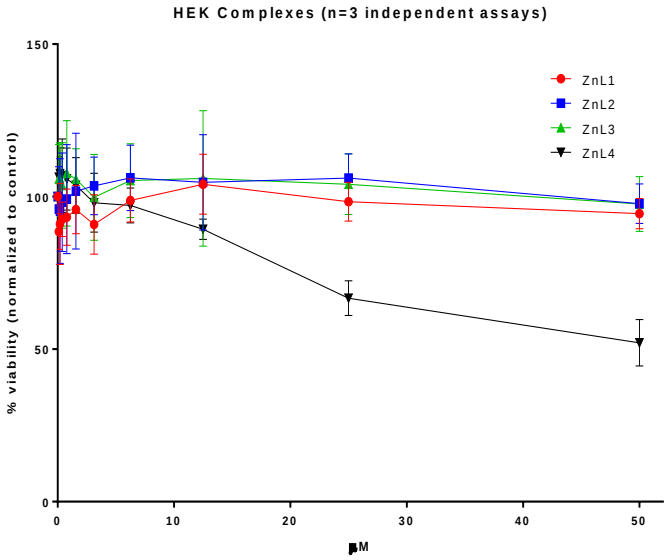

(D)

Figure 17: Dose-response curves of (A and C) ligands (B and D) Zinc(II) complexes and $ZnCl_2$. LNCaP and HEK cells were exposed to different concentrations of each test compound for 48 hours. Cell viability was determined using the resazurin reduction assay. Results were normalized to vehicle control and are presented as the mean ± SD of two independent assays.

The poor solubility of the Zn complexes seems to interfere with the cytotoxicity, such that it reduces the amount that remains in solution available for cell uptake. This assertion is made because, the ligands on their own are cytotoxic, but that effect is apparently lost or reduced when the ligands are complexed with the Zn^{2+}. This may be preventing the ligand from reaching its target or entering the cells. However, this does not mean that the complexes are not active. It just means that their physical properties may be masking their potential cytotoxic effects. It is therefore necessary for the introduction of hydrophilic substituents in order to improve aqueous solubility.[36]

Interestingly, the cell viability values observed for cells treated with the zinc complexes vary significantly between data sets obtained with the same cell line, which could probably be due to the poor solubility of the test compounds. This high variability is not observed with the counterpart ligands, which are readily soluble and remained solubilized during the treatment course.

IC_{50} values for LNCaP and HEK-293 could not be determined as no clear sigmoidal curve shape was observed with these cells. In the case of LNCaP cells, more date points are required, but due to the slow growth rate of these cells, more experiments could not be performed in time. Meanwhile, ZnL^4 is the most effective against LNCaP with an IC_{50} value of 7.6 µM attributed to its high solubility compared to the other complexes. In the case of HEK-293, no clear evidence of cytotoxicity could be identified, even at the highest concentration tested (50 µM), except with ZnL^4 *vs.* HL^4, which were able to reduce the viability of HEK-293 cells by ca. 50% at the highest concentration tested. As a result, it can be assumed that the tested compounds are non-toxic for HEK-293 cells.

Assays with Jurkat and MM.1S cell lines yielded interesting IC_{50} values, presented. Being the two most responsive cancer cell lines in this study, it would be interesting to further evaluate the cytotoxicity of the ligands in cultures of normal blood cells to probe the existence of specific anti-cancer activities.

The lower IC_{50} values observed for the ligands, instead of the complexes does not imply ruling out the complexes' cytotoxicity since some zinc complexes studied have been shown to improve permeability to cancer cells, reduced cell viability and demonstrate anti-tumour activity.[35,75,76] On the other hand, it can be proposed that the zinc complexes are serving as

vehicles for or transporters of the ligands and that the cytotoxic effect is actually from the ligands.[35] This could be supported by the cytotoxic effect and the IC_{50} observed with ZnL^4. All these hypotheses need to be further explored since the lower solubility of the complexes when compared with the ligands, would drastically reduce the amount of test compound in solution and available for cell internalization. One other aspect is the size of the complexes and their eventual net charge, which may hamper the crossing of the cell membrane.

3.7.2 Antimicrobial activity

All compounds were tested against Gram-positive and Gram-negative bacteria. However, there was no antimicrobial activity observed, with all assays reaching the same OD values as the 0.5% DMSO, at all concentration tested.

4. Conclusions

Four novel zinc(II) complexes were synthesized by reacting benzylhydrazone ligands with zinc acetate-2-hydrate. The ligands were synthesized by condensation reaction and characterized by various analytical techniques.

The synthesized complexes (ZnL^1-ZnL^4) had both 1:1 and 1:2 metal to ligand stoichiometries as proposed, demonstrating the coordinating flexibility of the selected ligand system. While ZnL^1 and ZnL^2 were seen to have similar stoichiometric structures, ZnL^3 has an acetate group and ZnL^4 shows the presence of two ligand molecules bidentate. Characterization of the complexes included spectrophotometric measurements in the μM range, elemental analysis, MS, FTIR and NMR spectroscopies. Difficulties in solubilizing the complexes posed challenges in the NMR measurements, yet it was possible to acquire ^1H NMR and HSQC spectra to support our structural proposals.

To evaluate their performance in biological studies, their behaviour in solution was studied. ZnL^4 demonstrated aggregation but lower precipitation than the other Zn-complexes in aqueous medium, however they all remained soluble and stable in the presence of BSA.

Thermodynamic studies carried out as well revealed that the predominant interactive force between the complexes and the BSA protein were moderate to strong hydrophobic forces. ZnL^4 was also the complex that showed lower ability to bind BSA, with the collected fluorescence

data not showing a good fitting, which would yield an accurate binding constant. Taking BSA as a model for HSA, it seems that albumin is a possible transporter of the complexes in blood. Given the presence of BSA in high amounts in culture media used in the cell studies, this suggest that the protein might help the compounds keep their solubility. Future studies considering the previous incubation of the complexes with BSA might help to further understand this point.

In vitro biological studies showed that all complexes and their ligands are cytotoxic, but none of them has antimicrobial activity. Overall, the cytotoxic screening showed higher antiproliferative activities for the ligands compared to their complexes. The exception was ZnL^4, which was better than H_2L^4 in prostate carcinoma (LNCaP) and myeloma (MM.1S) cell lines. ZnL^4 and H_2L^4 are both selective towards cancer cells and the relationship between IC_{50} (roughly half in the complex) suggests that the cytotoxic actively is due to the ligand. The properties of the zinc complexes in terms of solubility in aqueous media strongly affected their effect on cells. Their solubility, if enhanced, could help improve the cytotoxic effects as proven by the IC_{50} value of ZnL^4 against LNCaP cell line.

While the free ligands and the zinc complexes present interesting IC_{50} values, especially against leukaemia and myeloma cell lines, all compounds showed no significant cytotoxic activity against the non-cancer cell line HEK-293, demonstrating selective action against tumour cells.

Overall, the results of this study confirmed the capability of Schiff base ligands to coordinate metal ions, specifically zinc, and to create complexes suited for anti-cancer research. As proven in the group's earlier study[5], 8-Hydroxyquinoline hydrazones and their metal derivatives possess interesting anticancer potentials capable of enhancing cancer therapy. This work has shown other cell lines in which the ligands are cytotoxic against *per se* and a new zinc(II) complex that shows very interesting cytotoxic effects on, at least, two cell lines. Further developments are required in terms of ligands design or the use of targeting strategies to improve physiological solubility and to deliver compounds to their targets. Additional studies, on the ligands and ZnL^4, to evaluate effects in cell mechanisms and cell status, are required.

References

(1) Jemal, A.; Bray, F.; Center, M. M.; Ferlay, J.; Ward, E.; Forman, D. Global Cancer Statistics. *CA: Cancer J. Clin.* **2011**, *61* (2), 69–90. https://doi.org/10.3322/caac.20107.

(2) Horoszewicz, J. S.; Leong, S. S.; Kawinski, E.; Karr, J. P.; Rosenthal, H.; Chu, T. M.; Mirand, E. A.; Murphy, G. P. LNCaP Model of Human Prostatic Carcinoma. *Cancer Res.* **1983**, *43*, 10.

(3) Khalil, H.; Heulot, M.; Barras, D. Peptides and Biocomplexes in Anticancer Therapy. *Phy. Sci. Rev.* **2016**, *1* (6). https://doi.org/10.1515/psr-2016-0006.

(4) Zhang, H.; Liu, C.-S.; Bu, X.-H.; Yang, M. Synthesis, Crystal Structure, Cytotoxic Activity and DNA-Binding Properties of the Copper (II) and Zinc (II) Complexes with 1-[3-(2-Pyridyl)Pyrazol-1-Ylmethyl]Naphthalene. *J. Inorg. Biochem.* **2005**, *99* (5), 1119–1125. https://doi.org/10.1016/j.jinorgbio.2005.02.005.

(5) Ribeiro, N.; Bulut, I.; Pósa, V.; Sergi, B.; Sciortino, G.; Pessoa, J. C.; Maia, L. B.; Ugone, V.; Garribba, E.; Enyedy, É. A.; Acilan, C.; Correia, I. Solution Chemical Properties and Anticancer Potential of 8-Hydroxyquinoline Hydrazones and Their Oxidovanadium(IV) Complexes. *J. Inorg. Biochem.* **2022**, *235*, 111932. https://doi.org/10.1016/j.jinorgbio.2022.111932.

(6) Turnaturi, R.; Oliveri, V.; Vecchio, G. Biotin-8-Hydroxyquinoline Conjugates and Their Metal Complexes: Exploring the Chemical Properties and the Antioxidant Activity. *Polyhedron* **2016**, *110*, 254–260. https://doi.org/10.1016/j.poly.2016.02.025.

(7) Pippi, B.; Lopes, W.; Reginatto, P.; Silva, F. É. K.; Joaquim, A. R.; Alves, R. J.; Silveira, G. P.; Vainstein, M. H.; Andrade, S. F.; Fuentefria, A. M. New Insights into the Mechanism of Antifungal Action of 8-Hydroxyquinolines. *Saudi Pharm. J.* **2019**, *27* (1), 41–48. https://doi.org/10.1016/j.jsps.2018.07.017.

(8) Joaquim, A. R.; Gionbelli, M. P.; Gosmann, G.; Fuentefria, A. M.; Lopes, M. S.; Fernandes de Andrade, S. Novel Antimicrobial 8-Hydroxyquinoline-Based Agents: Current Development, Structure–Activity Relationships, and Perspectives. *J. Med. Chem.* **2021**, *64* (22), 16349–16379. https://doi.org/10.1021/acs.jmedchem.1c01318.

(9) Prachayasittikul, V.; Prachayasittikul, V.; Prachayasittikul, S.; Ruchirawat, S. 8-Hydroxyquinolines: A Review of Their Metal Chelating Properties and Medicinal Applications. *Drug Des. Devel. Ther.* **2013**, 1157. https://doi.org/10.2147/DDDT.S49763.

(10) Shah, P.; Abadi, L. F.; Gaikwad, S.; Chaudhari, D.; Kushwah, V.; Jain, S.; Bhutani, K. K.; Kulkarni, S.; Singh, I. P. Synthesis and Biological Evaluation of 8-Hydroxyquinoline-

Hydrazones for Anti-HIV-1 and Anticancer Potential. *ChemistrySelect* **2018**, *3* (38), 10727–10731. https://doi.org/10.1002/slct.201802283.

(11) Song, Y.; Xu, H.; Chen, W.; Zhan, P.; Liu, X. 8-Hydroxyquinoline: A Privileged Structure with a Broad-Ranging Pharmacological Potential. *Med. Chem. Commun.* **2015**, *6* (1), 61–74. https://doi.org/10.1039/C4MD00284A.

(12) de Freitas, L. V.; da Silva, C. C. P.; Ellena, J.; Costa, L. A. S.; Rey, N. A. Structural and Vibrational Study of 8-Hydroxyquinoline-2-Carboxaldehyde Isonicotinoyl Hydrazone – A Potential Metal–Protein Attenuating Compound (MPAC) for the Treatment of Alzheimer's Disease. *Spectrochim. Acta A: Mol. Bio. Spec.* **2013**, *116*, 41–48. https://doi.org/10.1016/j.saa.2013.06.105.

(13) Finkelstein, D. I.; Hare, D. J.; Billings, J. L.; Sedjahtera, A.; Nurjono, M.; Arthofer, E.; George, S.; Culvenor, J. G.; Bush, A. I.; Adlard, P. A. Clioquinol Improves Cognitive, Motor Function, and Microanatomy of the Alpha-Synuclein HA53T Transgenic Mice. *ACS Chem. Neurosci.* **2016**, *7* (1), 119–129. https://doi.org/10.1021/acschemneuro.5b00253.

(14) Ding, W.-Q.; Liu, B.; Vaught, J. L.; Yamauchi, H.; Lind, S. E. Anticancer Activity of the Antibiotic Clioquinol. *Cancer Res.* **2005**, *65* (8), 3389–3395. https://doi.org/10.1158/0008-5472.CAN-04-3577.

(15) Abouelhassan, Y.; Yang, Q.; Yousaf, H.; Nguyen, M. T.; Rolfe, M.; Schultz, G. S.; Huigens, R. W. Nitroxoline: A Broad-Spectrum Biofilm-Eradicating Agent against Pathogenic Bacteria. *Inter. J. Antimicrob. Agent* **2017**, *49* (2), 247–251. https://doi.org/10.1016/j.ijantimicag.2016.10.017.

(16) Cherdtrakulkiat, R.; Lawung, R.; Nabu, S.; Tantimavanich, S.; Sinthupoom, N.; Prachayasittikul, S.; Prachayasittikul, V. Nitroxoline: A Potent Antimicrobial Agent against Multidrug Resistant Enterobacteriaceae. *EXCLI J.; 18:Doc445; ISSN 1611-2156* **2019**. https://doi.org/10.17179/EXCLI2019-1378.

(17) Buteau, J.; Accili, D. Regulation of Pancreatic ?-Cell Function by the Forkhead Protein FoxO1. *Diabetes Obes. Met.* **2007**, *9* (s2), 140–146. https://doi.org/10.1111/j.1463-1326.2007.00782.x.

(18) Zheng, H.; Weiner, L. M.; Bar-Am, O.; Epsztejn, S.; Cabantchik, Z. I.; Warshawsky, A.; Youdim, M. B. H.; Fridkin, M. Design, Synthesis, and Evaluation of Novel Bifunctional Iron-Chelators as Potential Agents for Neuroprotection in Alzheimer's, Parkinson's, and Other Neurodegenerative Diseases. *Bioorg. Med. Chem.* **2005**, 11.

(19) Zheng, H.; Blat, D.; Fridkin, M. Novel Neuroprotective Neurotrophic NAP Analogs Targeting Metal Toxicity and Oxidative Stress: Potential Candidates for the Control of

Neurodegenerative Diseases. In *Oxidative Stress and Neuroprotection*; Parvez, H., Riederer, P., Eds.; Springer Vienna: Vienna, 2006; pp 163–172. https://doi.org/10.1007/978-3-211-33328-0_18.

(20) Zheng, H.; Youdim, M. B. H.; Weiner, L. M.; Fridkin, M. Synthesis and Evaluation of Peptidic Metal Chelators for Neuroprotection in Neurodegenerative Diseases. *J. Pept. Res.* **2005**, *66* (4), 190–203. https://doi.org/10.1111/j.1399-3011.2005.00289.x.

(21) Scott, L. E.; Telpoukhovskaia, M.; Rodríguez-Rodríguez, C.; Merkel, M.; Bowen, M. L.; Page, B. D. G.; Green, D. E.; Storr, T.; Thomas, F.; Allen, D. D.; Lockman, P. R.; Patrick, B. O.; Adam, M. J.; Orvig, C. N-Aryl-Substituted 3-(β-D-Glucopyranosyloxy)-2-Methyl-4(1H)-Pyridinones as Agents for Alzheimer's Therapy. *Chem. Sci.* **2011**, *2* (4), 642–648. https://doi.org/10.1039/C0SC00544D.

(22) Cukierman, D. S.; Pinheiro, A. B.; Castiñeiras-Filho, S. L. P.; da Silva, A. S. P.; Miotto, M. C.; De Falco, A.; de P. Ribeiro, T.; Maisonette, S.; da Cunha, A. L. M. C.; Hauser-Davis, R. A.; Landeira-Fernandez, J.; Aucélio, R. Q.; Outeiro, T. F.; Pereira, M. D.; Fernández, C. O.; Rey, N. A. A Moderate Metal-Binding Hydrazone Meets the Criteria for a Bioinorganic Approach towards Parkinson's Disease: Therapeutic Potential, Blood-Brain Barrier Crossing Evaluation and Preliminary Toxicological Studies. *J. Inorg. Biochem.* **2017**, *170*, 160–168. https://doi.org/10.1016/j.jinorgbio.2017.02.020.

(23) Bruijnincx, P. C. A.; Sadler, P. J. New Trends for Metal Complexes with Anticancer Activity. *Curr. Opin. Chem. Biol.* **2008**, *12* (2), 197–206. https://doi.org/10.1016/j.cbpa.2007.11.013.

(24) Renfrew, A. K. Transition Metal Complexes with Bioactive Ligands: Mechanisms for Selective Ligand Release and Applications for Drug Delivery. *Metallomics* **2014**, *6* (8), 1324–1335. https://doi.org/10.1039/C4MT00069B.

(25) Zhou, C.-Y.; Zhao, J.; Wu, Y.-B.; Yin, C.-X.; Pin, Y. Synthesis, Characterization and Studies on DNA-Binding of a New Cu(II) Complex with N1,N8-Bis(l-Methyl-4-Nitropyrrole-2-Carbonyl)Triethylenetetramine. *J. Inorg. Biochem.* **2007**, *101* (1), 10–18. https://doi.org/10.1016/j.jinorgbio.2006.07.011.

(26) Mahmood, K.; Hashmi, W.; Ismail, H.; Mirza, B.; Twamley, B.; Akhter, Z.; Rozas, I.; Baker, R. J. Synthesis, DNA Binding and Antibacterial Activity of Metal(II) Complexes of a Benzimidazole Schiff Base. *Polyhedron* **2019**, *157*, 326–334. https://doi.org/10.1016/j.poly.2018.10.020.

(27) Parsekar, S. U.; Velankanni, P.; Sridhar, S.; Haldar, P.; Mate, N. A.; Banerjee, A.; Sudhadevi Antharjanam, P. K.; Koley, A. P.; Kumar, M. Protein Binding Studies with

Human Serum Albumin, Molecular Docking and *in Vitro* Cytotoxicity Studies Using HeLa Cervical Carcinoma Cells of Cu(II)/Zn(II) Complexes Containing a Carbohydrazone Ligand. *Dalton Trans.* **2020**, *49* (9), 2947–2965. https://doi.org/10.1039/C9DT04656A.

(28) Correia, I.; Adão, P.; Roy, S.; Wahba, M.; Matos, C.; Maurya, M. R.; Marques, F.; Pavan, F. R.; Leite, C. Q. F.; Avecilla, F.; Costa Pessoa, J. Hydroxyquinoline Derived Vanadium(IV and V) and Copper(II) Complexes as Potential Anti-Tuberculosis and Anti-Tumor Agents. *J. Inorg. Biochem.* **2014**, *141*, 83–93. https://doi.org/10.1016/j.jinorgbio.2014.07.019.

(29) Ribeiro, N.; Bulut, I.; Cevatemre, B.; Teixeira, C.; Yildizhan, Y.; André, V.; Adão, P.; Pessoa, J. C.; Acilan, C.; Correia, I. Cu(II) and V(IV)O Complexes with Tri- or Tetradentate Ligands Based on (2-Hydroxybenzyl)- L -Alanines Reveal Promising Anticancer Therapeutic Potential. *Dalton Trans.* **2021**, *50* (1), 157–169. https://doi.org/10.1039/D0DT03331F.

(30) Ribeiro, N.; Di Paolo, R. E.; Galvão, A. M.; Marques, F.; Costa Pessoa, J.; Correia, I. Photophysical Properties and Biological Evaluation of a Zinc(II)-5-Methyl-1H-Pyrazole Schiff Base Complex. *Spectrochim. Acta A: Mol. Bio. Spec.* **2018**, *204*, 317–327. https://doi.org/10.1016/j.saa.2018.06.028.

(31) Zehra, S.; Shavez Khan, M.; Ahmad, I.; Arjmand, F. New Tailored Substituted Benzothiazole Schiff Base Cu(II)/Zn(II) Antitumor Drug Entities: Effect of Substituents on DNA Binding Profile, Antimicrobial and Cytotoxic Activity. *J. Bio. Struct. Dynam.* **2019**, *37* (7), 1863–1879. https://doi.org/10.1080/07391102.2018.1467794.

(32) De Freitas, L. V.; Dos Santos, A. L. da S. F.; Da Costa, F. C.; Calixto, J. B.; Miranda, P. V. P.; Silva, T. J. J.; Pereira, E. S.; Rocha, W. R.; De Almeida, W. B.; De Souza, L. A.; Freitas, M. C. R. Synthesis and Structural Characterization of a 8-Hydroxyquinoline Derivative Coordinated to Zn(II). *J. Mol. Struct.* **2018**, *1169*, 119–129. https://doi.org/10.1016/j.molstruc.2018.05.050.

(33) Kaya, B.; Yılmaz, Z. K.; Şahin, O.; Aslim, B.; Ülküseven, B. Structural Characterization of New Zinc(II) Complexes with N_2O_2 Chelating Thiosemicarbazidato Ligands; Investigation of the Relationship between Their DNA Interaction and *in Vitro* Antiproliferative Activity towards Human Cancer Cells. *New J. Chem.* **2020**, *44* (22), 9313–9320. https://doi.org/10.1039/D0NJ02149K.

(34) Ribeiro, N.; Albino, M.; Ferreira, A.; Escrevente, C.; Barral, D.; Pessoa, J.; Reis, C.; Gaspar, M.; Correia, I. Liposomal Formulations of a New Zinc(II) Complex Exhibiting

High Therapeutic Potential in a Murine Colon Cancer Model. *Int. J. Mol. Struct.* **2022**, *23* (12), 6728. https://doi.org/10.3390/ijms23126728.

(35) Porchia, M.; Pellei, M.; Del Bello, F.; Santini, C. Zinc Complexes with Nitrogen Donor Ligands as Anticancer Agents. *Molecules* **2020**, *25* (24), 5814. https://doi.org/10.3390/molecules25245814.

(36) Oliveri, V.; Vecchio, G. 8-Hydroxyquinolines in Medicinal Chemistry: A Structural Perspective. *Eur. J. Med. Chem.* **2016**, *120*, 252–274. https://doi.org/10.1016/j.ejmech.2016.05.007.

(37) Albrecht, M.; Fiege, M.; Osetska, O. 8-Hydroxyquinolines in Metallosupramolecular Chemistry. *Coord. Chem. Rev.* **2008**, *252* (8–9), 812–824. https://doi.org/10.1016/j.ccr.2007.06.003.

(38) Gupta, R.; Luxami, V.; Paul, K. Insights of 8-Hydroxyquinolines: A Novel Target in Medicinal Chemistry. *Bioorg. Chem.* **2021**, *108*, 104633. https://doi.org/10.1016/j.bioorg.2021.104633.

(39) Zheng, H.; Youdim, M. B. H.; Fridkin, M. Site-Activated Chelators Targeting Acetylcholinesterase and Monoamine Oxidase for Alzheimer's Therapy. *ACS Chem. Biol.* **2010**, *5* (6), 603–610. https://doi.org/10.1021/cb900264w.

(40) Fernández-Bachiller, M. I.; Pérez, C.; González-Muñoz, G. C.; Conde, S.; López, M. G.; Villarroya, M.; García, A. G.; Rodríguez-Franco, M. I. Novel Tacrine−8-Hydroxyquinoline Hybrids as Multifunctional Agents for the Treatment of Alzheimer's Disease, with Neuroprotective, Cholinergic, Antioxidant, and Copper-Complexing Properties. *J. Med. Chem.* **2010**, *53* (13), 4927–4937. https://doi.org/10.1021/jm100329q.

(41) da Silva, C. M.; da Silva, D. L.; Modolo, L. V.; Alves, R. B.; de Resende, M. A.; Martins, C. V. B.; de Fátima, Â. Schiff Bases: A Short Review of Their Antimicrobial Activities. *J. Adv. Res.* **2011**, *2* (1), 1–8. https://doi.org/10.1016/j.jare.2010.05.004.

(42) *GLOBOCAN 2020: New Global Cancer Data | UICC*. https://www.uicc.org/news/globocan-2020-new-global-cancer-data# (accessed 2022-09-24).

(43) Hameed, A.; al-Rashida, M.; Uroos, M.; Abid Ali, S.; Khan, K. M. Schiff Bases in Medicinal Chemistry: A Patent Review (2010-2015). *Expert Opin. Ther. Pat.* **2017**, *27* (1), 63–79. https://doi.org/10.1080/13543776.2017.1252752.

(44) Shahraki, S.; Heydari, A. Binding Forces between a Novel Schiff Base Palladium(II) Complex and Two Carrier Proteins: Human Serum Albumi and β-Lactoglobulin. *J. Bio.*

Struct. Dynam. **2018**, *36* (11), 2807–2821. https://doi.org/10.1080/07391102.2017.1367723.

(45) Facchinetti, V.; da R. Reis, R.; R.B. Gomes, C.; R.A. Vasconcelos, T. Chemistry and Biological Activities of 1,3-Benzothiazoles. *Mini-Rev. Org. Chem.* **2012**, *9* (1), 44–53. https://doi.org/10.2174/157019312799079929.

(46) Dehkhodaei, M.; Sahihi, M.; Amiri Rudbari, H. Spectroscopic and Molecular Docking Studies on the Interaction of Pd(II) & Co(II) Schiff Base Complexes with β-Lactoglobulin as a Carrier Protein. *J. Bio. Struct. Dynam.* **2018**, *36* (12), 3130–3136. https://doi.org/10.1080/07391102.2017.1380537.

(47) Chen, D.; Cui, Q. C.; Yang, H.; Barrea, R. A.; Sarkar, F. H.; Sheng, S.; Yan, B.; Reddy, G. P. V.; Dou, Q. P. Clioquinol, a Therapeutic Agent for Alzheimer's Disease, Has Proteasome-Inhibitory, Androgen Receptor–Suppressing, Apoptosis-Inducing, and Antitumor Activities in Human Prostate Cancer Cells and Xenografts. *Cancer Res.* **2007**, *67* (4), 1636–1644. https://doi.org/10.1158/0008-5472.CAN-06-3546.

(48) Kratz, F.; Beyer, U. Serum Proteins as Drug Carriers of Anticancer Agents: A Review. *Drug Del.* **1998**, *5* (4), 281–299. https://doi.org/10.3109/10717549809065759.

(49) Topală, T.; Bodoki, A.; Oprean, L.; Oprean, R. Bovine Serum Albumin Interactions with Metal Complexes. *Med. Pharm. Rep.* **2014**, *87* (4), 215–219. https://doi.org/10.15386/cjmed-357.

(50) Cao, X.; He, Y.; Liu, D.; He, Y.; Hou, X.; Cheng, Y.; Liu, J. Characterization of Interaction between Scoparone and Bovine Serum Albumin: Spectroscopic and Molecular Docking Methods. *RSC Adv.* **2018**, *8* (45), 25519–25525. https://doi.org/10.1039/C8RA04065F.

(51) Belatik, A.; Hotchandani, S.; Carpentier, R.; Tajmir-Riahi, H.-A. Locating the Binding Sites of Pb(II) Ion with Human and Bovine Serum Albumins. *PLoS ONE* **2012**, *7* (5), e36723. https://doi.org/10.1371/journal.pone.0036723.

(52) Dömötör, O.; Tuccinardi, T.; Karcz, D.; Walsh, M.; Creaven, B. S.; Enyedy, É. A. Interaction of Anticancer Reduced Schiff Base Coumarin Derivatives with Human Serum Albumin Investigated by Fluorescence Quenching and Molecular Modeling. *Bioorg. Chem.* **2014**, *52*, 16–23. https://doi.org/10.1016/j.bioorg.2013.10.003.

(53) Ruankham, W.; Phopin, K.; Pingaew, R.; Prachayasittikul, S.; Prachayasittikul, V.; Tantimongcolwat, T. In Silico and Multi-Spectroscopic Analyses on the Interaction of 5-Amino-8-Hydroxyquinoline and Bovine Serum Albumin as a Potential Anticancer Agent. *Sci. Rep.* **2021**, *11* (1), 20187. https://doi.org/10.1038/s41598-021-99690-2.

(54) Bernard Valeur. *Molecular Fluorescence, Principles and Applications*, 1st edition.; Wiley-VCH: New York, 2001.

(55) Peng, W.; Ding, F.; Jiang, Y.-T.; Peng, Y.-K. Bioavailability and Activity of Natural Food Additive Triterpenoids as Influenced by Protein. *J. Agric. Food Chem.* **2014**, *62* (10), 2271–2283. https://doi.org/10.1021/jf4049512.

(56) Fu, L.; Sun, Y.; Ding, L.; Wang, Y.; Gao, Z.; Wu, Z.; Wang, S.; Li, W.; Bi, Y. Mechanism Evaluation of the Interactions between Flavonoids and Bovine Serum Albumin Based on Multi-Spectroscopy, Molecular Docking and Q-TOF HR-MS Analyses. *Food Chem.* **2016**, *203*, 150–157. https://doi.org/10.1016/j.foodchem.2016.01.105.

(57) Kongot, M.; Maurya, N.; Dohare, N.; Parray, M. ud din; Maurya, J. K.; Kumar, A.; Patel, R. Enthalpy-Driven Interaction between Dihydropyrimidine Compound and Bovine Serum Albumin: A Spectroscopic and Computational Approach. *J. Bio. Struct. Dynam.* **2018**, *36* (5), 1161–1170. https://doi.org/10.1080/07391102.2017.1314834.

(58) Kongot, M.; Reddy, D. S.; Singh, V.; Patel, R.; Singhal, N. K.; Kumar, A. A Manganese (II) Complex Tethered with S-Benzyldithiocarbazate Schiff Base: Synthesis, Characterization, in-Vitro Therapeutic Activity and Protein Interaction Studies. *Spectrochim. Acta A: Mol. Bio. Spec.* **2020**, *231*, 118123. https://doi.org/10.1016/j.saa.2020.118123.

(59) Lakowicz, J. R. *Principles of Fluorescence Spectroscopy*, 3rd ed.; Springer: New York, 2006.

(60) Rezakhani, L.; Khazaei, M. R.; Ghanbari, A.; Khazaei, M. Crab Shell Extract Induces Prostate Cancer Cell Line (LNcap) Apoptosis and Decreases Nitric Oxide Secretion. *Cell J.* **2016**, *19* (2). https://doi.org/10.22074/cellj.2016.4879.

(61) *GraphPad Prism 9 Curve Fitting Guide - Equation: log(inhibitor) vs. response -- Variable slope*. https://www.graphpad.com/guides/prism/latest/curve-fitting/reg_dr_inhibit_variable.htm (accessed 2022-10-23).

(62) Slomp, G. Temperature Effects in Nuclear Magnetic Resonance Spectroscopy. *Rev. Sci. Instr.* **1959**, *30* (11), 1024–1027. https://doi.org/10.1063/1.1716411.

(63) Mehta, H. S.; Chen, Y.; Sears, J. A.; Walter, E. D.; Campos, M.; Kothandaraman, J.; Heldebrant, D. J.; Hoyt, D. W.; Mueller, K. T.; Washton, N. M. A Novel High-Temperature MAS Probe with Optimized Temperature Gradient across Sample Rotor for in-Situ Monitoring of High-Temperature High-Pressure Chemical Reactions. *Solid State Nuc. Mag. Res.* **2019**, *102*, 31–35. https://doi.org/10.1016/j.ssnmr.2019.06.003.

(64) Rani, M.; Jayanthi, S.; Kabilan, S.; Ramachandran, R. Synthesis, Spectral, Crystal Structure, Hirshfeld Surface, Computational Analysis, and Antimicrobial Studies of Ethyl-(E)-4-(2-(2-Arylidenehydrazinyl)-2-Oxoethyl)Piperazine-1-Carboxylates. *J. Mol. Struct.* **2022**, *1252*, 132082. https://doi.org/10.1016/j.molstruc.2021.132082.

(65) Nunes, P.; Correia, I.; Marques, F.; Matos, A. P.; dos Santos, M. M. C.; Azevedo, C. G.; Capelo, J.-L.; Santos, H. M.; Gama, S.; Pinheiro, T.; Cavaco, I.; Pessoa, J. C. Copper Complexes with 1,10-Phenanthroline Derivatives: Underlying Factors Affecting Their Cytotoxicity. *Inorg. Chem.* **2020**, *59* (13), 9116–9134. https://doi.org/10.1021/acs.inorgchem.0c00925.

(66) Levina, A.; Lay, P. A. Stabilities and Biological Activities of Vanadium Drugs: What Is the Nature of the Active Species? *Chem. Asian J.* **2017**, *12* (14), 1692–1699. https://doi.org/10.1002/asia.201700463.

(67) Sathyadevi, P.; Krishnamoorthy, P.; Jayanthi, E.; Butorac, R. R.; Cowley, A. H.; Dharmaraj, N. Studies on the Effect of Metal Ions of Hydrazone Complexes on Interaction with Nucleic Acids, Bovine Serum Albumin and Antioxidant Properties. *Inorg. Chim. Acta* **2012**, *384*, 83–96. https://doi.org/10.1016/j.ica.2011.11.033.

(68) van de Weert, M.; Stella, L. Fluorescence Quenching and Ligand Binding: A Critical Discussion of a Popular Methodology. *J. Mol. Struct.* **2011**, *998* (1–3), 144–150. https://doi.org/10.1016/j.molstruc.2011.05.023.

(69) Phopin, K.; Ruankham, W.; Prachayasittikul, S.; Prachayasittikul, V.; Tantimongcolwat, T. Insight into the Molecular Interaction of Cloxyquin (5-Chloro-8-Hydroxyquinoline) with Bovine Serum Albumin: Biophysical Analysis and Computational Simulation. *Int. J. Mol. Struct.* **2019**, *21* (1), 249. https://doi.org/10.3390/ijms21010249.

(70) Edwards, J. C.; Giammatteo, P. J. Process NMR Spectroscopy: Technology and On-Line Applications. In *Process Analytical Technology*; John Wiley & Sons, Ltd, 2010; pp 303–335. https://doi.org/10.1002/9780470689592.ch10.

(71) Liu, J.; He, Y.; Liu, D.; He, Y.; Tang, Z.; Lou, H.; Huo, Y.; Cao, X. Characterizing the Binding Interaction of Astilbin with Bovine Serum Albumin: A Spectroscopic Study in Combination with Molecular Docking Technology. *RSC Adv.* **2018**, *8* (13), 7280–7286. https://doi.org/10.1039/C7RA13272G.

(72) Ross, P. D.; Subramanian, S. Thermodynamics of Protein Association Reactions: Forces Contributing to Stability. *Biochem.* **1981**, *20* (11), 3096–3102. https://doi.org/10.1021/bi00514a017.

(73) Suryawanshi, V. D.; Walekar, L. S.; Gore, A. H.; Anbhule, P. V.; Kolekar, G. B. Spectroscopic Analysis on the Binding Interaction of Biologically Active Pyrimidine Derivative with Bovine Serum Albumin. *J. Pharm. Anal.* **2016**, *6* (1), 56–63. https://doi.org/10.1016/j.jpha.2015.07.001.

(74) Chen, W.-Y.; Huang, H.-M.; Lin, C.-C.; Lin, F.-Y.; Chan, Y.-C. Effect of Temperature on Hydrophobic Interaction between Proteins and Hydrophobic Adsorbents: Studies by Isothermal Titration Calorimetry and the van't Hoff Equation. *Langmuir* **2003**, *19* (22), 9395–9403. https://doi.org/10.1021/la034783o.

(75) Yu, H.; Zhou, Y.; Lind, S. E.; Ding, W.-Q. Clioquinol Targets Zinc to Lysosomes in Human Cancer Cells. *Biochem. J.* **2009**, *417* (1), 133–139. https://doi.org/10.1042/BJ20081421.

(76) Liu, Y.-C.; Wei, J.-H.; Chen, Z.-F.; Liu, M.; Gu, Y.-Q.; Huang, K.-B.; Li, Z.-Q.; Liang, H. The Antitumor Activity of Zinc(II) and Copper(II) Complexes with 5,7-Dihalo-Substituted-8-Quinolinoline. *Eur. J. Med. Chem.* **2013**, *69*, 554–563. https://doi.org/10.1016/j.ejmech.2013.08.033.

Annexes

A1. FTIR spectra

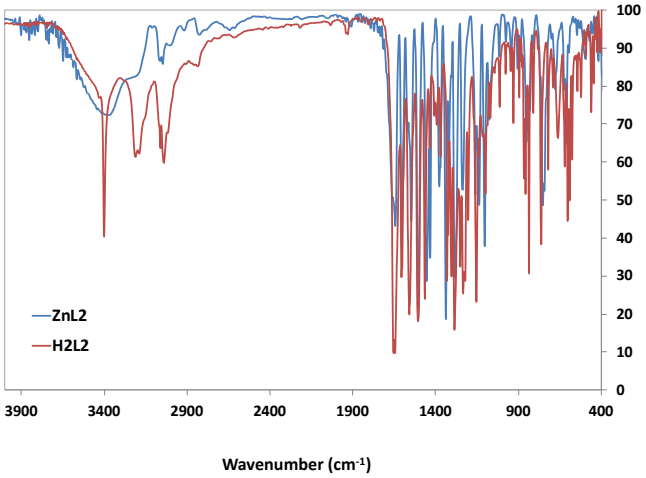

(A)

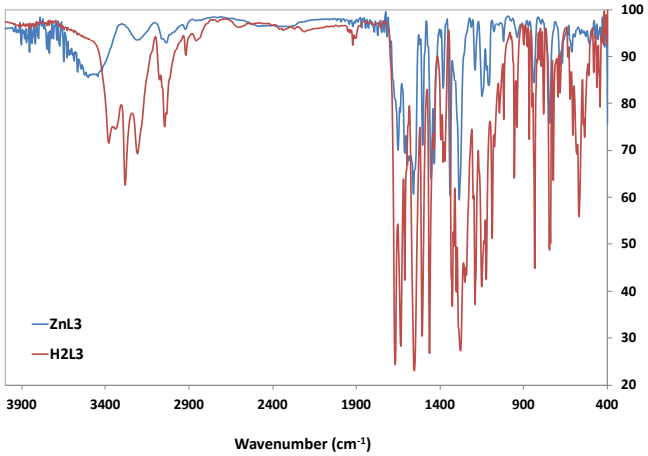

(B)

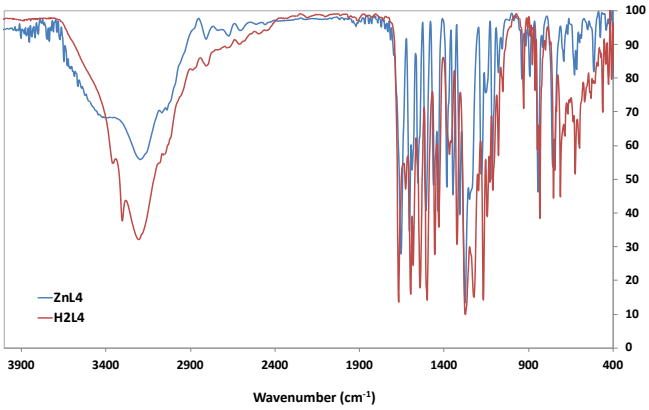

(C)

Figure A1. FTIR spectra (in KBr pellet) of the ligands and their corresponding zinc(II) complexes.

A2. NMR spectra at 50 ºC

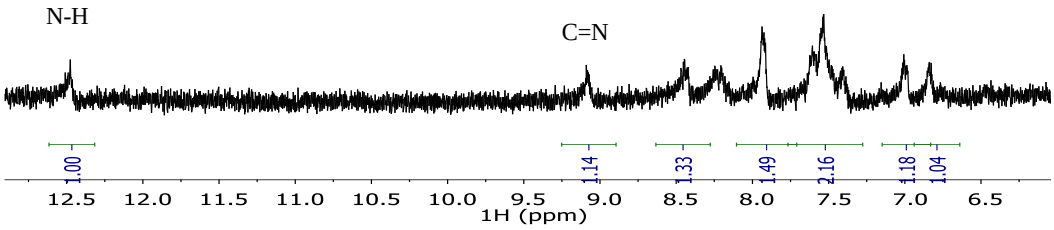

(A) ^{1}H-NMR spectra

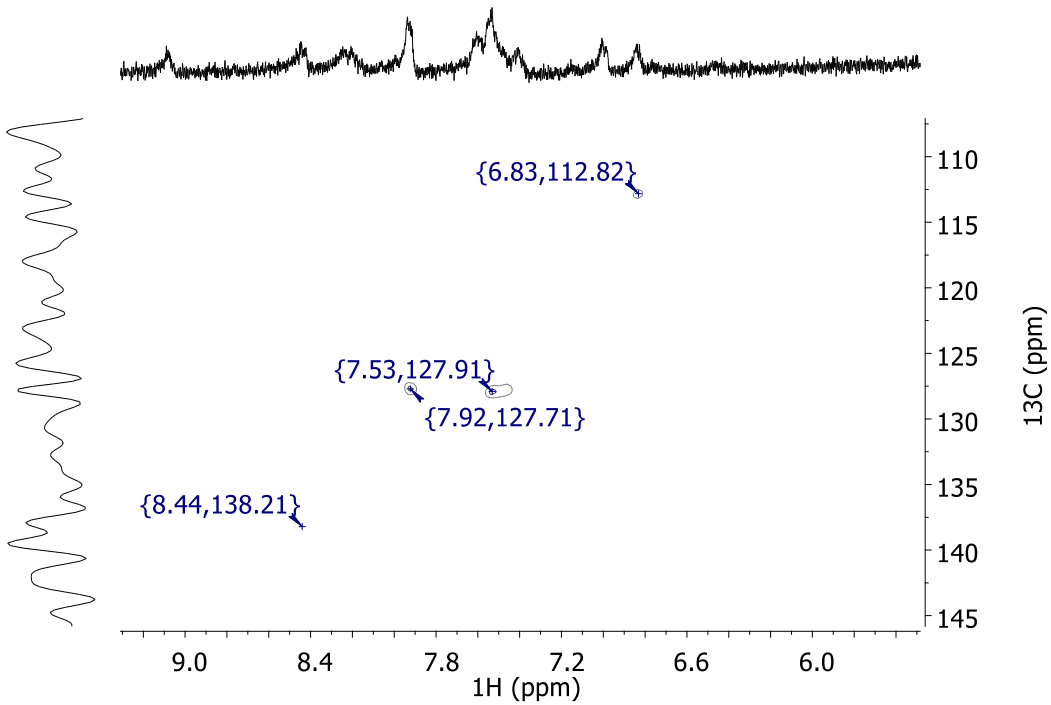

(B) HSQC spectra

Figure A2.1. NMR spectra of ZnL^{1} in DMSO_d_6 at 50 °C

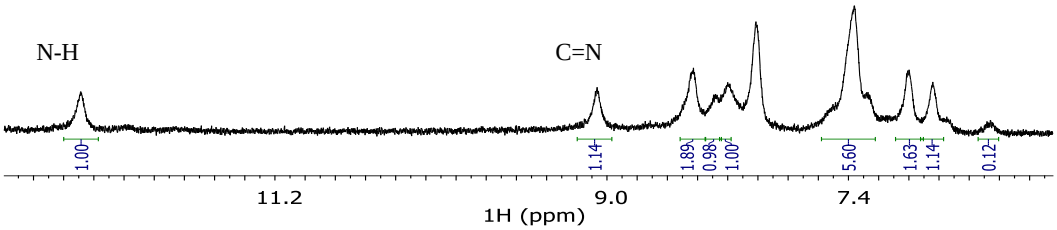

(A) ^{1}H-NMR spectra

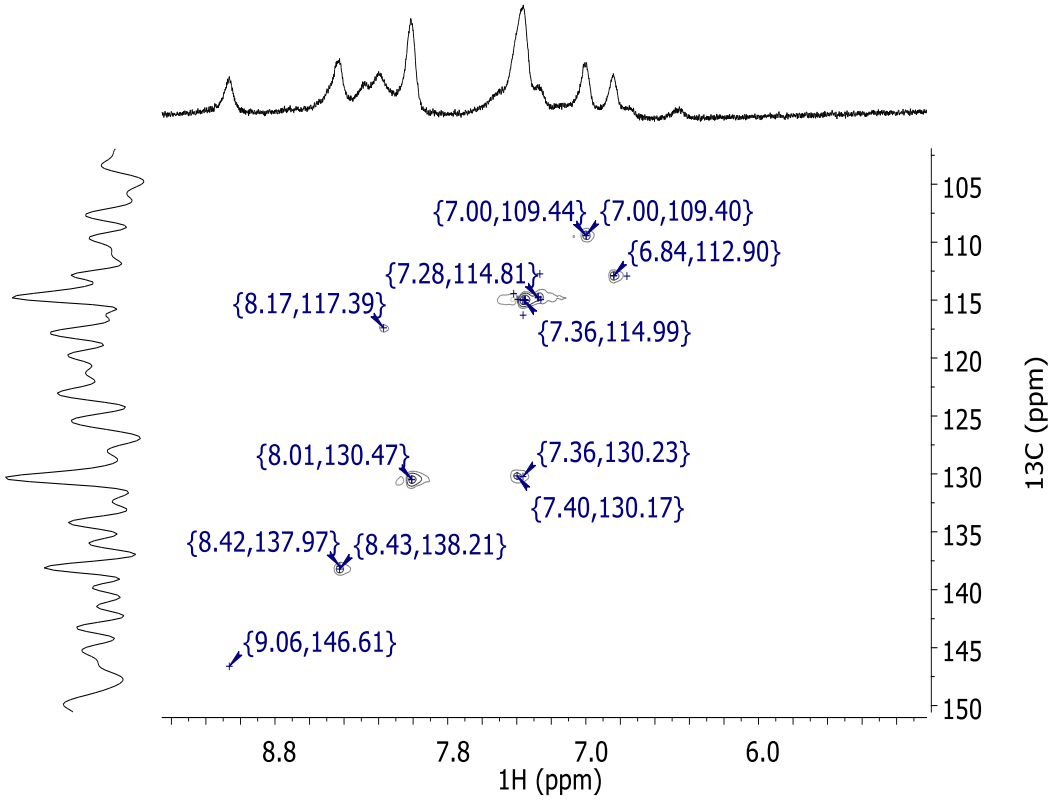

(B) HSQC spectra

Figure A2.2. NMR spectra of ZnL^2 in DMSO_d_6 at 50 ºC

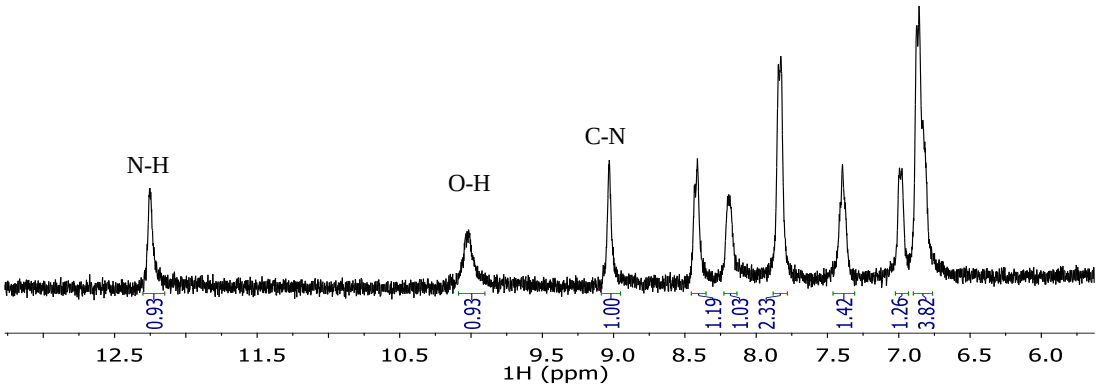

(A) ^{1}H-NMR spectra

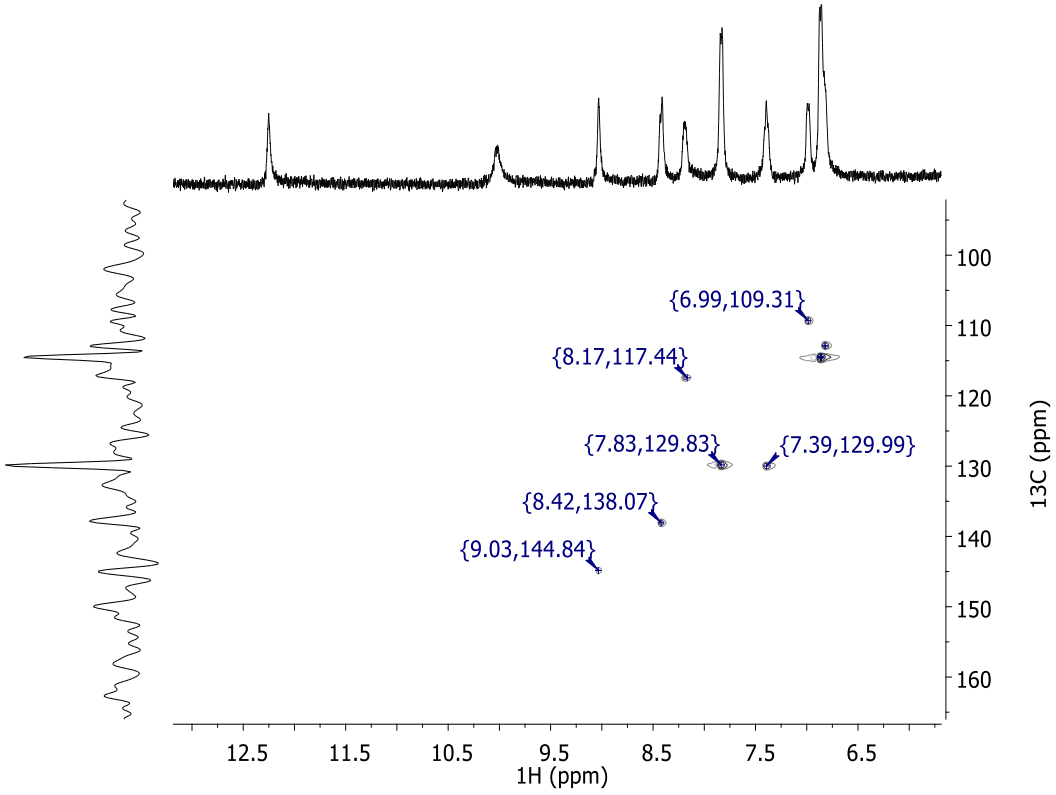

(B) HSQC spectra

Figure A2.3. NMR spectra of ZnL^{4} taken from 400 MHz apparatus in DMSO_d_6 at 50 ºC. Spectra output is double effect from the two ligands bound to the Zn^{2+}.

A3. UV-Visible absorption spectra

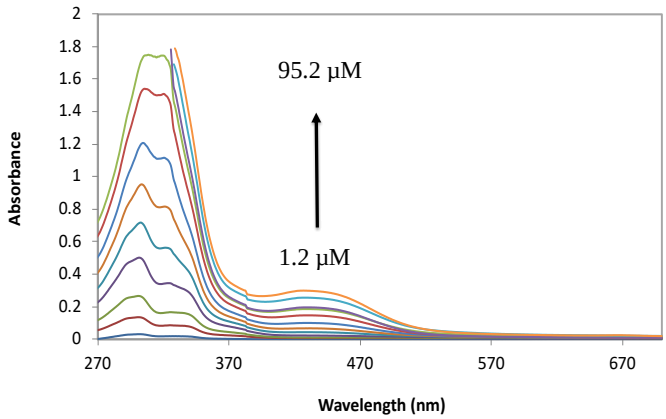

(A) ZnL^1

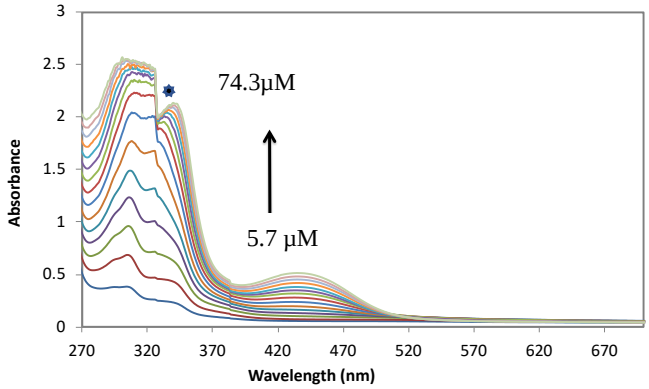

(B) ZnL^4

Figure A3.1. UV-Visible absorption spectra of ZnL^1 and ZnL^4 in DMSO with increasing concentrations indicated in the figure. * This is due to an electronic effect, when the lamp in changed from UV (deuterium) to vis (tungsten).

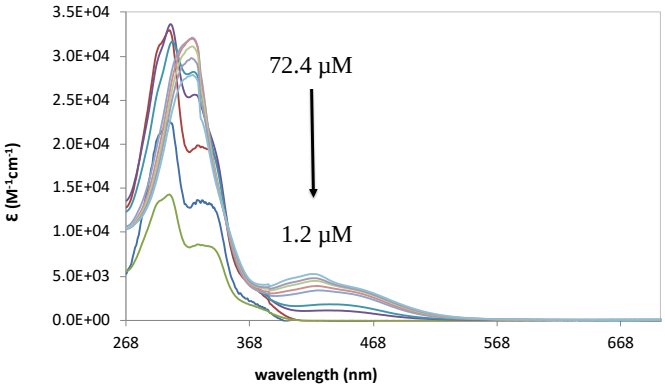

(A) ZnL^3

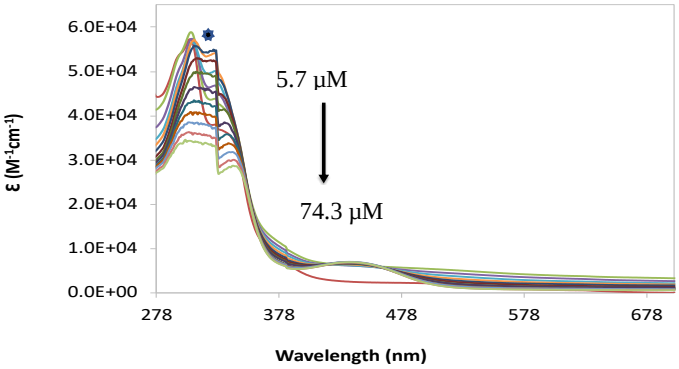

(B) ZnL^4

Figure A3.2. UV-Vis spectra (in molar absorptivity) of ZnL^3 and ZnL^4 in DMSO with increasing concentrations indicated in the figure. The increase in absorption in the visible region in (B) is due to light diffraction effects due to precipitation/aggregation. * This is due to an electronic effect, when the lamp in changed from UV (deuterium) to vis (tungsten).

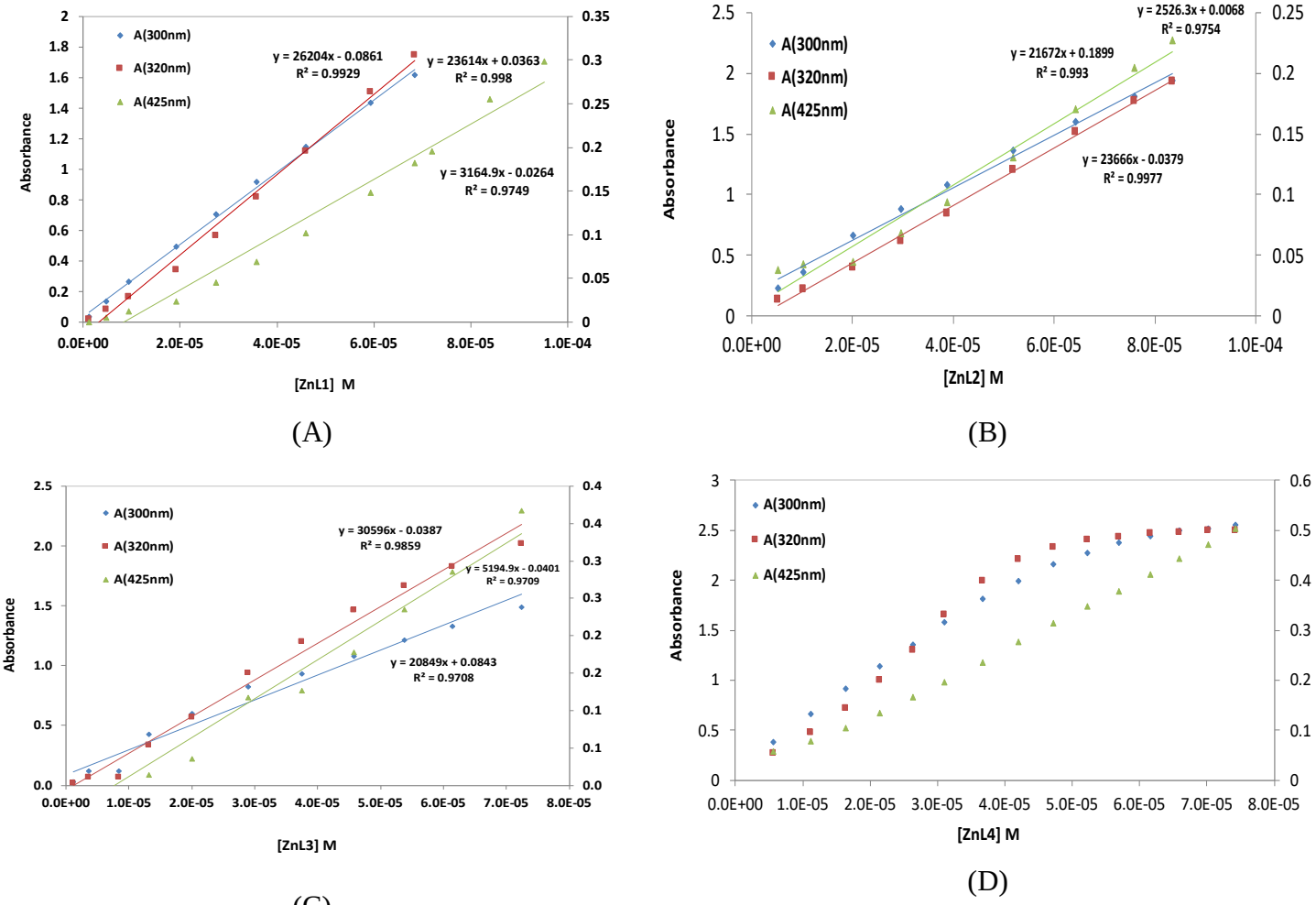

Figure A.3.3. Correlation graph (absorbance *vs.* concentration) of the zinc complexes at **λ** = 300, 320 and 425 nm. in DMSO

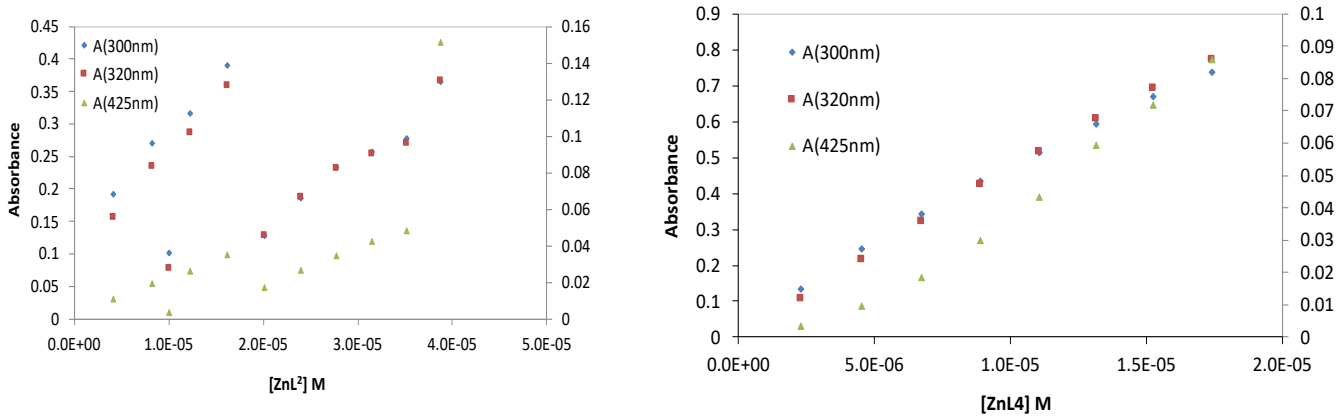

Figure A.3.4. Correlation graph (absorbance *vs.* concentration) of the zinc complexes ZnL^2 and ZnL^4 at **λ** = 300, 320 and 425 nm. in HEPES aqueous buffer (10 mM, pH 7.4).

A4. Stability studies

a) Stability in aqueous medium

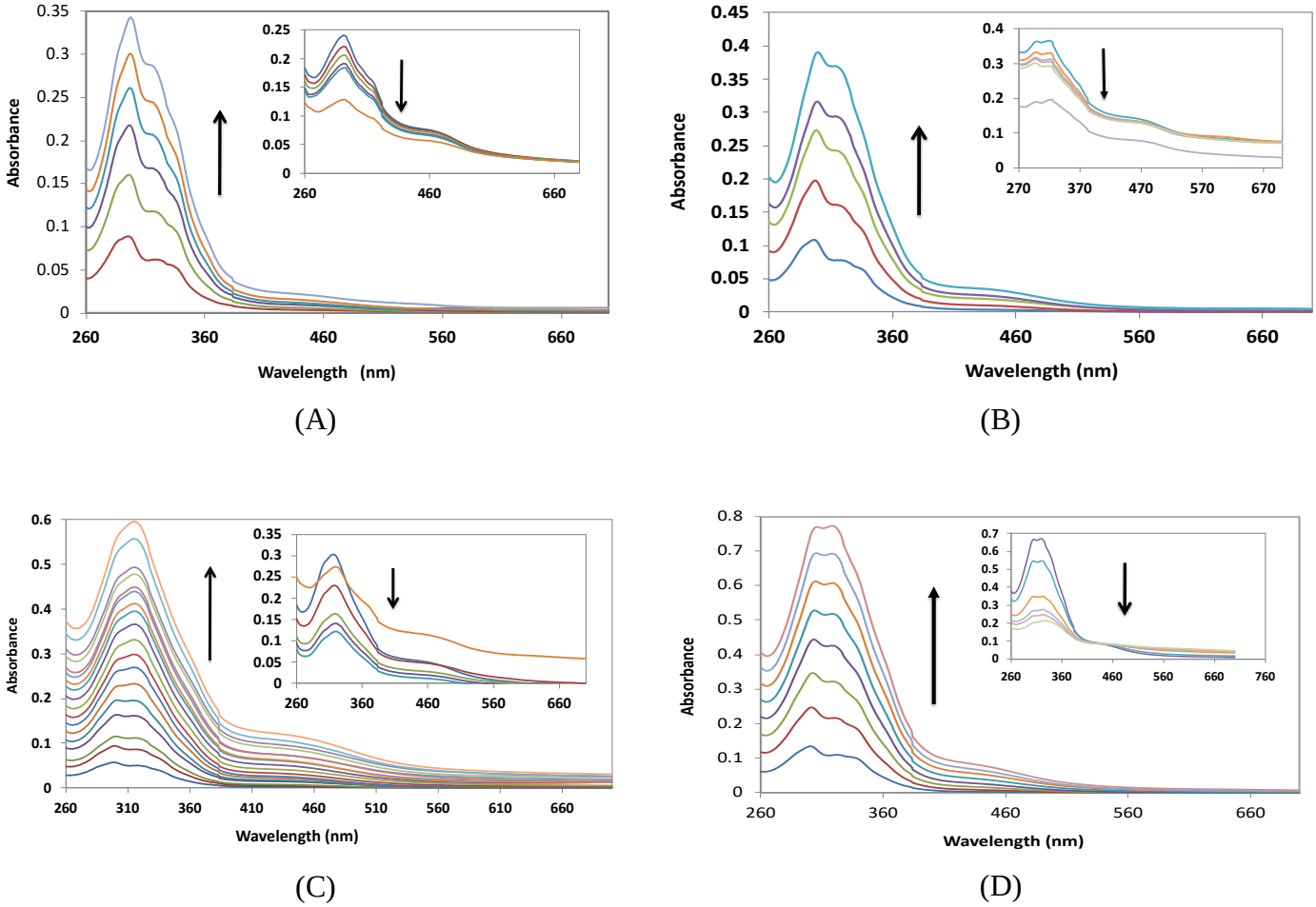

Figure A4.1. UV- Vis spectra in aqueous medium (HEPES: 10 mM, pH 7.4) of the zinc metal complexes with arrows indicating increasing concentration. (A) 3.8-25.6 µM ZnL^1 (B) 4.2-38.7 µM ZnL^2 (C) 2.4-44.8 µM ZnL^3 and (D) 2.3-17.8 µM ZnL^4. Stability (inset) for 5 consecutive hours and after 24 hours, arrows showing increasing time.

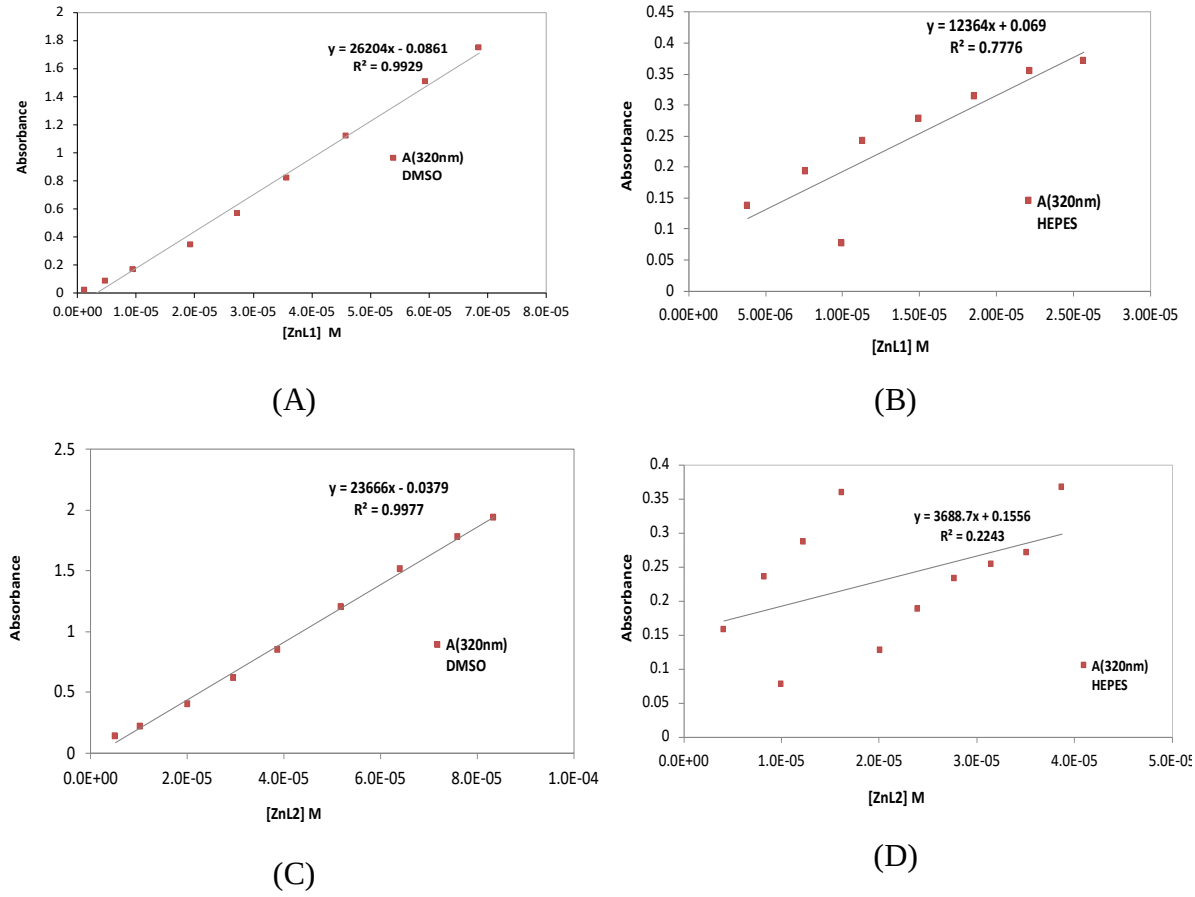

Figure A4.2. Correlation plots of absorbance *vs.* concentration for the complexes, ZnL^1 and ZnL^2 in both DMSO (left) and HEPES aqueous buffer (10 mM, pH 7.4) (right) at $\lambda = 320$ nm.

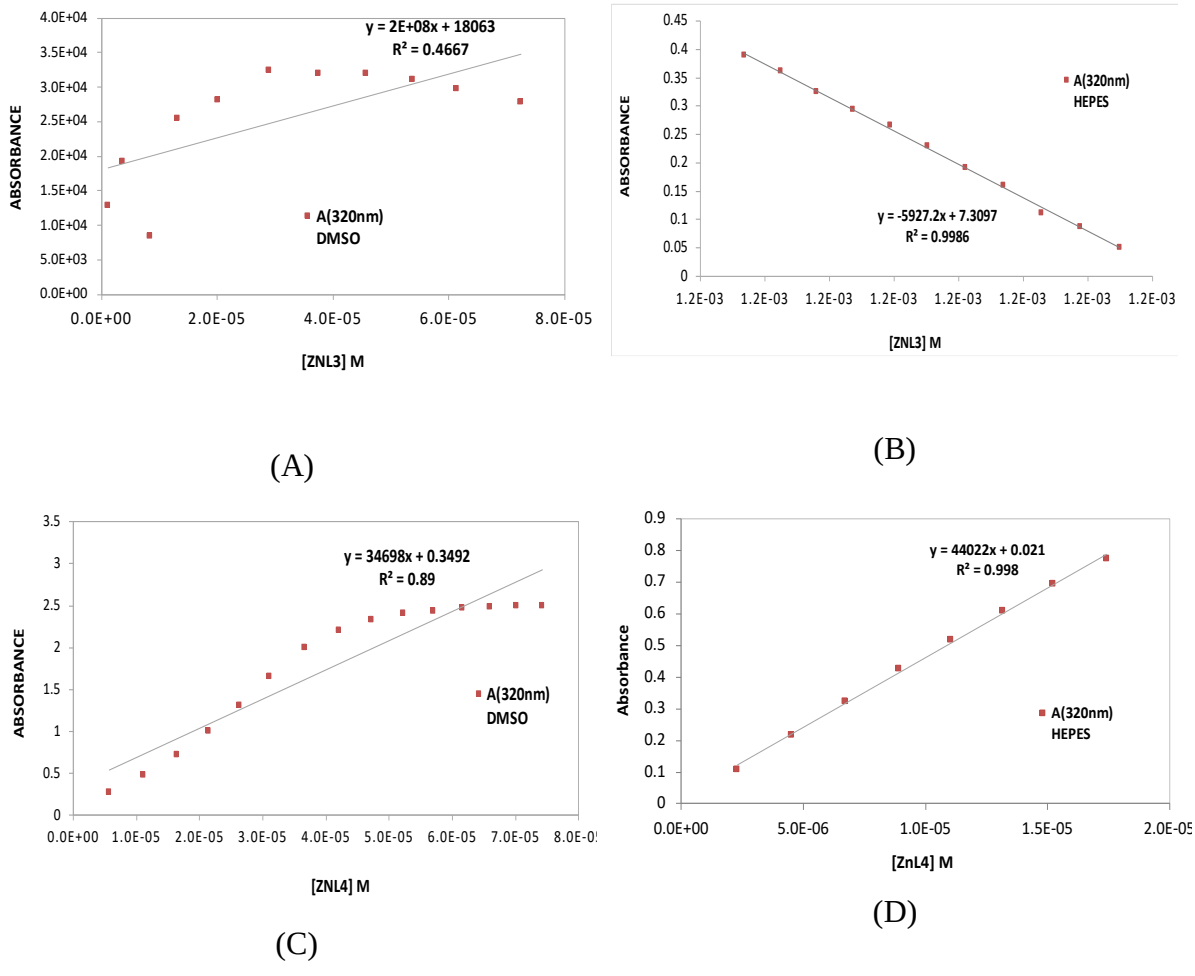

Figure A4.3. Correlation plots of absorbance *vs.* concentration for the complexes, ZnL^3 and ZnL^4 in both DMSO (left) and HEPES aqueous buffer (10 mM, pH 7.4) (right) at $\lambda = 320$ nm.

b) Stability in the presence of albumin

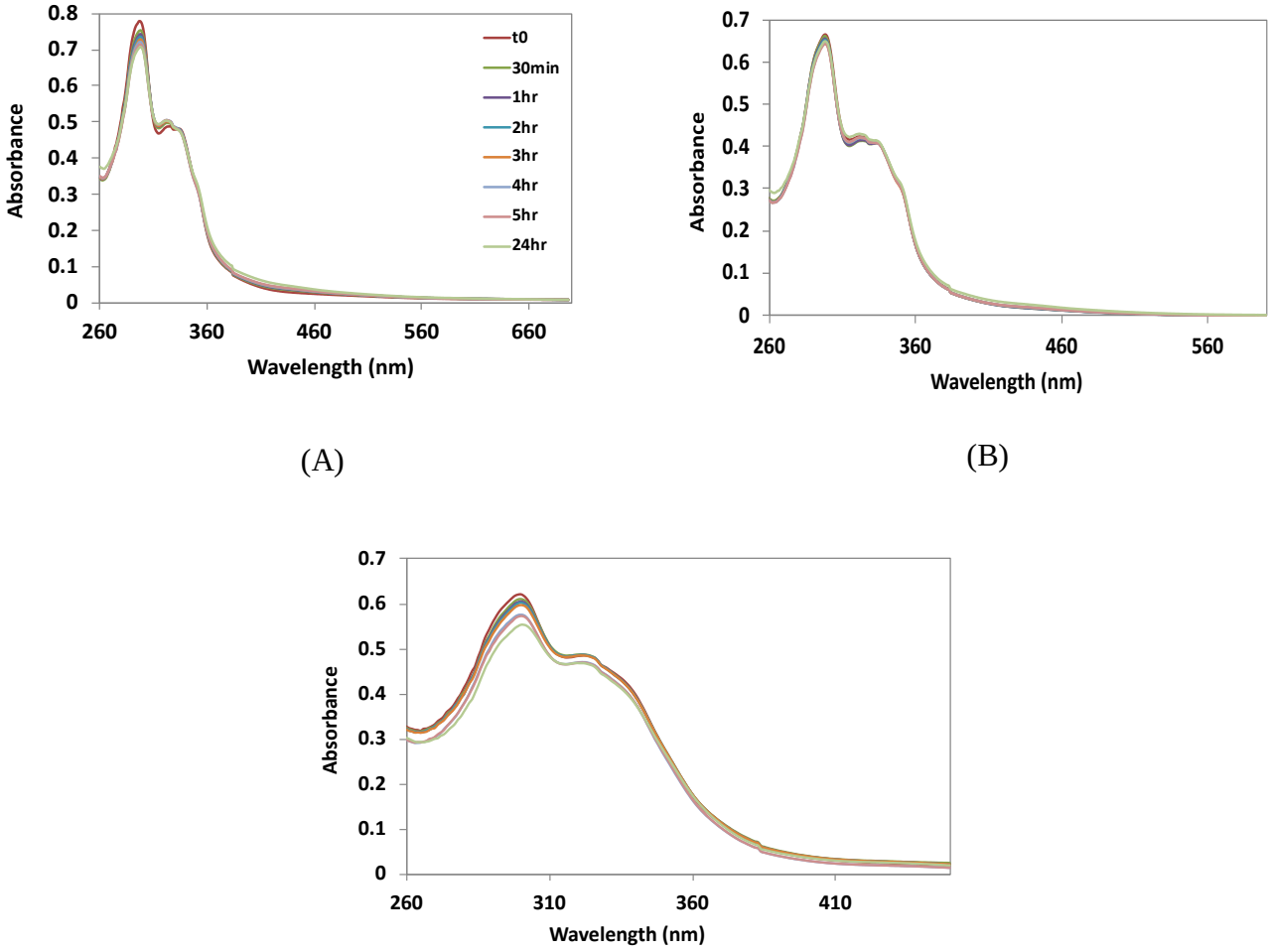

Figure A4.4. UV- Visible spectra of the zinc(II) complexes (in the presence of BSA) for 5 consecutive hours and after 24 hours. Ratio of [zinc complex] to [BSA] = 1:1~ 2.90×10^{-5} M. (A) ZnL^1, (B) ZnL^2, and (C) ZnL^3. Legend applies to all.

A5. UV- Visible fluorescence spectra

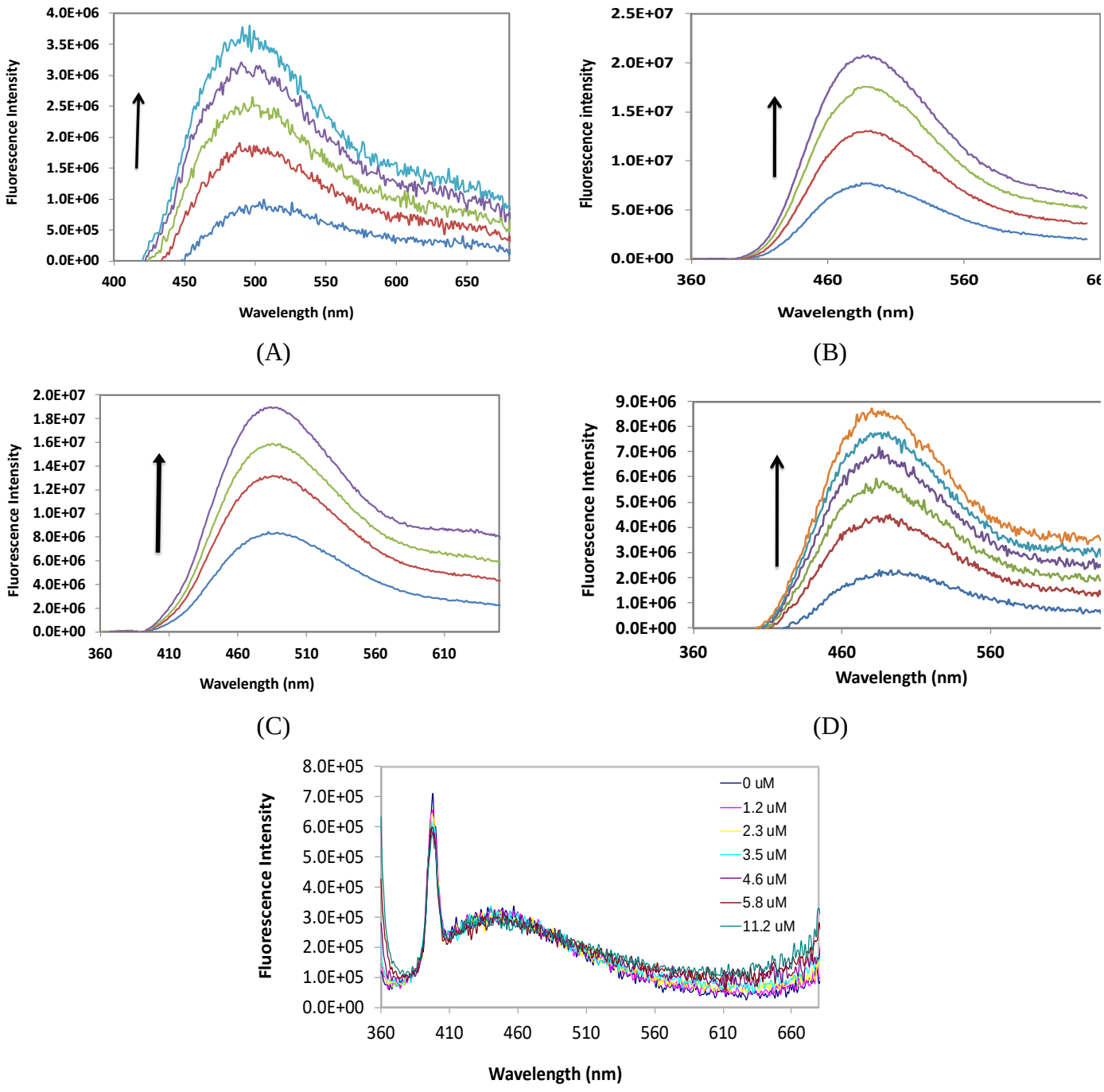

Figure A5. Fluorescence emission spectra (in DMSO) of the zinc metal complexes at λ_{ex}= 350 nm, with arrows indicating increasing concentration. (A) ZnL^1 (2.3-11.2×10^6 M). (B) ZnL^2 (2.1-8.2×10^6 M). (C) ZnL^3 (2.0-7.8×10^6 M) (D) ZnL^4 (1.2-6.9×10^6 M) and (E) Spectra of ZnL^4 exemplifying the non-emissive behaviour of the complexes in HEPES aqueous buffer (10 mM, pH=7.4)

A6. Quenching fluorescence spectra

A6.1. Fresh complex stock solutions

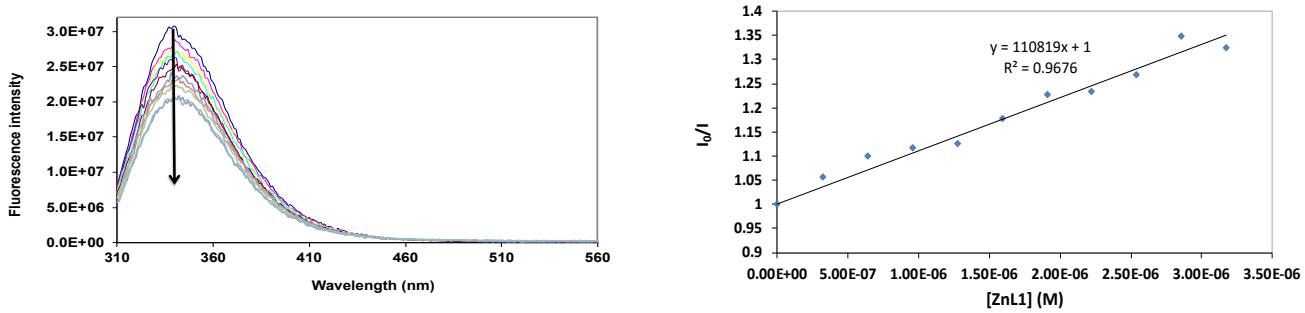

(A) ZnL^1

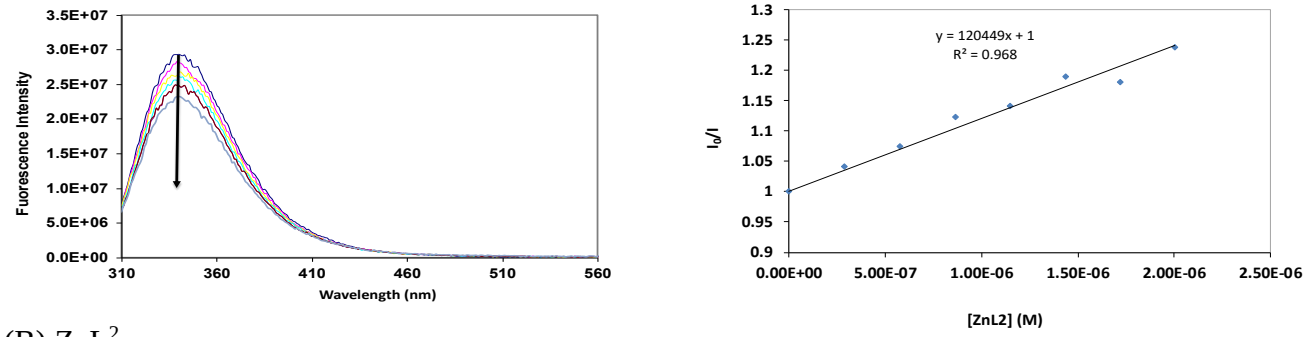

(B) ZnL^2

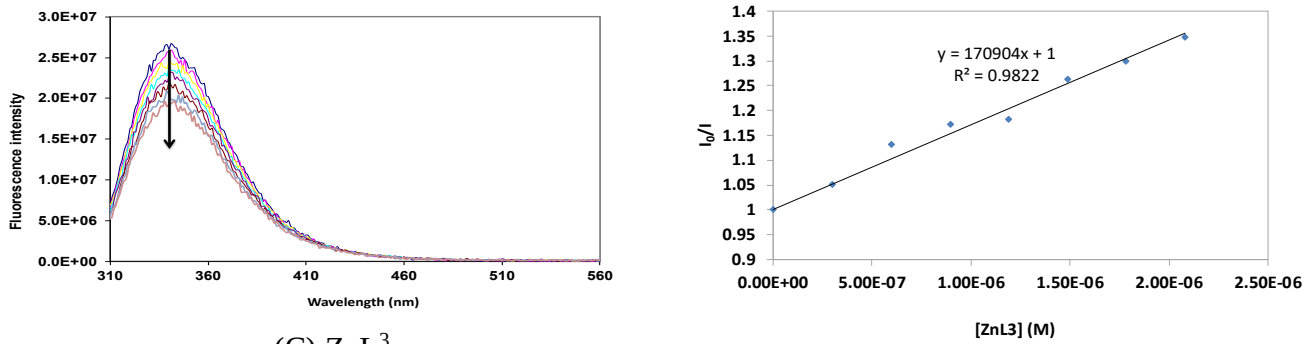

(C) ZnL^3

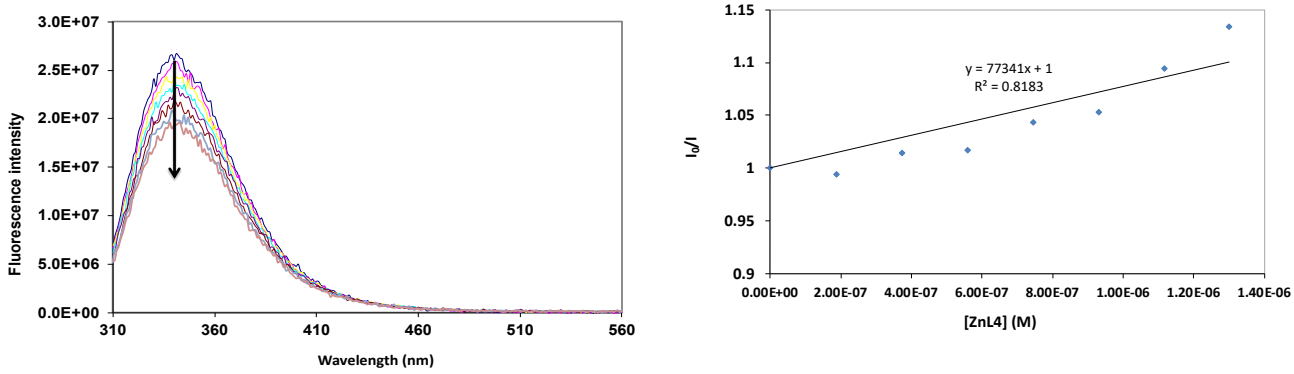

(C) ZnL^4

Figure A6.1. Fluorescence quenching spectra of BSA (~1.5 mM) by titration with fresh stock solutions of the zinc complexes with their Stern-Volmer plots (at 340 nm) and arrows indicating increasing complex concentrations from 0 to ~ 2.0×10^6 M.

A6.2. Aged complex stock solutions

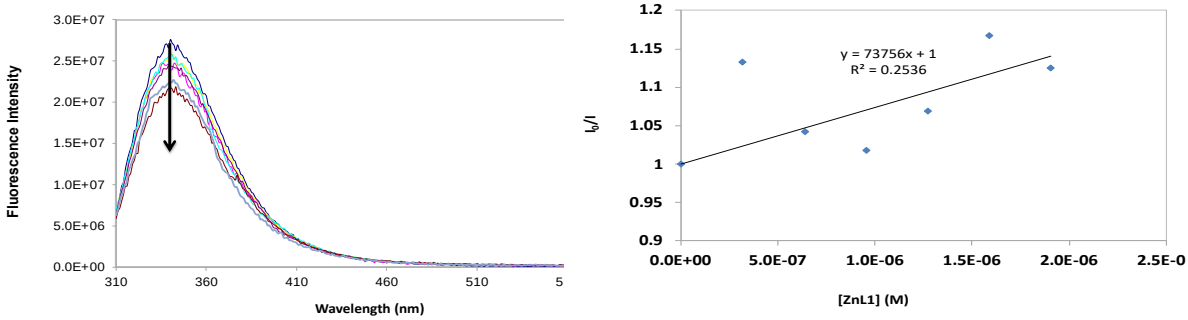

(A) ZnL^1

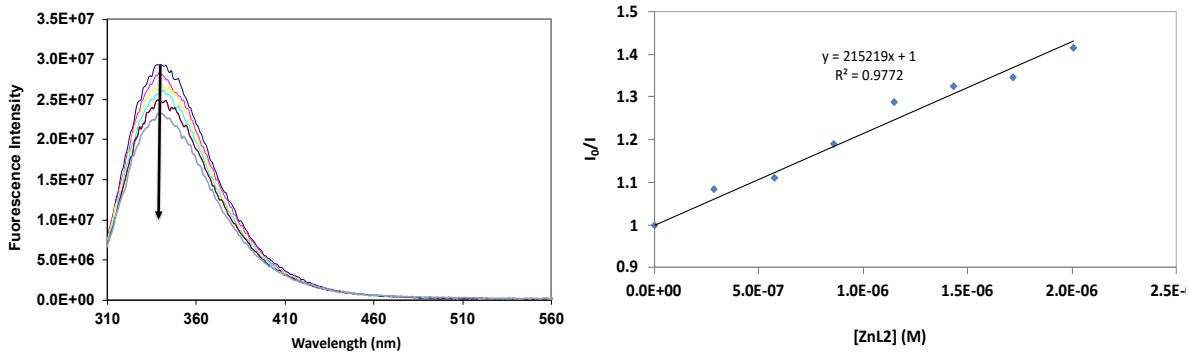

(B) ZnL^2

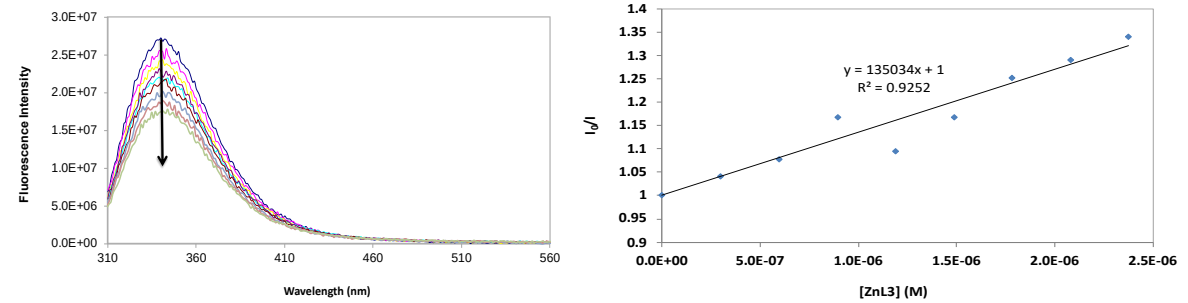

(C) ZnL^3

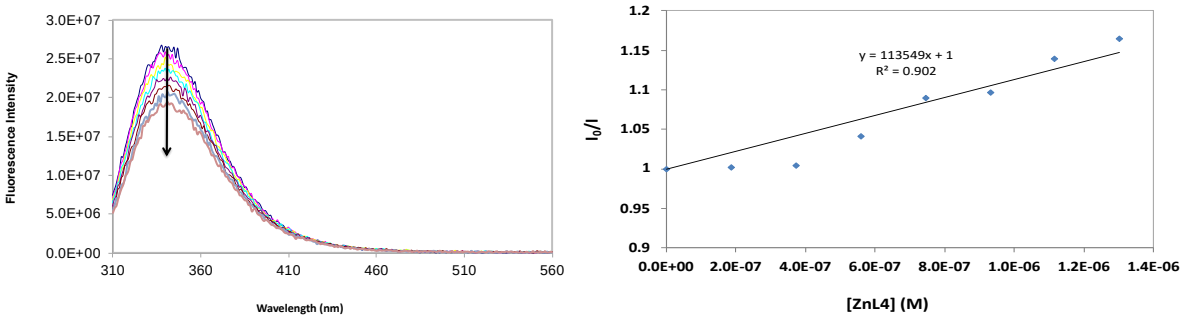

(D) ZnL^4

Figure A6.2. Fluorescence quenching spectra of BSA (~1.5 mM) by titration with aged stock solutions of the zinc complexes with their Stern-Volmer plots (at 340 nm) and arrows indicating increasing complex concentrations from 0 to ~ 2.4×10^6 M.

A7. Temperature studies with ZnL^3

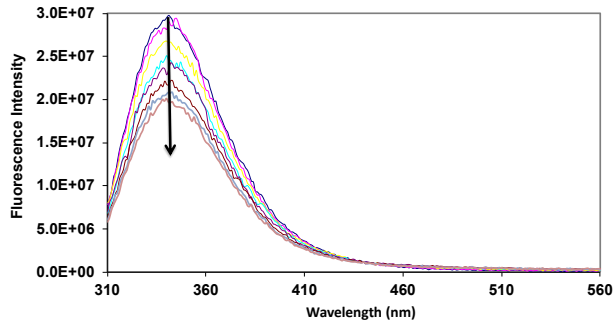

(A) 298K

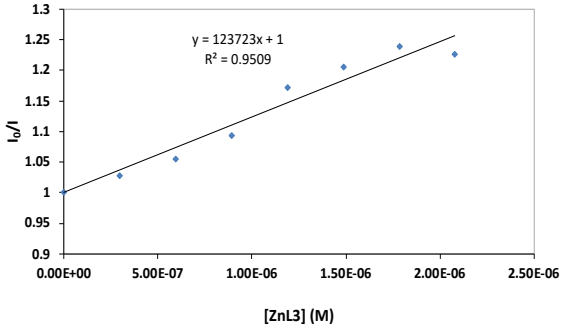

(B) 298K

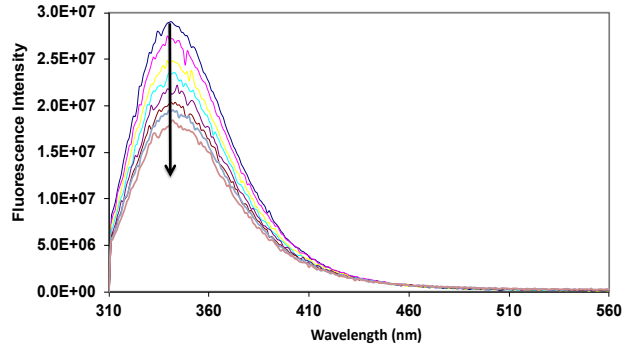

(C) 301K

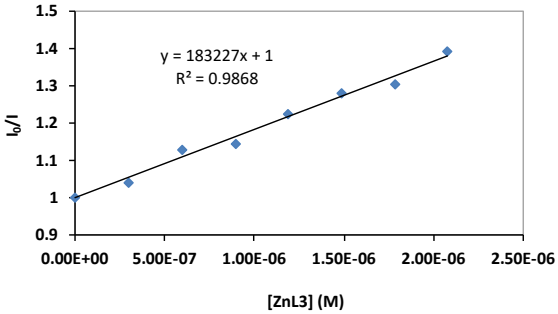

(D) 301K

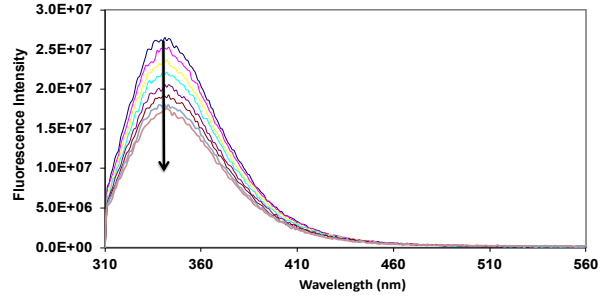

(E) 305K

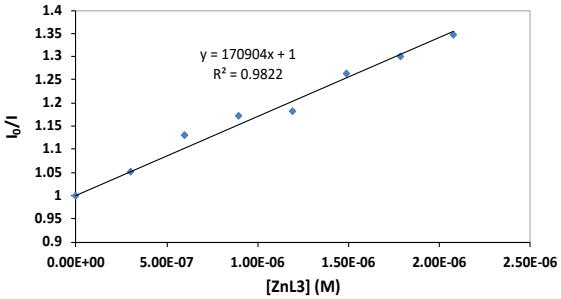

(F) 305K

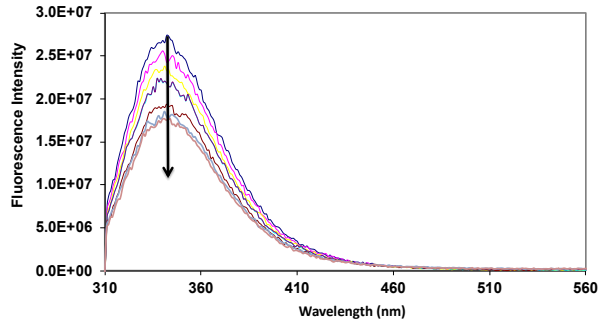

(G) 310K

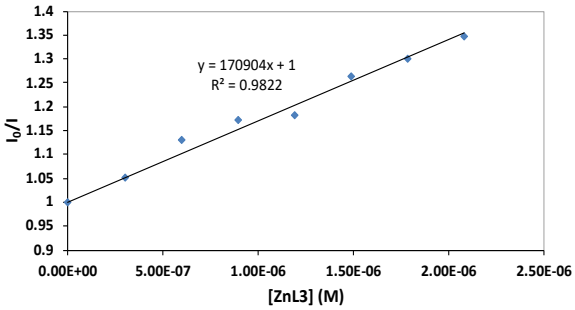

(F) 310K

Figure A7. Fluorescence quenching spectra of ZnL^3 in the presence of BSA (~1.5 mM) at different temperatures with their corresponding Stern-Volmer plots. Arrows indicating increasing complex concentration from 0 to ~ 2.0 M. (Temperature ± 1 ºC).

A.8. Cytotoxic activity

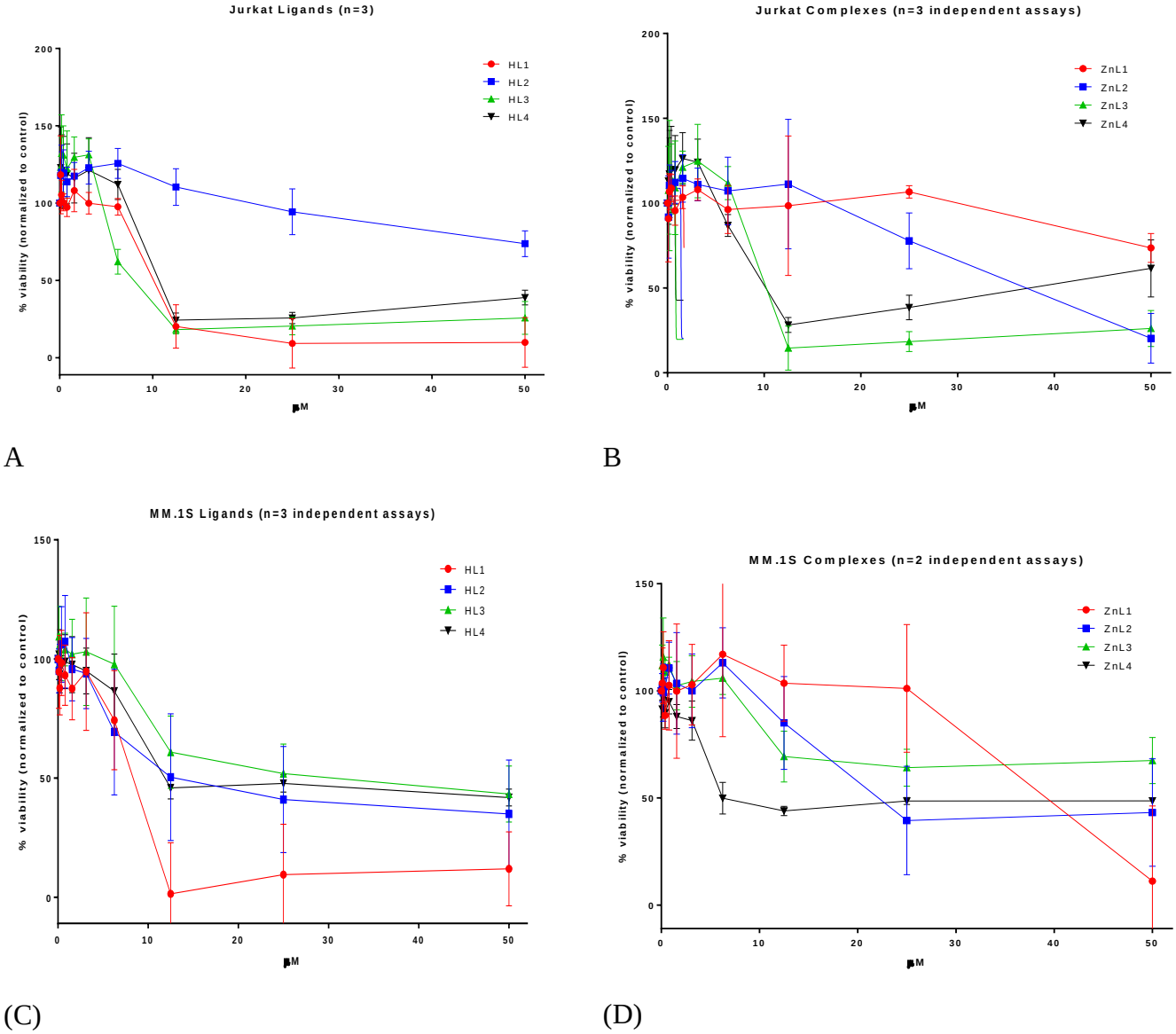

Figure A8.1. Dose-response curves of compounds. (A and C) Ligands and (B and D) Zinc complexes. Jurkat and MM.1S cells were exposed to different concentrations of each test compound for 48 h. Cell viability was determined using the resazurin reduction assay. Results were normalized to vehicle control and are presented as the mean ± SD of three independent assays.

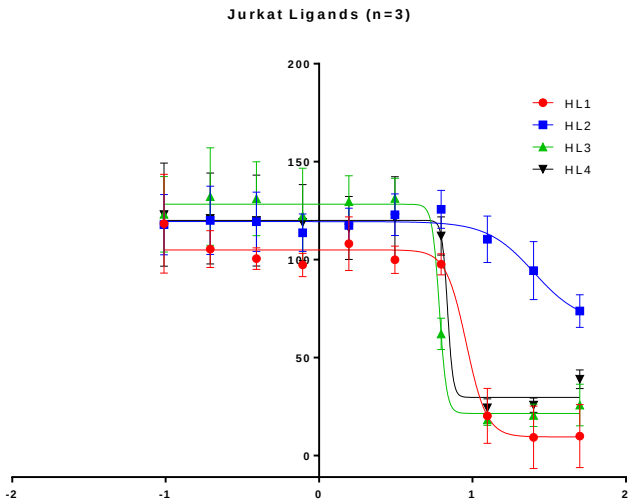

(A)

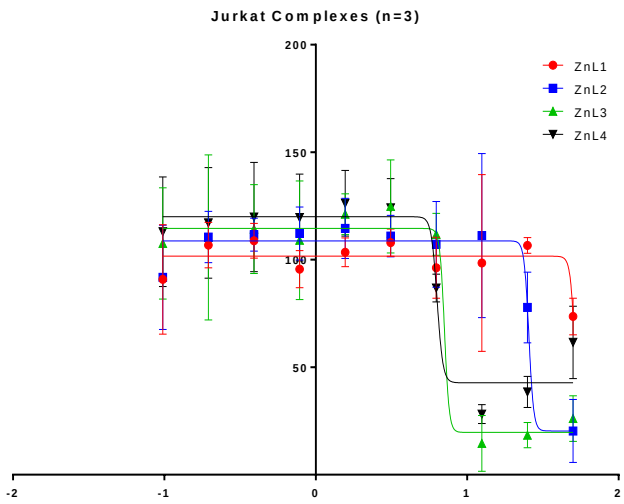

(B)

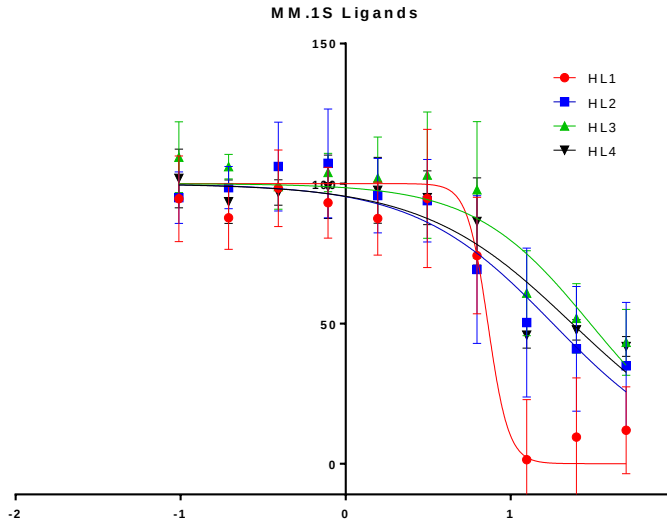

(C)

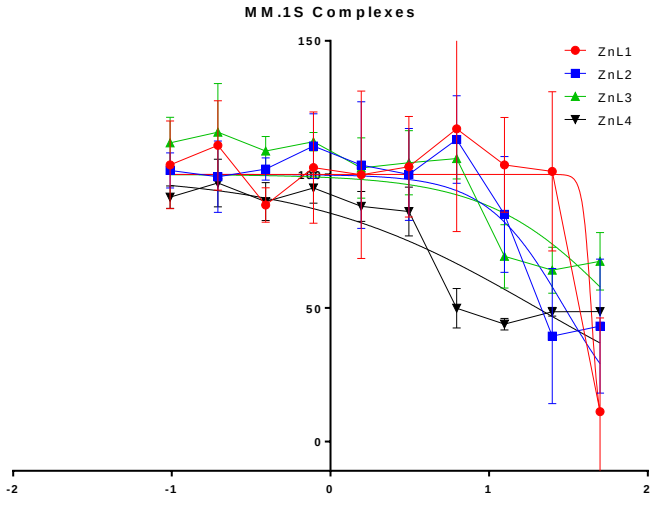

(D)

Figure A8.2. IC_{50} determination using a variable slope model. (A and C) Ligands and (B and D) Zinc(II) complexes.